

Bacterial cell cycle dynamics: size regulation during exponential growth and role of polyphosphate during starvation response

Thèse N° 8957

Présentée le 8 février 2019

à la Faculté des sciences de base

Laboratoire de biophysique expérimentale

Programme doctoral en approches moléculaires du vivant

pour l'obtention du grade de Docteur ès Sciences

par

ASTER LOUIS K VANHECKE

Acceptée sur proposition du jury

Prof. J. Lingner, président du jury

Prof. S. Manley, directrice de thèse

Prof. P. Levin, rapporteuse

Prof. A. Amir, rapporteur

Prof. J. McKinney, rapporteur

2019

Acknowledgements

First, I would like to thank my Thesis director Prof. Suliana Manley for granting me the opportunity to be a part of her lab and to meet and work with many different interesting people. Thanks for your honest feedback during so many meetings and presentations, I learned a lot about how to do good science.

Next I would like to thank my thesis jury for taking the time to evaluate my thesis. Thanks for the comments and suggestions for my thesis and for the great questions and the discussion during my oral exam. Thank you Prof. Petra Levin, Prof. Ariel Amir, Prof. John McKinney and Prof. Joachim Lingner.

I would like to thank all the people that I have worked with over the years. Seamus: thanks for making me at home in the lab and being my mentor for the first months. Thanks for teaching me how to break your microscope and, later, how to fix it again. Ambroise, thanks for your mentorship, it wasn't easy for both of us and we often thought differently about things, but in the end I learned a lot and had a lot of fun! Anna, grazie mille! It was a pleasure to work with you! Lisa, thanks for your enthusiasm and for teaching me about the mysterious polyphosphate, and for your patience during meetings when I spent all my time analyzing data but not thinking about how to present the analysis.

I would like to thank all the (ex-)lab members (in order of (dis)appearance): Thanks Seamus, Niklas, Sasha, Andrea, Kyle, Anna, Christian, Ambroise, Dora, Felix, Tatjana, Marcel, Baptiste, Charlotte, Timo, Armin, Emilie, Quentin, Sofia, Juliette, Guillaume and last but not least Robo-Kyle. Thanks for the great time we had together, all the discussions, feedback, weird lunch conversations and other fun stuff.

Special thanks to the people who took the time to give me feedback on parts of my thesis: Suliana, Ambroise, Dora, Christian and Clement.

To the friends I made here in Lausanne, thanks for making the last 4 years an amazing crazy adventure! Thanks for all the fun trips, dinners, drinks, parties and conversations.

Bedankt aan al mijn supporters aan het thuisfront, die achter ons stonden toen we beslisten om jullie te verlaten, sorry daarvoor. Bedankt om er steeds voor ons te zijn, als we terug in België waren, via skype/telefoon/briefkaart of op bezoek in Zwitserland (of in Italië, waarom niet?). En nog eens sorry dat ik Lynn heb meegenomen naar hier, maar zonder haar zou het echt niet gelukt zijn. Want Lynn, je bent mijn alles. Bedankt voor de goede zorgen, strenge woorden, steunende knuffels en de nodige lebbbers.

Contributions from others to chapters in this thesis

Chapter 2: The work in this chapter has been published: “Constriction rate modulation can drive cell size control and homeostasis in *Caulobacter crescentus*”, Ambroise Lambert*, Aster Vanhecke*, Anna Archetti, Seamus Holden, Felix Schaber, Zachary Pincus, Michael T. Laub, Erin Goley, Suliana Manley, iScience, 2018 (Lambert et al. 2018)

Conceptualization, A.L., A.V., S.M., E.G., M.T.L., S.H.; Methodology, A.L., A.V., S.M., E.G., M.T.L., S.H., A.A.; Software, A.V., A.A., F. S., S.H., Z.P., A.L.; Validation, A.L., A.V., S.M., S.H., A.A.; Formal Analysis, A.V., A.A., S.H., Z.P., A.L., S.M.; Investigation, A.L., A.V., E.G., S.H.; Resources, E.G., M.T.L., S.M.; Data Curation, A.V., A.L., A.A.; Writing – Original Draft: S.M., A.L., A.V., A.A.; Writing – Review & Editing: all authors.; Visualization, A.L., A.V., A.A., Z.P., S.M.; Supervision, S.M., E.G., A.L., S.H.; Funding acquisition, S.M., S.H.

Chapter 3: This project was a collaboration with Lisa Racki and Dianne Newman, California Institute of Technology, Pasadena, CA, USA.

Conceptualization, L.R., A.V., S.M., D.N.; Methodology, L.R., A.V., S.M., D.N.; Software, A.V.; Validation, A.V., L.R., S.M.; Formal Analysis, A.V., L.R., S.M.; Investigation, L.R., A.V.; Resources, L.R., D.N.; Data Curation, A.V., L.R.; Writing – Original Draft: A.V.; Writing – Review & Editing: all authors.; Visualization, L.R., A.V., S.M.; Supervision, S.M., D.N.; Funding acquisition, S.M., D.N.

Abstract

Bacteria are the most diverse and abundant kingdom of life and have adapted to survive and thrive in habitats around the globe. When provided with ample nutrients they grow and divide at staggering rates, increasing their population exponentially. Upon nutrient depletion on the other hand, they quickly adapt by drastically altering their metabolism, halting growth to survive for a very long time. Since bacteria are tiny -about a few micrometers-, visualizing these processes requires microscopy. To measure the dynamics of their shape and inner structures precisely, one needs to choose a technique that balances spatial resolution, temporal resolution and photo-toxicity. In this thesis, I present two projects using advanced dynamic microscopy, first to study cell size regulation during exponential growth in the abundance of nutrients and then to elucidate the role and positioning of polyphosphate granules during cell cycle exit in response to nutrient starvation.

During exponential growth, bacteria balance growth and division to regulate their size, resulting in a narrow size distribution, referred to as cell size homeostasis. Recent work has tried to uncover what cells sense to decide to divide in order to achieve size homeostasis: time, size, growth or a combination of those. Control of cell division is often equated to control of constriction onset; however, the constriction period still accounts for up to 40% of cell growth and could thus contribute significantly to cell size regulation. We used SIM microscopy to measure constriction kinetics and their impact on cell size regulation in *Caulobacter crescentus*. We found that constriction rate regulation can determine cell size. Moreover, constriction rate modulation compensates for variability in elongation before constriction, allowing a higher fidelity cell size homeostasis. We suggest a parsimonious model where excess cell wall precursors accumulate proportionally to elongation before constriction and set the rate of constriction. This is the first direct demonstration that constriction rate can contribute to cell size control and homeostasis in bacteria.

Upon nutrient starvation on the other hand, bacteria exit their cell cycle to preserve energy and nutrients. In many bacteria, such as *Pseudomonas aeruginosa*, this is associated with the accumulation of polyphosphate (polyP) in intracellular granules. PolyP is created by polyphosphate kinases (Ppk's), which are required for successful cell cycle exit and survival of and recovery from long-term starvation. Interestingly, these polyP granules are regularly spaced within the nucleoid. To date, it is not known during which stage polyP is required for cell cycle exit, and what causes the spacing of the granules. Here, we use fluorescence microscopy to probe the cell cycle stage of Δppk cells arrested during nutrient starvation as well as the localization and dynamics of Ppk's. We show that a majority of Δppk cells are arrested with open replication forks. Furthermore, we find that Ppk's localize in distinct patterns, already prior to starvation and polyP granule production, which could be responsible for the positioning of polyP granules. To this end, we developed a background subtraction algorithm to remove cytoplasmic fluorescence, improving accuracy of spot detection and localization.

Keywords

super-resolution microscopy, bacteria, cell size regulation, polyphosphate, stress response

Résumé

Les bactéries constituent le royaume de la vie le plus diversifié et abondant. Elles se sont adaptées pour survivre et prospérer dans différents habitats autour du monde. Lorsque les nutriments sont abondants, elles peuvent croître de manière exponentielle à des vitesses stupéfiantes. En cas de raréfaction des nutriments, elles modifient leur métabolisme radicalement afin de survivre. Elles sont minuscules, quelques micromètres, c'est la raison pour laquelle il faut l'aide de la microscopie pour les voir et les étudier. Pour mesurer la dynamique de leur forme et de leurs structures internes, il est important de trouver un équilibre entre résolution spatio-temporelle et phototoxicité. Dans cette thèse, je présente deux projets utilisant la microscopie dynamique avancée, d'abord pour étudier la régulation de la taille cellulaire lors de croissance exponentielle, puis pour élucider le rôle et le positionnement des granules de polyphosphate lors de la sortie du cycle cellulaire en réponse à un manque de nutriments.

Durant la phase exponentielle de croissance, les bactéries équilibrent la croissance avec la division afin de réguler leur taille, résultant à une distribution étroite de leur taille, nommé homéostasie de la taille cellulaire. Récemment, la recherche a tenté de découvrir ce que les bactéries perçoivent pour mener à leur division afin d'atteindre une homéostasie de taille : temps, taille, croissance ou une combinaison de ceux-ci. Le contrôle de la division est fréquemment assimilé au contrôle du début de la constriction; Cependant, la période de constriction représente jusqu'à 40% de la croissance cellulaire et pourrait donc contribuer à la régulation de la taille des cellules. Nous avons utilisé la microscopie SIM pour mesurer la cinétique de constriction et son impact sur la régulation de la taille de *Caulobacter crescentus*. Nous avons constaté que la régulation de la vitesse de constriction peut déterminer la taille des cellules. De plus, l'adaptation de la vitesse de constriction compense la variabilité d'élongation précédant la constriction, permettant ainsi une homéostasie de taille plus fidèle. Nous proposons un modèle dans lequel les précurseurs de la paroi cellulaire s'accumulent proportionnellement à l'allongement avant la constriction et déterminent la vitesse de constriction. Ceci est la première démonstration directe que la vitesse de constriction peut contribuer au contrôle de la taille des cellules et à l'homéostasie chez les bactéries.

Lorsque les nutriments se raréfient, les bactéries quittent leur cycle cellulaire pour économiser de l'énergie. Dans de nombreuses bactéries telles que *Pseudomonas aeruginosa*, ceci est associé à l'accumulation de polyphosphate (polyP) dans des granules intracellulaires. PolyP est produit par les polyP kinases (Ppk), indispensables à la sortie du cycle cellulaire et à la survie sans nutriments. À ce jour, on ne sait pas à quel stade de la sortie du cycle cellulaire polyP est requis et pourquoi les granules sont disposés régulièrement. Nous utilisons la microscopie à fluorescence pour sonder le stade du cycle cellulaire des cellules Δppk arrêtées, ainsi que la localisation de la protéine Ppk. Nous montrons qu'une majorité de cellules Δppk sont arrêtées au cours de la réplication de l'ADN. De plus, nous constatons que les Ppk sont placés régulièrement, déjà avant l'appauvrissement des nutriments et la production des granules, ce qui explique le positionnement des granules de polyP.

Mots-clés

Microscopie super-résolution, bactéries, régulation de taille cellulaire, poly-phosphate, réponse au stress

Contents

Acknowledgements	i
Abstract	iv
Keywords	iv
Résumé	v
Mots-clés	v
Contents	vii
List of Figures	x
List of Tables	xi
List of Equations	xi
Chapter 1 Introduction and background	13
1.1 Introduction	13
1.2 Structure and dynamics of the bacterial genome.....	14
1.3 Bacterial organelles.....	15
1.4 The bacterial cell envelope.....	16
1.4.1 Cell wall remodeling	16
1.5 Cell size regulation during exponential growth	19
1.5.1 Cell size control.....	19
1.5.2 Cell size homeostasis.....	20
1.6 Cell cycle regulation during nutrient starvation	21
1.7 Studying structural features of microscopic creatures	22
1.7.1 Classical microscopy.....	22
1.7.2 Super-resolution microscopy.....	23
Chapter 2 Constriction rate modulation can drive cell size control and homeostasis in <i>Caulobacter crescentus</i>	25
2.1 Abstract.....	25
2.2 Introduction	25
2.2.1 Importance of cell size regulation	25
2.2.2 Cell size control.....	26
2.2.3 Cell size homeostasis.....	26
2.2.4 Onset modulation versus rate modulation	26

2.2.5	Strategy.....	27
2.3	Results	27
2.3.1	Cell size control by constriction rate modulation.....	27
2.3.2	Constriction rate compensates variability in elongation before onset	29
2.4	Discussion.....	32
Chapter 3	The role of polyphosphate in the starvation response of <i>Pseudomonas aeruginosa</i>	35
3.1	Abstract.....	35
3.2	Introduction	35
3.2.1	The bacterial starvation response	35
3.2.2	Roles for polyP during the starvation response	35
3.2.3	Localization of polyP granules.....	36
3.2.4	Strategy.....	37
3.3	Results	37
3.3.1	Majority of starved Δ polyP cells stall with open replication forks	37
3.3.2	Localization of Ppk1 and Ppk2a	39
3.3.3	Cellular background subtraction improves localization accuracy.....	39
3.3.4	Dynamics of Ppk2a foci.....	42
3.4	Discussion.....	43
Chapter 4	Conclusion and outlook	45
4.1	Conclusion	45
4.2	Outlook.....	46
4.2.1	Mechanism of constriction rate compensation.....	46
4.2.2	Impact of variable constriction rate on pole shape.....	46
4.2.3	Location of Ppk foci.....	47
4.3	Final remarks	48
Chapter 5	Materials and Methods	49
5.1	Constriction rate modulation can drive cell size control and homeostasis in <i>Caulobacter crescentus</i>	49
5.1.1	Bacterial strains and growth conditions	49
5.1.2	Sample preparation	50
5.1.3	Image acquisition	50
5.1.4	Bleach correction	51
5.1.5	Quantification and statistical analysis.....	51
5.1.6	Detailed image analysis workflow.....	52
5.1.7	Pole shape analysis	54

5.1.8	Estimation of excess peptidoglycan precursor.	54
5.1.9	Empirical constriction model.....	55
5.1.10	Data and software availability.....	56
5.2	The role of polyphosphate in the starvation response of <i>Pseudomonas aeruginosa</i>	56
5.2.1	Bacterial strains and growth conditions	56
5.2.2	Image acquisition	57
5.2.3	Image segmentation and creation of cell contours	57
5.2.4	Alignment.....	57
5.2.5	Background subtraction and spot finding.....	57
5.2.6	Tracking analysis	58
5.2.7	Software availability	58
5.3	Outlook: Impact of variable constriction rate on pole shape	58
5.3.1	Figure 4-1A: prediction of pole contour.....	58
5.3.2	Figure 4-1B: Impact of pole shape on stalk position	58
	Appendix A Supplemental information to chapter 2.	61
	References	66
	Curriculum Vitae.....	84

List of Figures

Figure 1-1: The bacterial cell cycle: Chromosome conformation and cell shape. . .	18
Figure 1-2: Cell size regulation.....	20
Figure 2-1: Experimental strategy and constriction-related models for modulation of cell size.	27
Figure 2-2: Differences in constriction rate yield different cell sizes and pole shapes.	28
Figure 2-3: Compensation of elongation before and during constriction contributes to cell size homeostasis.	30
Figure 2-4: Early constriction rates compensate for elongation before onset.	31
Figure 3-1: A majority of Δ polyP cells did not finish DNA replication during cell cycle exit, as WT cells did.	38
Figure 3-2: Ppk1-mNeon localizes at midcell prior starvation and localizes uniformly throughout the central part of the cell.....	40
Figure 3-3: Ppk2a-mNeon tends to localize at the quarter positions, both before (0h) and after (3h) three hours of starvation.	41
Figure 3-4: Principle and validation of background subtraction method.....	42
Figure 3-5: Ppk2a-mNeon foci move subdiffusively and their motion is not significantly altered by starvation.....	43
Figure 4-1: Constriction rate, pole shape and impact on the cell.	47
Figure A-1: Image analysis pipeline.....	61
Figure A-2: Differences in size and elongation rate between populations.....	62
Figure A-3: Constriction rate drives compensation between LG-LC and LC-LB. ...	63
Figure A-4: Constriction rate shows influence of elongation before constriction decreases throughout constriction.....	64

List of Tables

Table 3-1: Results of validation of cellular background subtraction.....	42
Table 5-1: Experimental Models: Organisms and strains	49
Table 5-2: Plasmids	49
Table 5-3: Oligonucleotides	50
Table 5-4: Software packages	56
Table 5-5: Strains used in Chapter 3.....	56
Table 5-6: Spot detection parameters.....	58
Table 5-7: Camera setup parameters.....	59
Table 5-8: Localization analysis parameters.....	59

List of Equations

Equation 2-1: Estimation of area precursor excess at constriction onset.....	31
--	----

Chapter 1 Introduction and background

1.1 Introduction

Life is defined by its property to replicate itself. For bacteria, as for all cells, this entails growing and dividing. In order for one cell to transform into two, bacteria need to duplicate their genome, remodel their cell wall to create two cell walls and produce a new cell's worth of protein, RNA and metabolites. The synthesis of RNA and subsequent protein and metabolites is quite simple on the large scale; generally speaking, it requires no concerted efforts on the scale of a cell cycle, the synthesis of individual molecules is independent, so it consists of synthesizing "more stuff". The converse is the case for the doubling of the genome and the cell wall, both giant macromolecules whose duplication transcends the molecular scale, requiring cell-wide regulation. DNA replication initiates at one or a few specific places and should on average only occur once per cell cycle. Typically, the chromosome is organized and segregated while replication forks are still replicating it. Chromosome replication has to be coordinated with the duplication of the cell wall. The cell wall determines the shape of the cell, and to create two daughter cells of similar shape it cannot just grow randomly. For this reason, complex machineries remodel the cell wall, creating the cell wall that will separate the daughter cells, often preceded by a phase of growth. The regulation of cell wall remodeling will determine the size and shape of the daughter cells.

Growth and division require energy and nutrients from the environment and can deplete them rapidly. As a result, nutrient availability can fluctuate dramatically over time. Moreover, even maintenance of life without growth requires nutrients, as a result, nutrient starvation poses a significant challenge to bacteria. For this reason, bacteria need to sense and adapt to their environment. The starvation response requires major changes in bacterial physiology, and many aspects of it are still not well understood. It involves a few central relatively simple molecules with ancient origins. One of them is the polyphosphate (polyP) polymer, which seems to be involved in many different pathways and accumulates into spherical granules of up to 200 nm in size.

The behavior of bacteria in both nutrient rich and nutrient poor conditions have fascinated scientists for centuries. Their study has been complicated by their small size. Most bacteria are micron-sized and invisible to the naked eye; therefore, microscopy is required to visualize and study bacteria and their internal structures. Classical light and fluorescence microscopy have provided researchers with ample information on bacterial cell biology; however, they are limited to a resolution down to 200 nm due to the diffraction of light. Electron microscopy reaches a resolution that is roughly a hundred times smaller, but provides no dynamic information nor allows it for easy identification of protein species. With the development of several super-resolution microscopy techniques less than twenty years ago, the gap between fluorescence microscopy and electron microscopy became smaller (Gahlmann and Moerner 2014; Sigal, Zhou, and Zhuang 2018). Depending on the structure of interest and its dynamics, one has to choose the type of microscopy with the right balance of spatial resolution, temporal resolution and photo-toxicity (Z. Liu, Lavis, and Betzig 2015).

In this thesis, I present the two projects using advanced microscopy techniques and analysis. In the first project, we quantified the dynamics of the shape of the cell throughout the cell cycle to study the role of constriction rate modulation in cell size regulation during exponential growth. In the second project, we study the polyP granules and their dynamics during the starvation response. In the

current chapter, Chapter 1, I introduce the thesis and provide the necessary background to understand the following chapters of this thesis.

Chapter 2 describes the measurement of cell shape dynamics, more specifically the kinetics of constriction during the cell division of *Caulobacter crescentus*. We perturbed the constriction rate genetically and pharmacologically and measured its effect on cell size, showing that constriction rate modulation can be used to control cell size. Moreover, we found that early constriction rate compensates for variation in elongation before constriction, leading to a higher fidelity cell size homeostasis. We propose a parsimonious model, where the buildup of cell wall precursors during the elongation phase determines the rate of constriction.

In Chapter 3, we investigate the role of polyphosphate (polyP) in cell cycle exit during the starvation response of *Pseudomonas aeruginosa*. We localize and track polyphosphate kinases (Ppk's) as well as genomic markers (replication origins and replication forks). We found that polyP is often required for successful completion of DNA replication during cell cycle exit, and that Ppk's localize in distinct foci, already prior to starvation and the formation of polyP granules.

1.2 Structure and dynamics of the bacterial genome

Bacteria organize their components into structures to increase efficiency or to fulfill more complicated tasks (Mathews 1993; Surovtsev and Jacobs-Wagner 2018). Arguably the most important structure of each cell is the genome, which, for the majority of bacteria, exists as a single circular chromosome. Replication starts from a single locus, termed the origin of replication or *ori*, ending at a locus more or less on the opposite side of the chromosome, termed the terminus of replication or *ter* (Marsh and Worcel 1977; Meyenburg et al. 1979). The chromosome is always busy; it is being transcribed into RNA, replicated and segregated to form two daughter chromosomes and repaired after damages. It is being bound and unbound by proteins, and its three-dimensional organization is altered by gyrases, DNA structuring proteins, etc. To fit this polymer with a contour length of around 1 mm within a micron-sized cell, it must take on a highly compacted conformation. Nucleoid associated proteins (NAPs) and structural maintenance of chromosomes (SMC) proteins bind the chromosome and help compact and structure it (Dillon and Dorman 2010; Nolivos and Sherratt 2014).

The spatial organization of the nucleoid has been studied using sequence specific labels, such as fluorescence in situ hybridization (FISH) and fluorescent repressor operator systems (FROS). Interestingly, the spatial arrangement of the chromosome reflects the overall sequence of the genome. In *C. crescentus*, *P. aeruginosa* and *Mycobacterium smegmatis*, it was found that in cells with a single chromosome the origin of replication lies near the old cell pole, while the replication terminus lies near the new cell pole. Other loci are positioned in between at positions proportional to their genomic position. This is referred to as an "*ori-ter* configuration" (Figure 1-1B) (Viollier et al. 2004; Vallet-Gely and Boccard 2013; Logsdon et al. 2017). The *Escherichia coli* chromosome forms a different pattern; in slow growing cells, the origin of replication and terminus are found near the middle of the cell, with left and right arms of the chromosome in opposite halves of the cell (Nielsen et al. 2006; X. Wang et al. 2006). Fast growing *E. coli* cells, by contrast, organize their chromosome in an *ori-ter* fashion (Figure 1-1A) (Youngren et al. 2014). In all these cases, the chromosome is organized while it is being replicated, during the segregation process (Bates and Kleckner 2005; Viollier et al. 2004; Youngren et al. 2014; Vallet-Gely and Boccard 2013). In *C. crescentus*, replication initiation happens at the position of the origin near the old cell pole, after which the replication forks travel along the chromosomes to arrive at midcell, while one origin quickly localizes to the other cell pole. In *P. aeruginosa* the replisome stays at midcell, and each locus, including the origin of replication, travels to midcell just prior to its replication and subsequently travels to its new position in either half of the cell (Viollier et al. 2004; Vallet-Gely and Boccard 2013; X. Wang, Llopis, and Rudner 2013). For many species, the proper configuration of the chromosome is initiated by

the parABS-system or its homologs. ParB binds *parS* sites near the origin of replication and together with the ATPase parA it positions the origin of replication at its typical location, for instance near the cell poles for the *ori-ter* configuration (Mohl, Easter, and Gober 2001; P. S. Lee and Grossman 2006; Vallet-Gely and Boccard 2013; Badrinarayanan, Le, and Laub 2015). The chromosome is subdivided into macrodomains that co-localize partly due to aggregation of genes being regulated and expressed together (Valens et al. 2004; Le et al. 2013). DNA within these macrodomains forms extensive loops and often interacts, but interactions between different macrodomains are rare. The borders of these macrodomains are probably formed by highly transcribed regions, such as clusters of ribosomal genes. The growing amount of information on the conformation of the bacterial chromosome leads to ever more precise models of global chromosome conformation, providing a way to study the properties and behavior of the chromosome *in silico* (Hacker, Li, and Elcock 2017; Yildirim and Feig 2018).

1.3 Bacterial organelles

Unlike eukaryotes, bacteria usually do not have membrane-enclosed organelles or subcellular compartments. Nevertheless, many bacterial species create large subcellular structures with varying functions. Magnetotactic bacteria for instance create compass-like magnetic structures to orient themselves along a magnetic field (Uebe and Schüler 2016). They form crystals of magnetic iron minerals within membrane invaginations of their periplasm. The invaginations are pinched off and aligned with the cell long axis using a protein filament. This allows these cells to swim unidirectionally along the magnetic field, allowing them to quickly find microaerophilic environments (Popp, Armitage, and Schüler 2014). During cell division, the array of magnetosomes is positioned near midcell and divided in half, ensuring equal inheritance among daughter cells (Katzmann et al. 2011).

Bacterial microcompartments (BMC's) are large particles consisting of a regular shell made out of thousands of proteins filled with enzymes belonging to the same pathway. The most common example are the polyhedral carboxysomes in cyanobacteria. Carboxysomes massively increase the efficiency of carbon fixation by concentrating carbonic anhydrase and RubisCO. Carbonic anhydrase catalyzes the release of CO₂ from bicarbonate, increasing its local concentration; RubisCO enzymes then capture the CO₂. The protein shell prevents the CO₂ from escaping, further increasing efficiency. Many other BMC's exist, holding enzymes of different pathways (Yeates et al. 2008; Kerfeld, Heinhorst, and Cannon 2010; Chowdhury et al. 2014). Carboxysomes are regularly spaced within the cell. Recent work showed that this organization is caused by gradients of nucleoid-binding proteins in a Brownian-ratchet type mechanism: the parA-like protein McdA binds throughout the nucleoid when bound to ATP. McdB localizes to carboxysomes and to McdA, recruiting the carboxysomes to the nucleoid. McdB stimulates ATPase activity of McdA, causing it to unbind from the nucleoid, creating an McdA-depleted zone around the carboxysomes. The McdB-promoted motion of carboxysomes up the McdA gradient causes carboxysomes to spread out (MacCready et al. 2018). Thanks to this mechanism, carboxysomes are regularly spaced throughout the cell, ensuring equal partitioning over daughter cells during cell division.

One of the most widespread type of subcellular structures are polymer granules such as polyhydroxyalkanoate (PHA) granules and polyphosphate (polyP) granules (Anderson and Dawes 1990; Rao, Gómez-García, and Kornberg 2009). PHA granules are not enclosed by membranes, but do have many proteins associated to them (Bresan et al. 2016). PolyP granules are not enclosed by membranes and aggregation of polyP into granules is probably spontaneous since it also occurs *in vitro* (Miller 1984). These granules are often created as a stress response or during growth in nutrient-poor conditions. PHA granules mainly serve as a carbon and energy storage, while polyphosphate most likely also has regulatory roles during stress response, which will be discussed in section 1.6.

1.4 The bacterial cell envelope

The bacterial cell envelope delineates the boundary between the cell and the environment and in this capacity serves both as a physical barrier keeping the contents of the cell together and as the place of interaction between the bacterium and the environment (Silhavy, Kahne, and Walker 2010). Interaction with the environment goes from exchanging nutrients and waste products and sensing concentrations of these products, to interacting with the environment, for instance exerting force on it using flagellar motors or interacting with other organisms by exchanging nutrients or engaging in biological warfare. The cell envelope has multiple components or layers contributing to its functions.

The most important component of the cell envelope, present in all cells, is the lipid plasma membrane, which serves as the main permeability barrier, as well as a storage for energy-rich lipids (Raetz and Dowhan 1990; Meer, Voelker, and Feigenson 2008). Transmembrane channels allow for passive or active transport of molecules for which the membrane is impermeable. The plasma membrane can support large concentration or electrochemical gradients. This is essential in its role in metabolic pathways creating energy, such as the electron transport chain, which creates a proton gradient across the plasma membrane, known as the proton motive force.

The other components of the cell envelope differ between species and serve as a major factor in distinguishing groups of bacterial species. Most bacteria fall into one of two main groups, referred to as the Gram-positive and Gram-negative bacteria, named after their coloring by the Gram stain. Gram-positive bacteria have a thick cell wall surrounding their plasma membrane, retaining the gram stain. Gram-negative bacteria on the other hand have a much thinner cell wall and have a second outer membrane outside of the cell wall, allowing the gram stain to be washed away. Some bacteria, such as mycobacteria, do not fall into one of these two categories which often result in indecisive Gram-staining. The Gram-negative outer membrane is a lipid bilayer, but is very different from the plasma membrane in composition. The outer leaflet consists of glycolipids, such as the diverse lipopolysaccharides, which dictate most of the chemical properties of the cell's surface. One of the main functions of the outer membrane is to protect the cell from threats such as viruses or cell wall-targeting antibiotics or enzymes. The space between inner- and outer membrane is called the periplasm and contains many degradative enzymes such as RNase, also protecting from some viruses. Some Gram-negatives have an additional layer of surface protein called the surface layer (S-layer), providing additional protection (Silhavy, Kahne, and Walker 2010).

The cell wall is made of a material called peptidoglycan, which consists of a network of glycan strands cross-linked by peptide-bridges, containing D-amino acids which do not naturally occur in proteins (Vollmer, Blanot, and de Pedro 2008; de Pedro and Cava 2015). The building blocks of the cell wall, N-Acetyl glucosamine (GlcNAc) and N-acetyl muramic acid (MurNAc), are created in the cytoplasm. Then, MurNAc-pentapeptide is synthesized and added to the transport lipid undecaprenyl phosphate in the inner membrane, forming Lipid I, to which GlcNAc is added to form Lipid II. Lipid II is then flipped to the outer side of the plasma membrane, where it can be used for cell wall synthesis (Barreteau et al. 2008; Typas et al. 2012). The cell wall's main function is to give the cell its shape and rigidity, allowing it to resist expansion due to the high turgor pressure caused by high internal solute concentrations. Upon losing their cell wall, cells lose their shape and become spherical or burst, depending on the osmotic pressure. Purified cell walls retain the shape of the cell (Weidel and Pelzer 1964). Recent evidence shows that the outer membrane contributes in the resistance to internal pressure (Rojas et al. 2018). Nevertheless, the cell wall is still considered as the main load-bearing structure, and the sole structure maintaining the cell's shape.

1.4.1 Cell wall remodeling

To allow for growth and division, the cell wall constantly has to change shape, while retaining its integrity and rigidity. Cell wall synthesis consists of two main activities: transglycosylation,

the polymerization of glycan strands, and transpeptidation, the cross-linking of glycan strands by peptide bridges. The enzymes responsible for these activities are called penicillin binding proteins (PBP's), some PBP's combine both transglycosylase and transpeptidases activities. Transglycosylation and transpeptidation incorporates new material into the cell wall, however, in order for this material to contribute to the length (or more general, the surface area) of the cell wall, hydrolases have to break existing bonds to make place in between the old material (Typas et al. 2012).

PBP's by themselves can remodel the cell wall, adding material randomly. Very often however, they are part of a protein complex guiding cell wall remodeling to specific locations with specific orientations. In rod-shaped bacteria, the two most prevalent cell wall remodeling systems are the elongasome, responsible for elongation and leading to rod-like cells, and the divisome, directing cell wall remodeling inward, leading to cell division (Figure 1-1B).

The elongasome is organized around MreB, an actin homolog that forms filaments (Jones, Carbalido-López, and Errington 2001) (reviewed in (Shi et al. 2018)). Apart from MreB, this protein complex contains putative adaptor proteins MreC, MreD and RodZ, linking MreB with cell wall remodeling enzymes, such as RodA, a transglycosylase, and PBP2, an essential transpeptidases, which transiently binds MreB complexes (T. K. Lee et al. 2014; Morgenstein et al. 2015; Meeske et al. 2016). MreB filaments rotate circumferentially around the cells long axis, driven by cell wall synthesis (Garner et al. 2011; Teeffelen et al. 2011; Domínguez-Escobar et al. 2011). MreB orients along the greatest principle curvature, leading to a preferential localization to regions of negative curvature. This way, MreB directs cell wall synthesis to these regions, straightening non-uniform areas along rod-shaped cells (Ursell et al. 2014; Billings et al. 2014; Hussain et al. 2018). Additionally, cell wall insertion by MreB is dependent on mechanical strain. Consequently, mechanical forces leads to growth-dependent plastic deformations of cell shape and cells recover the rod-shape upon removal of the force (Wong et al. 2017). The orientation of the MreB filaments is believed to be parallel to the orientation of the incorporated glycan strands, which are preferentially oriented perpendicular to the long axis of the cell (Turner et al. 2018). The elongasome is responsible for the rod shape of the cell, and plays an important role in determining the constant diameter of the cell. Different studies in *E. coli* attributed cell diameter to specific properties of the MreB filaments, such as twist or curvature (S. Wang and Wingreen 2013; Ursell et al. 2014; Tropini et al. 2014; Ouzounov et al. 2016; Shi et al. 2017; Colavin, Shi, and Huang 2018). However, recent work in *B. subtilis* suggested that the cell diameter is set by the balance between random PG insertion by aPBPs, increasing the diameter, and the oriented PG insertion by the elongasome, reducing the diameter (Dion et al. 2018).

The divisome, the collection of proteins responsible for cell division, also has an important role for a filament-forming protein, FtsZ. FtsZ assembles in a ring-like structure around midcell (Bi and Lutkenhaus 1991; Ma, Ehrhardt, and Margolin 1996). FtsZ is a homolog of tubulin with which it shares many characteristics, the main ones being filament formation, GTPase activity and similar sequence and crystal structure (Erickson 1995, 1997; Löwe and Amos 1998). FtsZ assembly at midcell happens relatively early during the cell cycle, as was shown in *Bacillus subtilis*, where FtsZ assembled upon initiation of DNA replication (Harry, Rodwell, and Wake 1999). In *C. crescentus*, divisome assembly commences soon after replication and segregation of the origins of replication (Thanbichler and Shapiro 2006). Around 20 proteins with different functions are recruited to midcell, in different steps, leaving several points for regulation (Aarsman et al. 2005; Gamba et al. 2009; Goley et al. 2011; den Blaauwen, Hamoen, and Levin 2017). In the early stages of divisome assembly in *C. crescentus*, FtsZ recruits MreB, increasing cell wall elongation at midcell (Aaron et al. 2007).

Initially, it was thought that FtsZ forms some kind of force-generating ring structure (Li et al. 2007; Osawa, Anderson, and Erickson 2009; Erickson, Anderson, and Osawa 2010; Osawa and Erickson 2013; Szwedziak et al. 2014). However, this was put in doubt by reports that FtsZ did not form a

complete ring, incompatible with most force-generating models (Fu et al. 2010; Holden et al. 2014), and that cell wall synthesis, rather than FtsZ dynamics, is the rate-limiting step for constriction (Coltharp et al. 2016). Recently, it was shown that, very much like for MreB, individual FtsZ filaments rotate circumferentially and direct cell wall synthesis, leading to constriction (Bisson-Filho et al. 2017; Yang et al. 2017). An interesting difference between the elongasome and the divisome is that the motion of the elongasome depends on cell wall synthesis, while the motion of the divisome is determined by the treadmilling rate of FtsZ. This way, FtsZ directs and distributes cell wall remodeling around the septum.

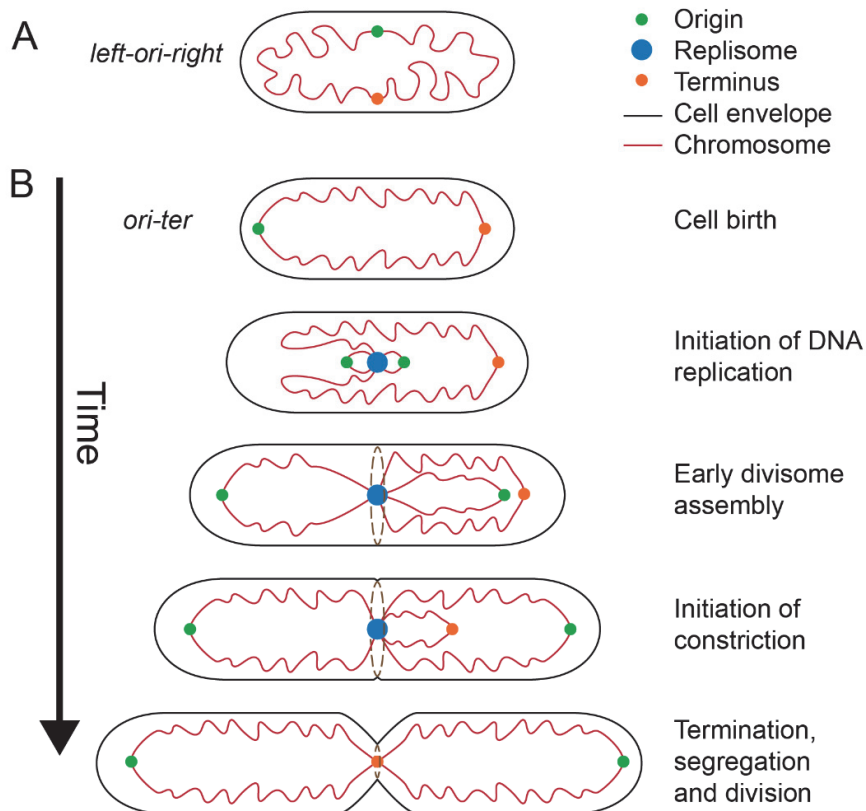


Figure 1-1: The bacterial cell cycle: Chromosome conformation and cell shape.

A) Chromosome in *left-ori-right* conformation, as in slow growing *E. coli*. **B)** Cell cycle for cell with the *ori-ter* chromosomal conformation, such as *C. crescentus* and *P. aeruginosa*, the replisome is shown centrally here as in *P. aeruginosa*. Cells are born with their chromosome in the *ori-ter* configuration, with the origin near the old pole and the terminus near the new pole. DNA replication starts with the origin of replication. The divisome starts to assemble only after DNA replication has initiated. After recruitment of late divisome proteins, the divisome initiates constriction. Before constriction can finish, DNA replication terminates and the daughter chromosomes are segregated, making way for the septum.

Many factors have been shown to influence divisome assembly and modulate constriction rate. The location of FtsZ assembly should occur around midcell, between segregated nucleoids. Bacteria have evolved a variety of mechanisms to control the position of divisome assembly. The Min system prevents divisome assembly near the cell poles, directing it to midcell, while in longer cells it creates periodic patterns of inhibition of divisome assembly (Bi and Lutkenhaus 1993; Raskin and Boer 1999b, 1999a; Hu and Lutkenhaus 1999; Wehrens et al. 2018). The nucleoid occlusion (NOC) system helps prevent divisome assembly near the nucleoid to prevent the septum from cutting the chromosome (Bernhardt and de Boer 2005; Adams, Wu, and Errington 2014; Bailey et al. 2014). In *C. crescentus*, no homolog to the Min or NOC system is present; instead, they have a protein called MipZ. MipZ interacts with ParB-*parS* complexes near the origin of replication and forms a

gradient, maintained by its ATPase- and DNA binding activity, peaking near the origins of replication. MipZ inhibits FtsZ assembly, therefore the divisome can only assemble near midcell, once the two copies of the origin of replication have been segregated (Thanbichler and Shapiro 2006; Kiebusch et al. 2012). The Min, NOC and MipZ systems not only help the divisome to find midcell, they also couple divisome assembly to cell length and/or chromosome segregation. Other factors mainly promote or delay FtsZ assembly. In both *B. subtilis* and *E. coli*, a metabolic enzyme links metabolism with cell division. In *B. subtilis* it is UgtP, involved in glycolipid synthesis, which is expressed proportional to nutrient availability. In *E. coli* this role is filled in by OpgH, which catalyzes the creation of osmoregulant periplasmic glucans from UDP-glucose. Both UgtP and OpgH localize to the division site and delay FtsZ assembly and divisome maturation, allowing cells to grow longer in nutrient rich conditions (Weart et al. 2007; Hill et al. 2013). Finally, some proteins couple the final stages of chromosome replication and segregation to cell division to prevent the septum to cut unsegregated nucleoids. In *E. coli* for instance, MatP is associated to the *ter* domain and slows down constriction (Harry, Rodwell, and Wake 1999; Buss et al. 2015; Espéli et al. 2012; X. Wang, Possoz, and Sherratt 2005).

By regulating division, cells can ensure DNA replication and segregation have finished prior to finishing division. Since cell elongation continues throughout the cell cycle, regulating cell division will have an effect on the size of the cell at division and thus the sizes of the daughter cells.

1.5 Cell size regulation during exponential growth

In the presence of sufficient nutrients, bacteria grow exponentially both in the length of individual cells as in their numbers (Godin et al. 2010; P. Wang et al. 2010). Nutrients are often scarce and only transiently available in the wild; therefore, bacteria attempt to use them as quickly and efficiently as possible. Bacteria have relatively little variation in cell size, especially during exponential growth, suggesting that cell size is regulated. There are many selective pressures that possibly act on cell size (Young 2006). Presumably, during exponential growth the main concerns are on one hand to provide enough space for chromosome segregation (Donachie and Begg 1989), cell division should take place only after chromosome segregation (Adams, Wu, and Errington 2014). On the other hand, the sooner or smaller cells divide, the sooner they become two independent cells, that can survive and thrive independently. Alternatively, changes in cell size could be a side effect of multifork replication and the coupling of DNA replication with cell division (Zheng et al. 2016; Amir 2017). As described above, cells first elongate followed by constriction leading to the creation of two daughter cells. The size of a cell at division could be controlled by changing many aspects of the cell cycle; regulation could be based on growth rate, time, size or amount of growth, and could be enforced at different points in the cell cycle, such as constriction onset or during the constriction phase. The challenge lies in identifying which ones the cell can and does regulate. Within cell size regulation, one can distinguish two types of regulation. First, the regulation of the average cell length in response to the environment, referred to as cell size control, and second, regulation of the size of single cells that make them regress towards the mean, leading to a narrow distribution of sizes, referred to as cell size homeostasis (Figure 1-2). Cell size control and homeostasis are closely related, but not all species show both of them, many bacteria, like *C. crescentus*, do not change their size depending on growth conditions. Cell size homeostasis however, is observed among all prokaryotes.

1.5.1 Cell size control

It was noted already in the fifties that for some species, such as *E. coli* and *Salmonella typhimurium*, the average cell size depends on nutrient derived growth rate (Schaechter, Maaløe, and Kjeldgaard 1958). More precisely, the logarithm of the average cell size (V) is proportional to the growth rate (λ , from length $L(t) = L_0 e^{\lambda t}$) multiplied by a constant time (T), equal to 60 minutes at 37°C, or

$\log V \sim \lambda T$, known as the growth law. This observation was combined with work showing DNA replication and subsequent division take approximately 60 minutes over a broad range of growth rates (Cooper and Helmstetter 1968), to form a model where DNA replication initiates at a constant volume per origin, followed by a constant time for DNA replication and subsequent division, leading to the observations of the growth law (Donachie 1968).

The molecular basis of the growth law is not clear. The main suspect for controlling DNA replication initiation with respect to cell size is DnaA, an ATPase. The concentration of DnaA-ATP remains constant during growth, while its absolute number increases with size. DnaA-ATP cooperatively binds the chromosome at an array of specific binding sites around the origin of replication and promotes initiation of DNA replication. Nevertheless, DnaA does not behave exactly as required for the model, so other factors must be involved (Løbner-Olesen et al. 1989; Westfall and Levin 2017). As discussed above, the divisome is controlled by many factors, some of which inhibit FtsZ assembly in the presence of (unsegregated) chromosomes (Bernhardt and de Boer 2005; Wu and Errington 2004; Adams, Wu, and Errington 2014; Coltharp et al. 2016). Nevertheless, there are other factors related to size and growth that regulate the divisome. Both in *B. subtilis* and *E. coli*, proteins have been found that sense nutrient availability and that influence FtsZ assembly accordingly (Weart et al. 2007; Hill et al. 2013; Vadia et al. 2017). The growth law has recently come under scrutiny, its implications have been reinterpreted as indicating that changes in cell size are mainly a product of the control of DNA replication (Amir 2014, 2017). Another meticulous work studied the relationship between size and growth rate under an exhaustive number of conditions and perturbations to formulate a more general form of the growth law: $V(V_0, T, \tau) = V_0 \times 2^{T/\tau}$, where V is the average volume at division, V_0 is the volume per *ori* at initiation, the minimal volume to initiate DNA replication, T is the time required for DNA replication and subsequent cell division and τ is the doubling time. All of these parameters can be modified by the environmental conditions or perturbations (Si et al. 2017).

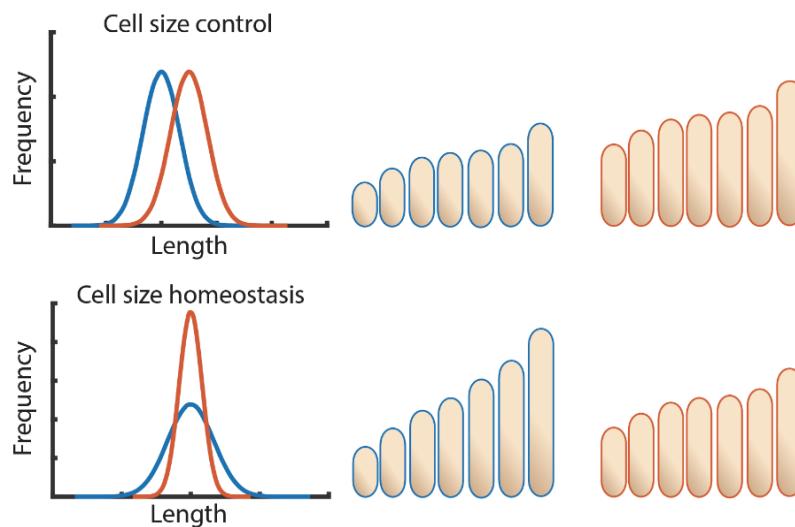


Figure 1-2: Cell size regulation.

Cell size control refers to the control of the mean cell size of a population, often as a function of growth rate. Cell size homeostasis refers to keeping the variation in cell size constant and relatively small.

1.5.2 Cell size homeostasis

How can cells within a population maintain a narrow distribution of cell sizes during growth at steady state? In order to achieve cell size homeostasis, there must be some mechanism driving cells with aberrant size towards the population's mean cell size. An initial theory was that there are size-sensing mechanisms promoting cell division at a critical cell size (Rashevsky 1938; Koch and

Schaechter 1962). A candidate mechanism came when it was observed that replication of DNA was always initiated at a constant mass or volume per origin, followed by a constant time for replication and subsequent division (Cooper and Helmstetter 1968; Donachie 1968). Note that in this study cell mass was measured, but volume and mass are assumed interchangeable in this model and later studies often measured cell volume rather than mass. More recently, evidence from time-lapse microscopy of many generations of bacteria kept at constant conditions in microfluidic devices reputed the sizer model. It showed that cells do not divide at a constant size, independent from their size at birth, as the sizer predict. Instead all cells, independent from their size at birth, divide after growing for a certain amount, which is the on average the same for all cells. This model is termed the “adder” (Campos et al. 2014; Taheri-Araghi et al. 2015; Jun and Taheri-Araghi 2015).

How cells could possibly measure their increase in length or volume since birth is not entirely clear, but the proposed models generally rely on the accumulation of a certain factor that when reaching a threshold concentration, triggers a cell cycle event. Such a mechanism has been proposed to trigger DNA replication, in the context of the constant volume or growth per origin (Sompayrac and Maaløe 1973; Ho and Amir 2015). Another mechanism was proposed to directly trigger cell division. In this study, it was shown the balance between volume- and surface growth controls the cell surface area-to-volume ratio. Both volume and surface growth are dependent on metabolic activities in the cytoplasm, proportional to the cell volume, thus allowing for homeostasis of surface to volume ratio (Harris and Theriot 2016). Here it was noted that over the cell cycle, the surface area to volume ratio oscillates, decreasing during the elongation phase and increasing again during the constriction phase. Assuming constant biosynthesis of surface precursors, a surplus of precursors would build up during elongation phase, proportional to the volume increase since growth. It was proposed that constriction was triggered by the precursor surplus reaching a threshold. The surplus of cell wall precursors would be used to build the septum and thus the new cell poles, which have a high surface area-to-volume ratio.

However, Donachie’s model, i.e. initiation of DNA replication at a critical mass followed by a constant period of DNA replication and subsequent division, was shown to be still consistent with recent data in single *E. coli* cells, leading to an adder at fast growth, but tending more towards a sizer-like behavior at slow growth (Wallden et al. 2016). Despite major research effort over decades, the details of cell size homeostasis are not clear.

1.6 Cell cycle regulation during nutrient starvation

Exponential growth quickly depletes available nutrients and in most environments nutrient availability is low and fluctuating (De Nobili et al. 2001; Garcia et al. 2013). Nutrient starvation is one of many stresses that bacteria can face in their environment. Each stress elicits a specific response, but most of them include a decrease in growth rate, or even a complete cell cycle exit. This way cells can drastically decrease their nutrient requirements and protect their chromosome from damage (Saint-Ruf et al. 2007). Most stress responses, including the starvation response, have a common core, depending on the alternative sigma factor RpoS (Battesti, Majdalani, and Gottesman 2011). As a sigma factor, RpoS complexes with RNA polymerase and alters its specificity, massively altering which genes it transcribes (H. Weber et al. 2005).

Starvation-related stresses usually elicit the stringent response, characterized by high levels of the “alarmone” guanosine penta-phosphate and guanosine tetra-phosphate, (p)ppGpp, as the central signaling molecule. (p)ppGpp stimulates translation of RpoS (Lange, Fischer, and Hengge-Aronis 1995). The enzymes responsible for synthesis and hydrolysis of (p)ppGpp differ between bacteria. They are extensively described in *E. coli*, but these enzymes and the general mechanisms of the stringent response are believed to be well-conserved between proteobacteria and, to a certain extent, other bacteria (K. Liu, Bittner, and Wang 2015). In proteobacteria, RelA and SpoT can both synthesize and hydrolyze (p)ppGpp. RelA is bound to the ribosomes, where it senses unloaded

tRNA's indicative of amino acid scarcity and responds by producing (p)ppGpp (Agirrezabala et al. 2013; English et al. 2011). (p)ppGpp then alters transcription by binding to the RNA polymerase, together with the transcription factor DskA (Barker et al. 2001; Barker, Gaal, and Gourse 2001; Paul et al. 2004; Durfee et al. 2008; Traxler et al. 2011). (p)ppGpp also has many effects on translation, DNA replication and metabolism, although it is hard to discern which effects are primary and which ones are secondary. (p)ppGpp induction has been shown to increase RpoS levels, probably by combined effects on transcription, translation and stability (Battesti, Majdalani, and Gottesman 2011). Elevated (p)ppGpp levels decreases growth rate and drastically changes metabolism (Traxler et al. 2008; Potrykus et al. 2011), ultimately leading to higher resistance to stress, even to stresses different from what initially caused the response (Khakimova et al. 2013; Nguyen et al. 2011).

(p)ppGpp promotes the accumulation of another interesting stress-related molecule, polyphosphate (polyP) (Kuroda et al. 1997). PolyP accumulates into spherical granules clearly visible in electron micrographs and sometimes even in phase contrast microscopy. They are created in response to stress in many bacteria, including *Klebsiella aerogenes*¹ (Smith, Wilkinson, and Duguid 1954), *Acetonebacter longum* (Tocheva et al. 2013), *E. coli* and *P. aeruginosa* (Ault-Riché et al. 1998; Amado and Kuzminov 2009), while polyP granules are always present in *C. crescentus* and *Campylobacter jejuni* (Müller et al. 2014; Henry, Crosson, and Chang 2013). PolyP has been suggested to be a storage or a sequestration mechanism for energy and phosphate or even metal ions, which it binds due to its high negative charge. When the polyP producing enzymes, polyphosphate kinases (Ppk's), are knocked out, no polyP granules are formed, decreasing the survival chances of the cells during stationary phase (Crooke et al. 1994; Rao and Kornberg 1996). PolyP seems to play a variety of roles during starvation, for instance by activating the Lon protease which degrades ribosomal proteins (Kuroda et al. 2001). PolyP, together with (p)ppGpp, slows down the cell cycle in *C. crescentus* (Boutte, Henry, and Crosson 2012). Recent work has shown that polyP plays a role as a chaperone to protect proteins from oxidative stress (Gray and Jakob 2015). Moreover, it has been shown that polyP is required for proper cell cycle exit during starvation in *P. aeruginosa* (Racki et al. 2017). PolyP is a multifunctional molecule; it is quite likely that not all its functions are known yet. Moreover, it remains to be seen what the relative importance of these different functions is during stress response and cell cycle exit, i.e. the absence of which function causes failure in cell cycle arrest in the absence of polyP.

1.7 Studying structural features of microscopic creatures

1.7.1 Classical microscopy

Bacteria are small, and their discovery only came with the development of a microscope strong enough to resolve them, developed by Antonie Van Leeuwenhoek in the 17th century. Microscopy still remains one of the main tools to study bacteria and their underlying structures. Since most bacteria are on the order of a micrometer, most of their subcellular features cannot be resolved by light microscopy. Instead, most subcellular features in bacteria were discovered and described using electron microscopy, reaching a resolution in the order of a few nanometers (Baker and Pease 1949; Dubochet et al. 1983; Oikonomou, Chang, and Jensen 2016).

Apart from resolution, contrast is another important limiting parameter, it describes the ability to discern a structure of interest from the background signal. In bright-field light microscopy, contrast is created when the sample absorbs light, while in electron microscopy it is created by the absorption or scattering of electrons. Many biological samples however are highly transparent to visible light. Modalities like phase contrast and differential interference contrast (DIC) microscopy increase

¹ Previously known as *Enterobacter aerogenes* or *Aerobacter aerogenes* (Tindall, Sutton, and Garrity 2017).

contrast between the cell and the background and allows to better discern certain compartments. But, as is also a limitation of electron microscopy, all these techniques rely on the inherent contrast of the sample and do not allow to specifically highlight a structure or protein of interest. This limitation was overcome by the use of specific staining, initially mainly fluorescent dyes. A higher specificity is possible with immunostaining, where fixed, permeabilized cells are stained with an antibody tagged with a fluorescent dye or an electron-dense particle (Stirling 1990). With the discovery and cloning of the green fluorescent protein (GFP) it became possible to genetically create fluorescent chimeras with any protein of interest (Tsien 1998), given that the chimera is still functional or at least localizes like the native protein (Swulius and Jensen 2012). This allowed researchers to selectively look at the localization and structures formed by their protein of interest.

1.7.2 Super-resolution microscopy

Despite the ease of specific labelling provided by fluorescent labels, fluorescence microscopy was still limited in resolution by the diffraction limit, while electron microscopy with nanometer-resolution could only be performed on fixed samples that were not easily labeled. This gap was addressed by the development of several super-resolution microscopy modalities. These techniques overcome the diffraction limit in different ways, by temporally separating or varying the intensity of different subsets of the fluorophores by using non-uniform illumination and/or special fluorophore properties. In stimulated emission depletion (STED), a type of scanning microscopy, the effective illuminated volume is decreased by inactivating fluorophores around the center of the illuminated volume (Hell and Wichmann 1994; Klar et al. 2000). This is done using a second, donut-shaped laser beam around the center of the illuminated volume, promoting stimulated emission in a wavelength that is filtered out of the detection channel. Single molecule localization microscopy (SMLM), such as stochastic optical reconstruction microscopy (STORM) or photo-activated localization microscopy (PALM), temporally separates the emission of single fluorophores by stochastic blinking or photo-activation events. Fluorescence of a single fluorophore can be localized with nanometer precision (Betzig et al. 2006; Hess, Girirajan, and Mason 2006; Rust, Bates, and Zhuang 2006; Heilemann et al. 2008). Recording a video of blinking frames can allow to localize enough molecules to reconstruct a super-resolved image. The observation of single molecule blinking events can be used to estimate molecule numbers, taking into account possible biases (Annibale et al. 2011; Rollins et al. 2014). It can also allow to follow the motion of single molecules in live cells (Manley et al. 2008). Structured illumination microscopy (SIM) uses structured illumination patterns to achieve frequency shifting with the structure in the sample. Combining differently oriented shifted patterns, one can access higher frequency information of the sample structure, achieving a resolution doubling in classical SIM (M. G. L. Gustafsson 2000; Mats G. L. Gustafsson et al. 2008).

All these methods have inherent strengths and weaknesses, which have to be balanced for the question at hand (Reviewed in (Z. Liu, Lavis, and Betzig 2015)). The most prominent feature of super-resolution modalities is their spatial resolution. Diffraction limited microscopy has a resolution of 200 nm or higher, depending on the wavelength of the light used. SIM improves this twofold, to 100 nm at best, while STED and SMLM reach resolutions on the order of 20 nm. It is to be noted that for SMLM the resolution is a combination of localization precision and sampling rate, since enough single fluorophores have to be localized to reconstruct the fine structure of the target.

While wide-field fluorescence microscopy is only limited by the framerate of the camera and the brightness of the sample and can reach acquisition times down to the order of a millisecond, super-resolution methods typically need much more time. Since STED is a scanning method, the resolution improvement is proportional to the increased scanning time in each dimension. Typical acquisition times at 20 nm resolution can be more than a minute. But video-rate imaging is possible at ~60 nm resolution for a bright sample (Westphal et al. 2008). In PALM and STORM, the acquisition time is set by the blinking rate of the fluorophores in the sample and the density of molecules to acquire to achieve sufficient sampling, and is typically a few minutes, but can be down to a few

seconds when pushing the limits (Shim et al. 2012). In this aspect, SIM excels over the other modalities, since it only requires 9 or 15 frames to be acquired, which can be done in 0.1-2 s, depending on the brightness of the sample. Instant SIM, which replaces some of the digital image processing steps in SIM by optical operations, achieves single-frame super-resolution and can reach framerates up to 100 frames per second (York et al. 2013).

Super-resolution techniques typically require much higher laser powers than wide-field fluorescence microscopy. This can cause damage to the cell, or at least heat it up considerably, perturbing the processes being studied. The irradiances which a cell can endure depends on the species, the dye, the wavelength and many other factors. STED requires between 10^4 and 10^9 W/cm², while SMLM requires 10^3 to 10^4 W/cm², noting that PALM often requires damaging short wavelengths for photo-activation. SIM on the other hand, only requires 10 - 10^2 W/cm², being much more compatible with live-cell time lapse imaging.

All these features need to be taken into consideration when choosing a super-resolution imaging modality. STED and SMLM are most suited for structural questions, where mostly the labelling strategy will determine which modality to use. SMLM has already shown to be useful to explore bacterial cell biology (Gahlmann and Moerner 2014). SIM is most suited for time-lapse microscopy, and has already proven its use in understanding bacterial cell division (Strauss et al. 2012; Bisson-Filho et al. 2017; Yang et al. 2017).

Chapter 2 Constriction rate modulation can drive cell size control and homeostasis in *Caulobacter crescentus*.

The work in this chapter has been published: “Constriction rate modulation can drive cell size control and homeostasis in *Caulobacter crescentus*”, Ambroise Lambert*, Aster Vanhecke*, Anna Archetti, Seamus Holden, Felix Schaber, Zachary Pincus, Michael T. Laub, Erin Goley, Suliana Manley, iScience, 2018 (Lambert et al. 2018)

2.1 Abstract

Rod-shaped bacteria typically grow first via sporadic and dispersed elongation along their lateral walls and then via a combination of zonal elongation and constriction at the division site to form the poles of daughter cells. Although constriction comprises up to half of the cell cycle, its impact on cell size control and homeostasis has rarely been considered. To reveal the roles of cell elongation and constriction in bacterial size regulation during cell division, we captured the shape dynamics of *Caulobacter crescentus* with time-lapse structured illumination microscopy and used molecular markers as cell-cycle landmarks. We perturbed the constriction rate using a hyperconstriction mutant or fosfomycin inhibition. We report that the constriction rate contributes to both size control and homeostasis, by determining elongation during constriction and by compensating for variation in pre-constriction elongation on a single-cell basis.

2.2 Introduction

2.2.1 Importance of cell size regulation

Cell size regulation is observed nearly universally among prokaryotes (Koch 1996), allowing them to both control their size at birth and to homeostatically maintain it over multiple generations (P. Wang et al. 2010). Cell size control and homeostasis are critical for survival: once too small, cells lack the volume required to host the essential machinery of life (National Research Council (US) Steering Group for the Workshop on Size Limits of Very Small Microorganisms 1999) or initiate chromosome segregation (Donachie and Begg 1989). On the other hand, dividing increases cell number and thus overall survival chances. Moreover, cells that are much too large may even suffer limitations in nutrient uptake (Beveridge 1988) and distribution (Schulz and Jørgensen 2001) because of their reliance on diffusive transport.

Size regulation is linked to cell cycle progression, which is marked by several key processes, including chromosome replication, segregation, and division into two daughter cells. These processes occur once per cell cycle in bacteria such as *Caulobacter crescentus* (Marczynski 1999), in contrast to rapidly proliferating organisms such as *Escherichia coli* (Cooper and Helmstetter 1968) and *Bacillus subtilis* in which cells often have multi-fork replication and which can, following nutrient upshifts, initiate replication multiple times in a single cell cycle. In *C. crescentus*, differentiation from a swarmer to a stalked cell and the initiation of chromosome replication and segregation mark the

transition from cell cycle phase G1 to S. The completion of replication marks the end of S phase. Once DNA segregation is completed, cells finish cytokinesis to form sibling stalked and swarmer cells during G2/M (Skerker and Laub 2004).

2.2.2 Cell size control

From the perspective of the cell wall, individual *C. crescentus* cells elongate exponentially throughout the cell cycle, as is typical for rod-shaped bacteria. Their growth is divided into an initial stage of dispersed pure elongation as peptidoglycan is inserted sporadically along the lateral walls, followed by a stage of zonal elongation and then mixed elongation and constriction in G2/M phase during which peptidoglycan is inserted at mid-cell to build two new poles (Aaron et al. 2007; Kuru et al. 2012). In *B. subtilis*, in strains where cells are on average longer at the onset of constriction, they are also on average longer at division (Taheri-Araghi et al. 2015; Weart et al. 2007). This suggests a model for cell size control, by modifying the cell length at which the divisome, the multi-protein complex which guides division, begins to generate constriction. Similarly, in *C. crescentus*, chromosome segregation must initiate before the cytokinetic Z-ring can assemble at mid-cell, coordinated by the gradient-forming FtsZ inhibitor MipZ (Thanbichler and Shapiro 2006). Another possibility is that the rate of constriction is modulated; this was shown to be the case for MatP, which coordinates chromosome segregation and constriction in *E. coli* (Coltharp et al. 2016).

2.2.3 Cell size homeostasis

For a population to maintain its size over generations, “size homeostasis,” different rules have been proposed. In a “sizer” model, cells require a critical size to divide, in an “adder” model, cells add a fixed volume between birth and division, and in a “timer” model, cells maintain the time between divisions (Amir 2014). Note that a pure timer model cannot correct for fluctuations in cell size. Mixed models that combine aspects of each have had success in capturing a wide range of observations (Banerjee et al. 2017; Osella, Nugent, and Cosentino Lagomarsino 2014), and are often justified through their connections with specific cell cycle phases. In *E. coli*, the period of chromosome replication until the end of the subsequent cell division may take a constant duration, underlying a timer (Cooper and Helmstetter 1968). The initiation of chromosome replication requires a fixed volume per origin of replication, and a fixed time to divide after replication initiation (Donachie 1968). This leads to a sizer under slow growth conditions and a phenomenological adder under fast growth, multi-origin conditions (Wallden et al. 2016; Ho and Amir 2015). Putative molecular mechanisms have generally relied on the accumulation of proteins above a threshold, such as an “initiator” of unknown identity triggering replication (Sompayrac and Maaløe 1973; Ho and Amir 2015), possibly DnaA (Løbner-Olesen et al. 1989) or accumulation of excess peptidoglycan (PG) cell wall precursors triggering constriction (Harris and Theriot 2016). A model of the latter case predicts a constant addition of volume per cell cycle, or adder. Indeed, an adder has been observed for *C. crescentus* under a wide range of growth conditions (Campos et al. 2014). Deviations from a pure adder toward a mixed relative timer and adder have also been reported for stalked cells, observed over many generations and a range of different temperatures (Banerjee et al. 2017). Any model incorporating a sizer or adder will allow smaller cells to increase while larger cells decrease in size over generations until both converge to a size set by the constant of addition (Jun and Taheri-Araghi 2015). Thus, both provide a clear means for a population to achieve size homeostasis.

2.2.4 Onset modulation versus rate modulation

Remarkably, although constriction makes up a significant portion of the cell cycle in many bacteria (den Blaauwen, T., Hamoen, and Levin 2017), for example up to 40% for *E. coli* (Reshes et al. 2008) or *C. crescentus* grown in minimal media (Laub et al. 2000), its impact on cell size control and homeostasis has rarely been considered. Intriguingly, budding yeast may use constriction rate to modulate their size in response to changes in growth conditions (Leitao and Kellogg 2017). However, a single-cell study of the contribution of the constriction stage in bacteria has been

challenging, in part due to the diffraction-limited size of the constriction site, and the need for corroboration by divisome markers to identify constriction onset unambiguously. Furthermore, direct measurement of the instantaneous constriction rate has not been possible.

2.2.5 Strategy

Here, we investigated whether, and how cells adjust their constriction rate to achieve cell size control and homeostasis. We used structured illumination microscopy (SIM) (M. G. L. Gustafsson 2000) to resolve the constriction site diameter and measure the size of synchronized *C. crescentus* cells as they progressed through their cell cycle. We show that perturbing the constriction rate changes cell size, independent of elongation rate. Furthermore, we found that within a population the onset of constriction and its rate are coordinated: cells that elongate more than average before constriction undergo a more rapid constriction, leading to less elongation during constriction, and vice-versa. This compensation leads to a higher fidelityadder than permitted by onset control alone, allowing *C. crescentus* to better maintain its size in the face of biological noise.

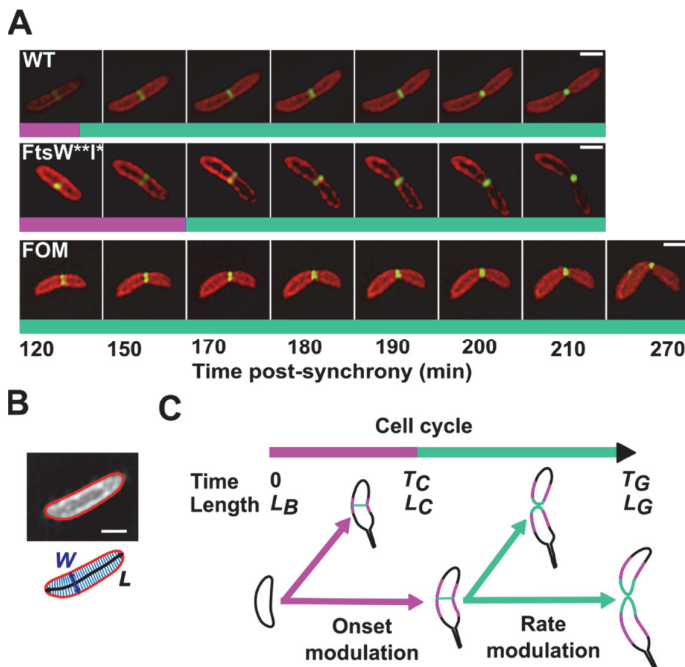


Figure 2-1: Experimental strategy and constriction-related models for modulation of cell size. **A)** Time-lapse SIM images: inner membrane (mCherry-MTS₂, red), FtsZ (FtsZ-GFP, green). Shown are example wild-type (WT), FtsW*** mutant, and fosfomycin-treated (FOM) cells through constriction, until separation. Images were bleach corrected for visualization (see Materials and Methods 5.1.4). **B)** Analysis of cell shape parameters using sDaDa (see Materials and Methods 5.1.6 and Figure A-1): the central line (black) is used to measure length (L); the width (W) is extracted from each perpendicular segment; the cell contour defines cell shape (red line). **C)** Constriction rate or onset control mechanisms for length. Cells are born at time 0 with length at birth L_B , and elongate exponentially. T_C and L_C are the time and length at constriction onset. T_G and L_G are the time and length at the end of the cell cycle. Magenta parts of the cell contour represent lateral elongation, and cyan parts represent septal elongation. Scale bars: 500 nm. Bicolor bars indicate the stage: pre-constriction (magenta) and constriction (cyan).

2.3 Results

2.3.1 Cell size control by constriction rate modulation

To test the role of constriction, we perturbed its rate pharmacologically and genetically, more specifically, we looked for perturbations to cell size that could act through changing constriction rate. Fosfomycin inhibits the peptidoglycan (PG) synthesis enzyme MurA (Kahan et al. 1974), thus slowing down PG synthesis and therefore possibly the constriction rate. Interestingly, fosfomycin treatment leads to an increase in cell size. For a perturbation leading to smaller cells,

we looked at the divisome. The divisome includes cell wall remodeling enzymes including the late-arriving FtsW and FtsI. Several point mutants of the glycosyltransferase FtsW (Meeske et al. 2016) and its cognate transpeptidase FtsI (Adam et al. 1997), referred to as FtsW^{**1*}, resulted in a gain-of-function phenotype in *C. crescentus*, able to overcome inhibition of constriction and leading to smaller cells (Modell et al. 2014). It was hypothesized that these mutations maintain the enzymes in their active state, and thereby increase the constriction rate (Modell et al. 2014).

We resolved cell shape dynamics during the cell cycle by performing dual-color imaging of the inner membrane and divisome proteins (FtsZ-GFP, FtsW-GFP) with time-lapse SIM (Figure 2-1A, Materials and Methods 5.1 and Table 5-1) on a synchronized population of cells. We used automated image analysis to quantify cell shape parameters during the cell cycle (Figure 2-1B, Figure A-1, Methods 5.1.6). The overall cell length relative to the wild-type strain was shorter for FtsW^{**1*} and longer for fosfomycin-treated cells (Figure 2-2A, Figure A-2A, B), consistent with previous studies (Harris and Theriot 2016; Modell et al. 2014).

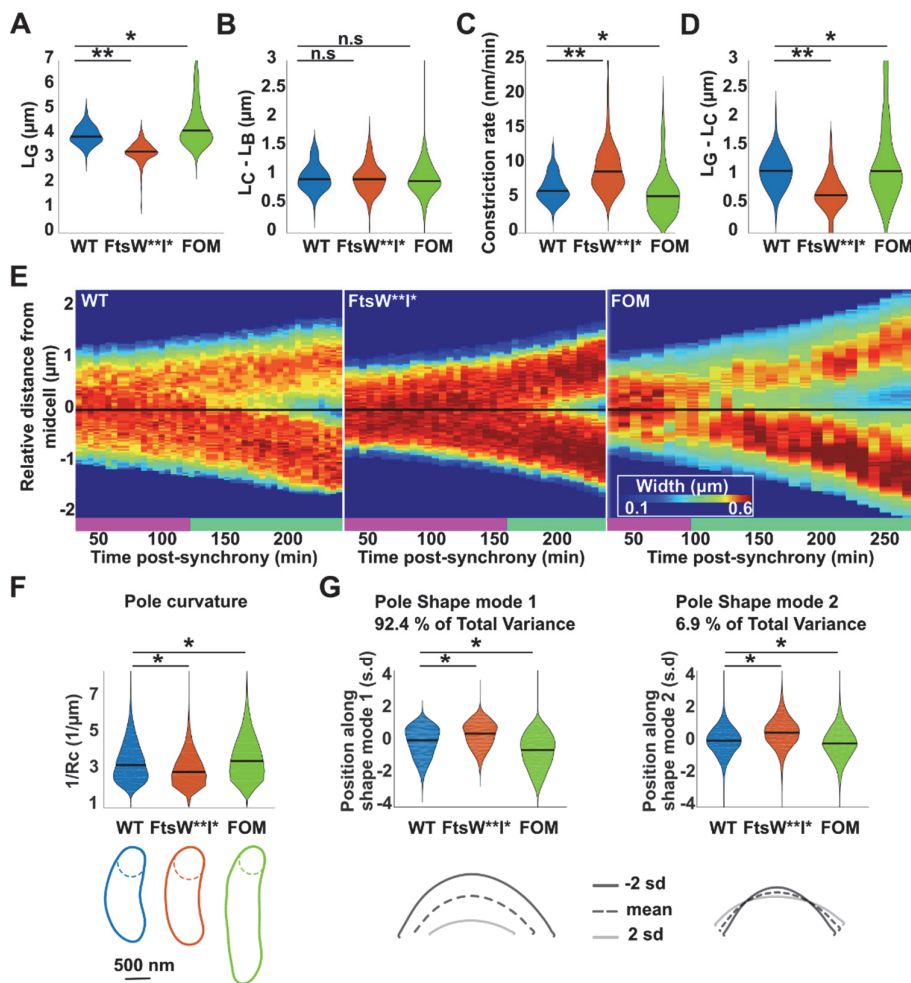


Figure 2-2: Differences in constriction rate yield different cell sizes and pole shapes.

Single-cell distributions of **A**) length at division; **B**) elongation before constriction; **C**) mean constriction rate; **D**) elongation during constriction. (**A-D**), black bars represent the median of the population. Number of cells N: WT: N=208, FtsW^{**1*}: N=212, FOM: N=220. Significance: **: $p < 0.005$, *: $p < 0.05$, n.s.: not significant. **E**) Kymographs of representative cells, displaying cell diameter along the cell's length (vertical axis), versus growth time post-synchrony (horizontal axis), red indicates large diameter, blue small diameter. The black horizontal line indicates the middle of the cell. Bicolor bars indicate the stage: pre-constriction (magenta) and constriction (cyan). **F**) Pole curvature analysis. The curvature is the reciprocal of the radius (Rc) of a circle tangent to the curve at a given point, here taken to be the pole. Each cell contour represents a representative single cell from each condition; the distribution of curvatures is plotted above (median value, black bar). **G**) The pole region was extracted from each contour (>6000 cells per condition) and analyzed using principal component analysis (Celltool, (Pincus and Theriot 2007)). Shape mode 1 mostly accounts for variation in the length of the pole; shape mode 2

mostly accounts for variation in the bluntness of the pole independent of length. The distributions of each shape mode is plotted, with examples of corresponding shapes.

Could elongation before the onset of constriction set the differences in final length between FtsW**I* mutant, fosfomycin-treated and WT cells (Figure 2-1C, onset modulation)? The appearance of a measurable constriction in SIM data corresponded well with the arrival of FtsW (Figure A-1C) and allowed us to separate elongation before and after constriction onset. Differences in elongation before constriction for all conditions (Figure 2-2B) were insufficient to account for the observed differences in final length (Figure 2-2A). Thus, we examined shape changes during constriction (Figure 2-1C). Individual cells continued to elongate exponentially with the same apparent rate, even as they changed from pure elongation to mid-cell remodeling and constriction (Figure 2-2C, E). However, the mean constriction rate was increased for the FtsW**I* mutant and decreased for fosfomycin-treated cells when compared to WT (Figure 2-2C). The rate of constriction determined the duration of the constriction phase, leading to differences in overall cell elongation during the constriction phase (Figure 2-2D). We also examined the impact of MreB on cell size control using the point mutant MreBQ26P (Aaron et al. 2007), which participates only in side-wall elongation and not septal elongation. We found that cells were longer on average than WT, with a higher elongation rate, indicating that this is a gain-of-function mutation. Interestingly, the average constriction rate increased, resulting in a nearly unchanged elongation during constriction (Figure A-2D). Instead, here the increased elongation before constriction was responsible for the difference in cell size. Thus, we have demonstrated that constriction rate modulation can be a mechanism for cell size control, independent from onset modulation (Taheri-Araghi et al. 2015; Weart et al. 2007) or elongation.

We found that individual cells continued to elongate at the same rate prior to and during constriction, although different perturbations modulated their constriction rate. Thus, faster constriction as in the case of FtsW**I* implies cells should have shorter, blunter poles, while slower constriction as in the case of fosfomycin treatment implies they should have longer, sharper poles. Indeed, kymographs show a more extended gradient in cell width at the poles of fosfomycin-treated cells (Figure 2-2E). In contrast, FtsW**I* cells show a steeper gradient at the poles. This was confirmed quantitatively by measuring the radius of curvature at the poles (Figure 2-2F). Furthermore, a population-wide analysis of pole shape demonstrated that over 95% of the total shape variance is accounted for with two principle shape modes, which primarily capture variation in the length and bluntness of the poles (Figure 2-2G). FtsW**I*, fosfomycin-treated, and WT cells were all distinct along each of these shape axes. We also observed differences in the width of the Z-ring, which appears laterally extended in the fosfomycin case (Figure A-2C). This may result from changes in length at constriction onset, since the region of low MipZ concentration will be more extended in longer cells (Thanbichler and Shapiro 2006).

2.3.2 Constriction rate compensates variability in elongation before onset

To better decipher the relative role of the constriction rate in cell size regulation we further analyzed its contribution to cell size homeostasis. Our experiments were designed to precisely measure the relative contributions to total elongation and not to distinguish between different general models of homeostasis, which would require measurement over thousands of generations. We found that cells elongated with a distinct mean value for each condition (Figure 2-3), and that the more individual cells elongated before, the less they elongated during constriction across all conditions tested, including in *E. coli* wild-type cells (Figure 2-3, Figure A-3). Indeed, the total elongation was independent of the relative time cells spent in elongation and constriction phases, with the exception of fosfomycin-treated cells (Figure 2-3), generally consistent with an “adder.” Consequently, the variance in the total elongation was lower than the variances in elongation before and during constriction would have independently suggested. This was true for all populations, including

under perturbed conditions (Figure A-3A). These results demonstrate compensation, or over-compensation in the case of fosfomycin (Figure 2-3, Figure A-3B), between elongation before and during constriction resulting in a higher fidelity homeostasis for total elongation (Figure A-3A-C).

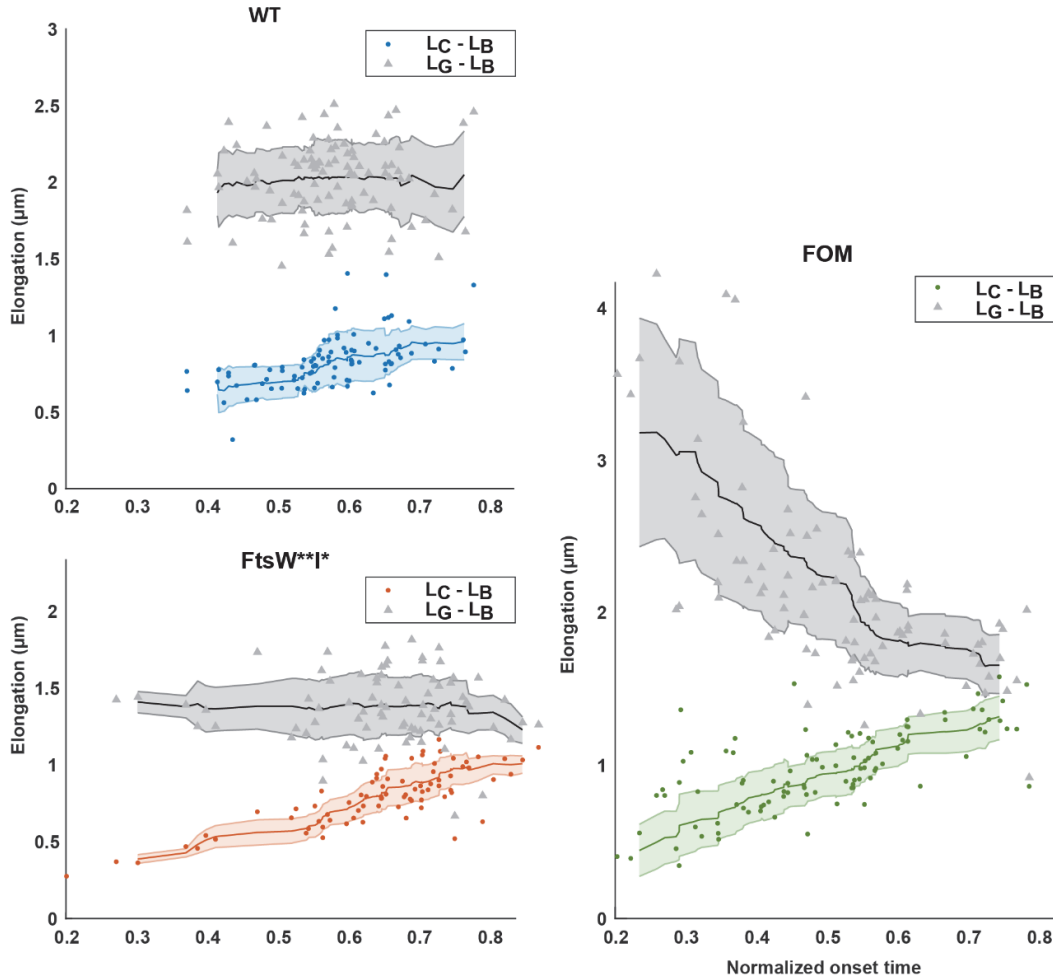


Figure 2-3: Compensation of elongation before and during constriction contributes to cell size homeostasis. Total elongation (gray) and elongation before constriction (color) for individual Wild Type (WT), *FtsW**I** and fosfomycin (FOM)-treated cells, as a function of normalized onset time (T_c/T_0). Lines represent the 20 cells moving average; the shaded zones represent the moving standard deviation. Extreme outliers, more than 2 standard deviations from the mean, were omitted for the calculation of the moving average.

What could be the mechanism for this compensation? Elongation rate and constriction rate together determine elongation during constriction. Compensation could occur if cells which elongate less before onset subsequently elongate more rapidly or constrict more slowly. However, elongation rate during constriction did not negatively correlate with elongation before constriction (Figure A-4A). To better understand constriction dynamics, we examined single cell waist widths as a function of relative duration of constriction (Figure 2-4A). Cells which elongated more before constriction also spent relatively less time constricting, indicating a higher overall constriction rate. The converse was true for cells which elongated less before constriction, but this observation alone does not rule out the possibility of a very late regulatory step being responsible for changes in average constriction rate. Single cells constricted with increasing rate until division; thus, we defined two rates, corresponding to early and late constriction (Figure A-4B), similar to (Banerjee et al. 2017). Interestingly, early constriction rate correlated positively with elongation before constriction, but late rate did not (Figure 2-4B, C). Hence, early constriction rate changes at the single cell level to adjust elongation during and compensate elongation before constriction.

While molecular mechanisms ensuring homeostasis have been proposed, the identity of the underlying regulatory factors remains controversial. A previous model estimated PG precursor excess as a function of the cell cycle (Harris and Theriot 2016). Each cell is assumed to be born with negligible excess, then generating an increasing excess of PG precursors during elongation. PG precursors are synthesized in the cell volume, at a volume-dependent rate, while being depleted as they become integrated into the cell wall (see section 5.1.8). Using this model and experimentally measured cell contours to estimate the changes in surface area (ΔA) and volume (ΔV), we calculated the excess precursor area (A_{excess}) at the onset of constriction (T_c) for individual cells at onset of constriction:

$$A_{excess}(T_c) = \left\langle \frac{\Delta A}{\Delta V} \right\rangle_{cell\ cycle} \Delta V(T_c) - \Delta A(T_c)$$

Equation 2-1: Estimation of area precursor excess at constriction onset.

Here, $\langle \rangle_{cell\ cycle}$ refers to the value averaged over the cell cycle. Since it took on average 30 minutes to set up each experiment, we underestimated the volume and area at birth, leading to an offset toward negative estimated precursor excess (Figure 2-4D). However, we expect the trends to be insensitive to this shift.

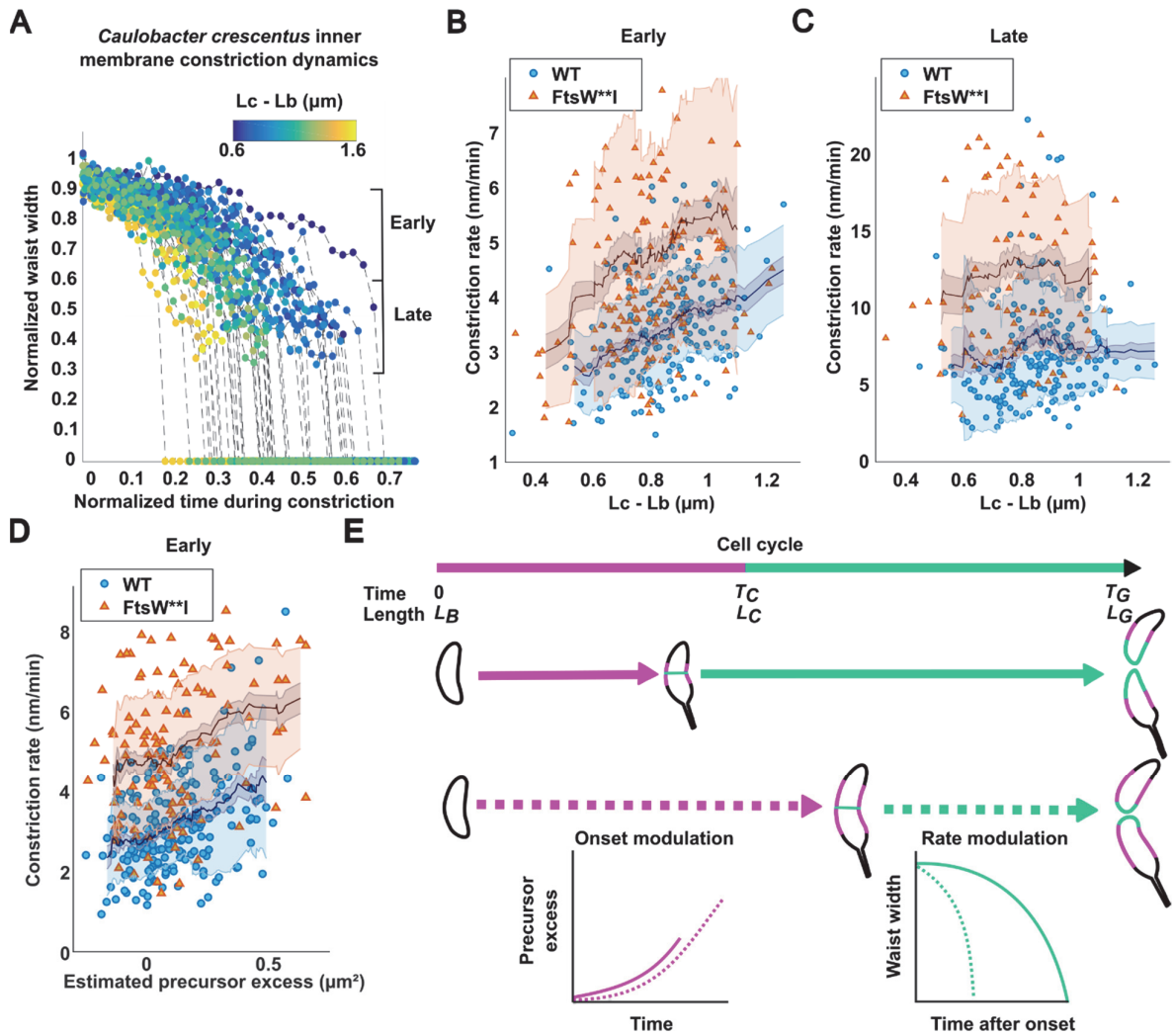


Figure 2-4: Early constriction rates compensate for elongation before onset.

A) Normalized waist width as a function of normalized time during constriction, color map represents the elongation before constriction. The measurable constriction was divided into early (0.9-0.6) and late (0.6-0.3) stages. **B)** Testing correlation between early constriction rate and elongation before constriction in both WT and FtsW**I strains, WT: $r=0.45$, $p-$

value <0.01 FtsW**I*: $r=0.24$, $p\text{-value}<0.01$ (Pearson correlation coefficient). **C)** Testing correlation between late constriction rate and elongation before constriction, WT: $r=0.05$, $p\text{-value}>0.48$, FtsW**I*: $r=0.02$, $p\text{-value}>0.8$ (Pearson correlation coefficient). **D)** Testing correlation between estimated PG precursor excess and early constriction rate, WT: $r=0.33$, $p\text{-value}<0.01$, FtsW**I*: $r=0.29$, $p\text{-value}<0.01$ (Pearson correlation coefficient). $N \geq 200$ for each strain. Lines in **(B-D)** represent the 20 cells moving average; the shaded zones represent the moving standard deviation. Extreme outliers, more than 2 standard deviations from the mean, were omitted for the calculation of the moving average. **E)** Schematic of size regulation in *C. crescentus* with mixed modulation of constriction onset and rate. Magenta parts of the cell contour represent lateral elongation, and cyan parts represent septal elongation. Later onset leads to higher PG precursor excess, which drives more rapid initial constriction (dashed trajectories), and vice-versa.

2.4 Discussion

To explain our finding that constriction rate modulation is dependent on elongation prior to constriction, we speculate on a parsimonious model in which PG precursor excess also sets the rate of PG remodeling at the constriction site, and therefore the rate of constriction: the higher the excess the shorter the constriction duration. Indeed, we observed a positive correlation between the early rate of constriction and estimated excess PG precursor for WT and FtsW**I* cells (Figure 2-4D, Figure A-4). This is also consistent with measurements of compensation in the MreBQ26P mutant, in which cells elongate slightly faster. According to this model, an increased elongation rate with a constant PG precursor production rate implies that cells will be longer when they achieve a critical concentration to initiate constriction, without a disruption to compensation. This is consistent with our findings (Figure A-3E), indicating that MreB does not play a major role in setting constriction rates. Furthermore, as the new cell poles are built, the excess PG precursor should diminish, leading to a decreased creation of area per time. This is indeed what we observe (Equation 2-1 and 5.1.9.2), consistent with models of constriction rate in *E. coli* (Coltharp et al. 2016). Fosfomycin inhibits PG synthesis, so we can no longer use the same mathematical expression to estimate precursor excess, since the activity of fosfomycin would introduce an extra depletion term. Interestingly, within our model this should lead to a slower constriction, consistent with our observations (Figure 2-2C). Moreover, fosfomycin treatment could decouple PG precursor levels from the growth in the elongation phase and this way disrupt the compensation mechanism and cell size homeostasis, as suggested by the results in Figure 2-3.

Recent work showed that *C. crescentus* follows the adder model at 37°C, but not at lower temperatures (Banerjee et al. 2017). In our data, we did not see any meaningful deviation from the adder model. As stated above, we only examined only one condition (28°C, M2G poor media), and could only measure shape dynamics over a single cell cycle, which could have prevented us to see deviations from the adder model. On the other hand, we could measure constriction dynamics with a higher precision, including the onset of constriction. Moreover, we independently confirmed constriction onset measurements using FtsW as a late divisome marker. For our data, a threshold invagination was much more robust, as well as consistent with FtsW-arrival, compared to the piecewise exponential fit in the mentioned study.

Although we have posed the regulatory factor to be PG precursors, this remains controversial because there is only indirect evidence for their role. Any “X-factor” regulatory molecule for constriction rate following the functional relationship described for surface area and volume would fit within the model we suggest. Within the context of size homeostasis, this proposed mechanism neither precludes nor requires any given overall model, but does suggest a means to achieve higher fidelity in adder-type models. The fact that this compensation occurs as a late step in the cell cycle is consistent with observations by Campos *et al.*, suggesting that the adder would act on a regulatory step late in the cell cycle, after assembly of the Z-ring (Campos et al. 2014).

The proposed model relies on the kinetic properties of the cell wall remodeling enzymes and could be conserved in other species than *C. crescentus*. We also observed a positive correlation between the overall rate of constriction and elongation before constriction in *E. coli* (Figure A-3F), although here we were not able to independently measure early and late constriction rates. Constriction rate

could possibly impact cell size regulation in any species that elongates significantly during constriction. On the other hand, cells that do not elongate during the constriction phase should be insensitive to constriction rate compensation.

Under nutrient-enriched growth conditions, *Salmonella typhimurium*, *E. coli* and *B. subtilis* can coordinate their cell size with nutrient availability, perhaps to allow sufficient room for multi-fork replication (Donachie and Begg 1989; Sargent 1975; Schaechter, Maaløe, and Kjeldgaard 1958) and a concomitant increase in cell size to maintain a constant volume per origin (Amir 2017; Zheng et al. 2016). Remarkably, *C. crescentus* shows no such nutrient adaptation (Beaufay et al. 2015; Campos et al. 2014), and how its size is modulated in the face of mutations or pharmacological perturbations has remained a mystery. Our findings clearly show that growth during the constriction stage of the cell cycle contributes to cell size control. Modulation of constriction dynamics changes the overall length of cells, in a manner which has implications for cell shape. By modulating constriction onset and rate together (Figure 2-4E), cells may arrive at a variety of pole shapes, an emerging control mechanism for bacterial cell shape (Lariviere et al. 2018).

Intriguingly, the cell wall itself can have differential properties at the division site. In *B. subtilis*, the division septum contains an enrichment of pentapeptides compared to the rest of the cell envelope (Morales Angeles et al. 2017), perhaps due to a change in the crosslinking or PG composition. In *E. coli*, glycan strands lacking stem peptides are enriched at the septum, allowing proteins containing the PG binding (SPOR) domain to be recruited (Yahashiri, Jorgenson, and Weiss 2015). In *C. crescentus*, the hydrolase DipM is recruited to the division site by its PG binding LysM domains, suggesting a distinct PG chemistry (Goley et al. 2010; Möll et al. 2010; Poggio et al. 2010). Consistently, we observed a differential, reduced staining by wheat germ agglutinin (WGA) at midcell for later stages of the cell (Figure A-4I) (Douglass et al. 2016). We expect that in future studies it will be important to use fluorescent cell-cycle markers in conjunction with fluorescent D-amino acids (Kuru et al. 2012), which together can identify cell-cycle timing and modes of growth. It would be interesting to investigate whether the rate of constriction also affects cell wall chemistry at the division site.

Different factors have been demonstrated to be important for determining constriction dynamics. Before cells can build a septal wall, chromosomes must be partitioned; accordingly, machinery which coordinates the two such as MatP in *E. coli* can also modulate constriction rate (Coltharp et al. 2016). Similarly, dynamically treadmilling FtsZ filaments act as a scaffold to direct cell wall remodelers to the division site, and can even modulate the rate of cell wall remodeling in *B. subtilis* (Bisson-Filho et al. 2017; Yang et al. 2017; Lariviere et al. 2018). Nevertheless, the activity of PG remodeling enzymes involved in constriction might depend on PG precursor concentrations, and thus may act as a part of a responsive machine. Since, for individual cells, elongation proceeds exponentially with a single rate constant even as PG precursor excess is predicted to increase over the cell cycle, the elongation machinery is presumably relatively insensitive to changes in PG precursor amounts. By coupling the elongation machinery to the PG precursor-sensitive constriction machinery, the cell may have arrived at a simple means of compensating for variation in the growth during the elongation phase. This compensation still has its limitations as we observed in the case of FtsW**1* (Figure A-3B); in the case of large elongation before onset, cells must still elongate by a minimum amount during constriction. In the future, it will be interesting to identify the molecular partners responsible for constriction rate modulation and PG sensing, and to experimentally investigate the mechanism behind compensation of elongation.

Chapter 3 The role of polyphosphate in the starvation response of *Pseudomonas aeruginosa*

3.1 Abstract

Bacteria are often faced with nutrient starvation. As they transition from exponential growth to stationary phase, many bacteria accumulate granules of the inorganic polymer polyphosphate (polyP). PolyP is created by polyphosphate kinases (Ppk's), its accumulation has many effects and is required for successful cell cycle exit. Interestingly, polyP granules are evenly spaced throughout the nucleoid. The origin of this pattern is unknown. To find out why polyP is required for cell cycle exit, we probe during which stage cells without polyP are arrested. Moreover, we investigated the localization and mobility of Ppk foci. We found that a majority of Δppk cells are arrested with open replication forks, much more often than reported previously. We saw that the Ppk's form foci with a distinct localization pattern, already before starvation and the presence of polyP granules. Moreover, their mobility is not altered by starvation, but is quite slow, suggesting that the foci are tethered to a larger structure, possibly polyP or the nucleoid.

3.2 Introduction

3.2.1 The bacterial starvation response

Many studies of bacteria look at their behavior during exponential growth. The conditions bacteria face in the environment however often are very different from laboratory conditions allowing for exponential growth. Periods of nutrient abundance are rare and transient (De Nobili et al. 2001). In order to survive, bacteria have to sense and adapt to their environment. When starved for nutrients, bacteria downregulate the energy draining processes that drive the cell cycle, such as DNA replication, transcription and translation. Since not much energy will be available for DNA repair, it is essential that bacteria finish replicating their DNA and store it in a protected state (Chiancone and Ceci 2010; Martinez and Kolter 1997). This starvation response leads to cell cycle exit, and many of its aspects are controlled by the small signaling molecule Guanosine tetra/(penta)-phosphate, (p)ppGpp (Chatterji and Kumar Ojha 2001; Traxler et al. 2008; Bergkessel, Basta, and Newman 2016). (p)ppGpp production promotes production of another molecule, polyphosphate (polyP), an inorganic polymer often found in granules that plays a role during starvation (Kuroda et al. 1997).

3.2.2 Roles for polyP during the starvation response

PolyP granules have been observed in bacteria a long time ago. While some bacteria have polyP granules in all examined conditions, other bacteria accumulate polyP into granules under conditions

of nutrient limitation or other stresses. Examples are *Klebsiella aerogenes*¹ (Smith, Wilkinson, and Duguid 1954), *Escherichia coli* and *Pseudomonas aeruginosa* (Ault-Riché et al. 1998; Amado and Kuzminov 2009). Since polyP can serve as a source of energy, phosphate and chelated metal ions, it has been suggested that polyP can function as a buffer or storage for all of these. If this is the case, it is probably not used during early starvation, when the granules are produced, but rather deep into starvation or during cell cycle re-entry when nutrient levels rise again, at which point the granules are consumed again (Tocheva et al. 2013; Racki et al. 2017).

The reversible synthesis of polyP from ATP or GTP is catalyzed by poly-phosphate kinases, of which two types exist and are widely conserved in bacteria, archaea and some eukaryotes (A. Kornberg, Kornberg, and Simms 1956; S. R. Kornberg 1957; Ahn and Kornberg 1990; Ishige, Zhang, and Kornberg 2002; Zhang, Ishige, and Kornberg 2002). *P. aeruginosa* has four *ppk* genes: *ppk1*, *ppk2a*, *ppk2b* and *ppk2c*, deletion of these *ppk* genes, Δ polyP, leads to loss of polyP production and its accumulation in granules, which can be rescued by reintroduction of either *ppk1* or *ppk2a* (Racki et al. 2017). Δ polyP mutants grow exponentially at a normal rate in the presence of nutrients. However, they have a decreased survivability during stationary phase (Crooke et al. 1994; Rao and Kornberg 1996).

In wild type (WT) *P. aeruginosa* cells, starvation induced cell cycle exit entails inhibition of new DNA replication, termination of ongoing DNA replication, chromosome segregation and cell division. This results in small daughter cells with a single copy of the chromosome. Δ polyP cells fail to exit their cell cycle upon starvation; they do not divide and often have two origins of replication, indicating their chromosome has been copied at least partially. Labeling of replication forks with single stranded binding protein fused to the fluorescent protein mCherry (SSB-mCherry), yields fluorescent foci in one out of five cells, indicating that a fraction of the cells failed to finish replication (Racki et al. 2017). These results indicate that polyP already has a function when its levels are still rising, possibly independent from its putative storage function.

Multiple reports indicate that polyP has different roles than storing and providing energy or phosphate. In *Caulobacter crescentus*, it was shown that polyP decelerates the cell cycle, by inhibiting DNA replication initiation and swarmer-to-stalked differentiation (Boutte, Henry, and Crosson 2012). Moreover, in *E. coli*, during a shift from rich to poor medium, polyP activates degradation of free ribosomal proteins by Lon protease. The absence of either polyP or Lon causes an extended lag phase. PolyP can bind both the Lon protease and free ribosomal proteins, promoting complex formation and degradation of the ribosomal proteins. This is believed to downregulate translation as well as to provide free amino acids for the translation of proteins required for the adaptation to the medium shift. polyP production requires a rise in ppGpp concentration. In a WT strain, the concentrations of both ppGpp and polyP decreases again at the end of the lag phase. In the absence of polyP however, ppGpp concentration stays high for much longer (Kuroda et al. 1999, 2001).

3.2.3 Localization of polyP granules

PolyP granules can be found in specific subcellular localizations depending on the organism, some more specific than others. PolyP granules are found near the cell poles in *Campylobacter jejuni*, in between nucleoid and ribosome exclusion zone, possibly caused by exclusion from these two regions (Müller et al. 2014). In *Acetonebma longum*, around 8 up to 12 polyP granules are formed during sporulation, at the leading edge of the membrane engulfing the endospore (Tocheva et al. 2013). Newborn *C. crescentus* cells have a single polyP granule near the middle of the cell, associated with a Ppk1 cluster. DNA replication and segregation are required for the relocation of the Ppk1 cluster, which produces a second polyP granule. By this time the two granules are localized around the two quarter positions, ensuring that both daughter cells receive a single granule

¹ Previously known as *Enterobacter aerogenes* or *Aerobacter aerogenes* (Tindall, Sutton, and Garrity 2017).

during cell division (Henry, Crosson, and Chang 2013). In *P. aeruginosa*, multiple granules can be found in the nucleoid region and appeared to be spaced (Racki et al. 2017). Although some localization patterns can arise spontaneously due to the physical properties of the granules and their surroundings, some probably require active processes, such as localized polyP production by Ppk's in the case of *C. crescentus*.

Molecular crowding can lead to aggregation of large particles through an entropic force termed the "depletion force" (Asakura and Oosawa 1958), an example is the aggregation of large protein-DNA complexes such as those involved in replication and transcription (Marenduzzo, Micheletti, and Cook 2006). The depletion force could possibly drive aggregation of large structures such as polyP granules to the nucleoid. Active positioning mechanisms exist for other bacterial organelles. Magnetosomes, for instance, are membrane invaginations containing magnetic iron crystals used by bacteria for navigation. They are aligned on an actin-like filament and positioned at midcell during division, to ensure equal partitioning between daughter cells (Komeili et al. 2006; Uebe and Schüler 2016). Carboxysomes on the other hand, are large protein shells containing enzymes for the Calvin cycle. Their position is controlled by a pair of parAB-like proteins which use the nucleoid as a scaffold to regularly space the carboxysomes (Yeates et al. 2008; MacCready et al. 2018).

3.2.4 Strategy

Here, we examined the role of polyP and the Ppk's during cell cycle exit in *P. aeruginosa*. We reassessed the fraction of Δ polyP cells that are stalled with an open replication fork and found significantly higher numbers than previously observed. We examined the localization of Ppk1 and Ppk2a, and found that they form foci with distinct patterns and localize already before starvation and production of polyP granules. We measured the dynamics of Ppk2a foci and found that their mobility is not altered upon starvation and the associated polyP granule production. On the other hand, their motion is orders of magnitude smaller than expected for a protein complex, suggesting that they could be associated to a larger particle.

3.3 Results

3.3.1 Majority of starved Δ polyP cells stall with open replication forks

Δ polyP cells fail to exit their cell cycle during starvation, however it is not known whether they are arrested during DNA replication, chromosome segregation or septation (Racki et al. 2017). A fraction of these cells formed foci of SSB-mCherry, labeling open replication forks. However, most of these foci were quite dim and it is not known whether SSB always remains associated to all open replication forks during starvation. In other words, there could be undetected open replication forks. For this reason, we decided to use a core component of the divisome to examine the presence of open replication forks. More specifically DnaX, coding for the τ and λ subunits of the DNA polymerase III complex, serving as the β -clamp loader. Additionally, we used a brighter fluorescent protein, mApple (Shaner et al. 2008). We reintroduced the cells to a nutrient-rich medium to allow for reassembly of the replisomes and thus DnaX-mApple. We used strains expressing GFP-ParB^{pMT1} able to bind a parS^{pMT1} site introduced on the chromosome near the Origin of replication (GFP-ParB^{pMT1} targeted to this locus will be referred to as Ori-GFP) (Racki et al. 2017) and an mApple-tagged DnaX, expressed from its native genomic locus. As previously reported, WT cells are small and have a single copy of their chromosome, resulting in a single Ori-GFP focus and no DnaX foci (Figure 3-1)(Racki et al. 2017). Δ polyP cells on the other hand, have similar lengths as during exponential growth, and often contain two Ori-GFP foci (>90% of cells), as well as at least one DnaX-mApple focus (>50% of cells) (Figure 3-1). This indicates that a majority of the Δ polyP cells have open replication forks when failing cell cycle exit, significantly more than what could be observed previously (Racki et al. 2017).

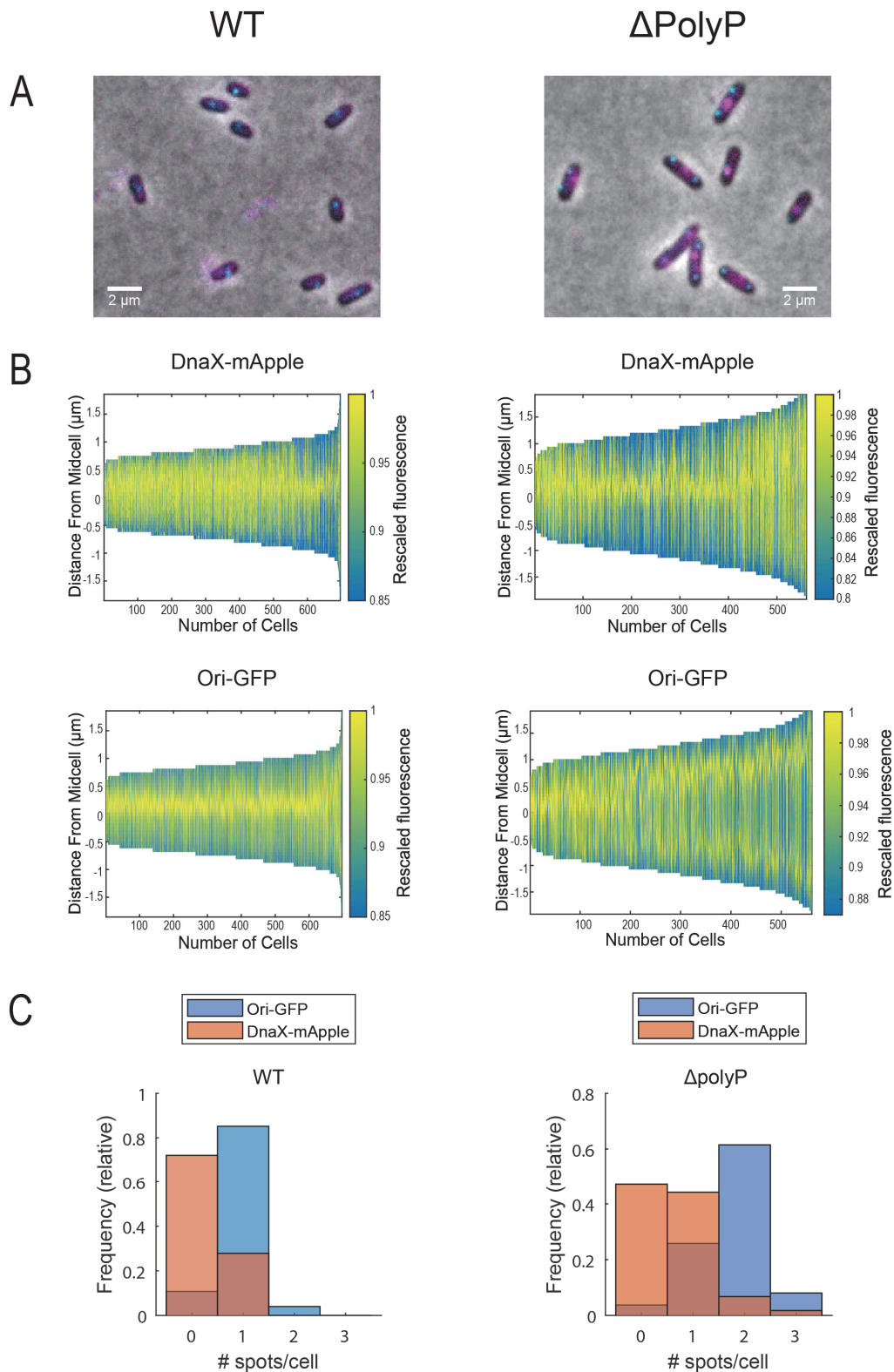


Figure 3-1: A majority of Δ polyP cells did not finish DNA replication during cell cycle exit, as WT cells did.
A) Example multicolour images of WT and Δ polyP cells reintroduced to nutrient-rich media after overnight starvation. The images are an overlay of phase contrast (grayscale), Ori-GFP fluorescence (cyan) and DnaX-mApple fluorescence (magenta). **B)** Demographs showing the distribution of fluorescence along cell length (y-axis) for cells ordered by length (x-axis). The fluorescent signal was rescaled to the maximal fluorescence per cell to correct for cell-to-cell variation. **C)** Histograms showing the distribution of number of fluorescent spots per cell in both fluorescence channels, DnaX-mApple in orange, and Ori-GFP in blue.

3.3.2 Localization of Ppk1 and Ppk2a

The Ppk's are important for both production and use of polyP and could play a role in localizing polyP granules. We examined the subcellular localization of Ppk2a and Ppk1 during nutrient starvation using fusions to a green fluorescent protein mNeonGreen (mNeon) (Shaner et al. 2013). The fluorescent protein fusion genes replaced the respective native *ppk* gene, with the native promoter and are supposedly expressed at levels close to the WT proteins. Moreover, they were able to rescue polyP granule production and the cell cycle exit upon starvation response in a Δ polyP strain, indicating that the fluorescent protein fusion did not interrupt gene function. Interestingly, Ppk1 and Ppk2a localized as foci with a different localization pattern after 3 hours in nitrogen-limited media. While *ppk1* foci could be found throughout the cell, except for the poles (Figure 3-2), Ppk2a showed a tendency to localize close to the quarter positions (Figure 3-3). To our surprise, both Ppk1 and Ppk2a also formed foci in nutrient rich conditions, when no polyP granules are present. Ppk2a had a similar localization pattern as during starvation (Figure 3-3), but Ppk1 localized preferentially around midcell, especially when only a single fluorescent focus was present (Figure 3-2).

3.3.3 Cellular background subtraction improves localization accuracy

We noticed that the images of Ppk1 and Ppk2a had relatively high cellular background fluorescence, affecting the fine measurement of foci localization. Background fluorescence is often present when imaging bacterial cells and is caused by a fraction of the labeled protein diffusing through the cytoplasm as well as autofluorescent metabolites. This cellular background fluorescence is usually uniform throughout the cytoplasm, taking the shape of the bacterium. While it usually poses little problem in qualitatively assessing the localization of a protein, cellular background fluorescence affects the measurement of their brightness and position. For this reason, it is key to estimate and subtract cellular background fluorescence (Moolman, Kerssemakers, and Dekker 2015). To do so, we developed a MATLAB function, which uses the cell outlines and the raw fluorescence image to create an estimation of the background in the image and subtract it from the raw image (Figure 3-4 A). For details, see Materials and Methods, 5.2.5).

To validate this method, we used images of cell expressing cytosolic YFP, on which we simulated fluorescent foci with known positions. We compared the precision and detection efficiency of fitting spots in three types of images: images with background after background subtraction as the test scenario, images with background without background subtraction as the worst-case scenario and finally images with spots in the absence of background as the best-case scenario (Figure 3-4 B). The dimensions and intensities were chosen at levels comparable to the Ppk2a-mNeon data. We found that background subtraction improved detection efficiency, Jaccard index of 69% as opposed to 25%, as well as localization precision, 22 nm compared to 79 nm. It even came relatively close to the best-case scenario, with a Jaccard index of 84% and a localization precision of 14 nm (Table 3-1). This remaining difference is due to the absence of noise in the "spots only" images.

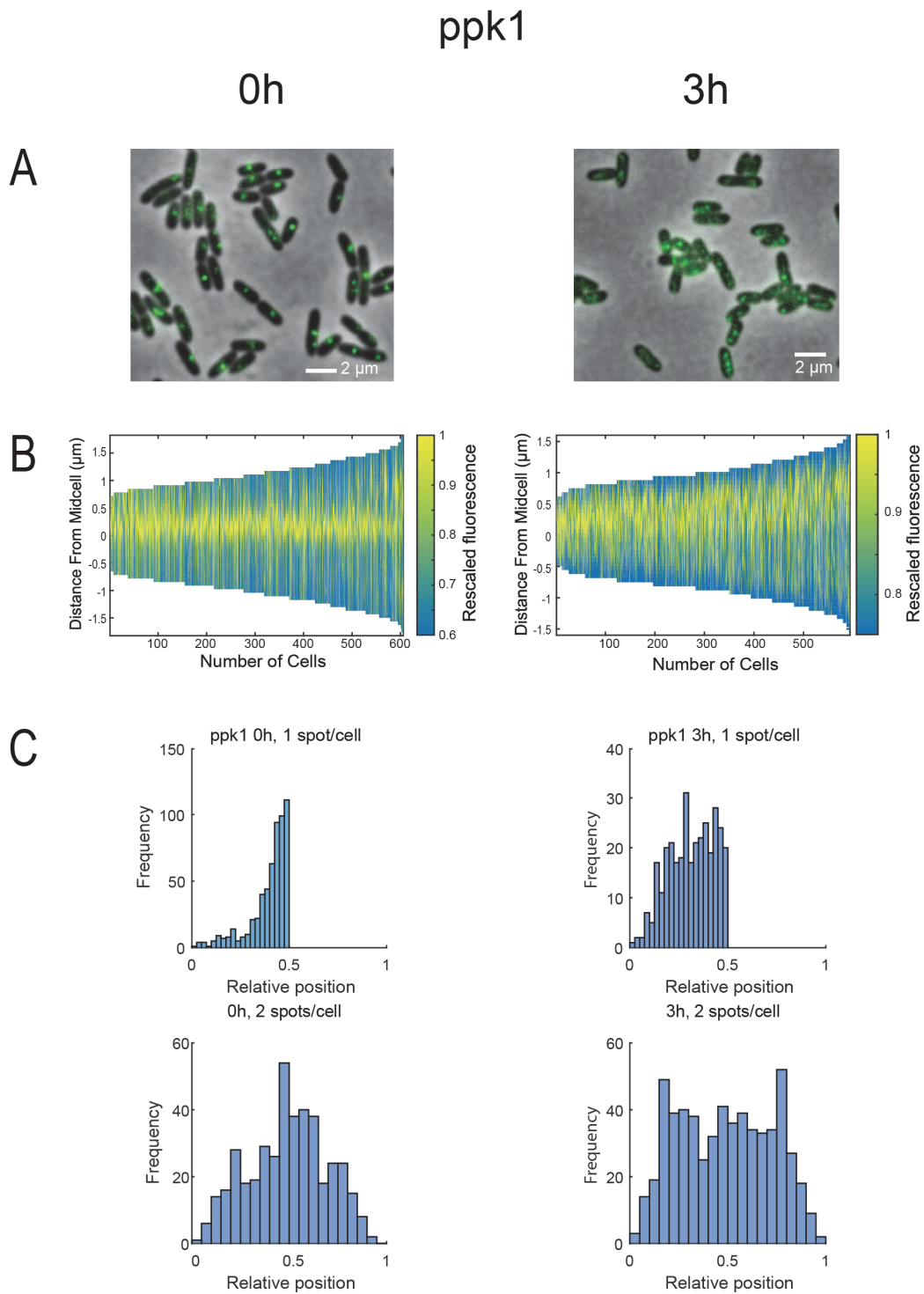


Figure 3-2: Ppk1-mNeon localizes at midcell prior starvation and localizes uniformly throughout the central part of the cell.

A) Example multicolor images of WT in nutrient-rich medium (0h) or after three hours in nitrogen-limited medium (3h). The images are an overlay of phase contrast (grayscale) and Ppk1-mNeon fluorescence (green). **B)** Demographs showing the distribution of fluorescence along cell length (y-axis) for cells ordered by length (x-axis). The fluorescent signal was rescaled to the maximal fluorescence per cell to correct for cell-to-cell variation. **C)** Histograms showing the distribution of the relative localization of Ppk1-mNeon foci along the long axis of the cell, both before (0h) and after 3h of starvation. The data was split up into one or two foci per cell. Data from cells with more than two foci is not shown. Note that for cells with one focus, the pole closest to the focus is defined as zero.

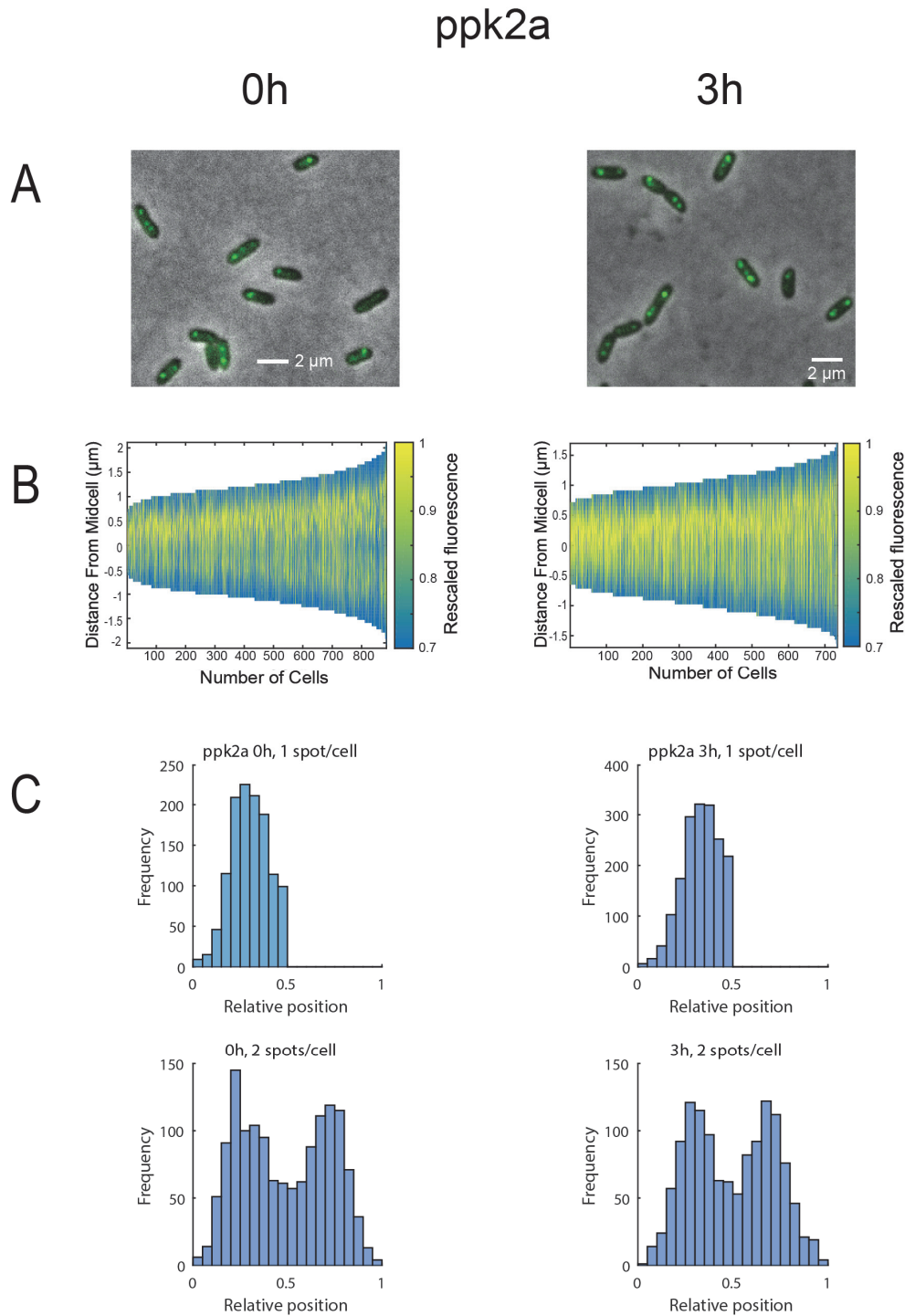


Figure 3-3: Ppk2a-mNeon tends to localize at the quarter positions, both before (0h) and after (3h) three hours of starvation.

A) Example multicolor images of WT in nutrient-rich media (0h) or after three hours of in nitrogen-limited medium (3h). The images are an overlay of phase contrast (grayscale) and Ppk2a-mNeon fluorescence (green). **B)** Demographs showing the distribution of fluorescence along cell length (y-axis) for cells ordered by length (x-axis). The fluorescent signal was rescaled to the maximal fluorescence per cell to correct for cell-to-cell variation. **C)** Histograms showing the distribution of the relative localization of Ppk1-mNeon foci along the long axis of the cell, both before (0h) and after 3h of starvation. The data was split up into one or two foci per cell. Data from cells with more than two foci is not shown. Note that for cells with one focus, the pole closest to the focus is defined as zero.

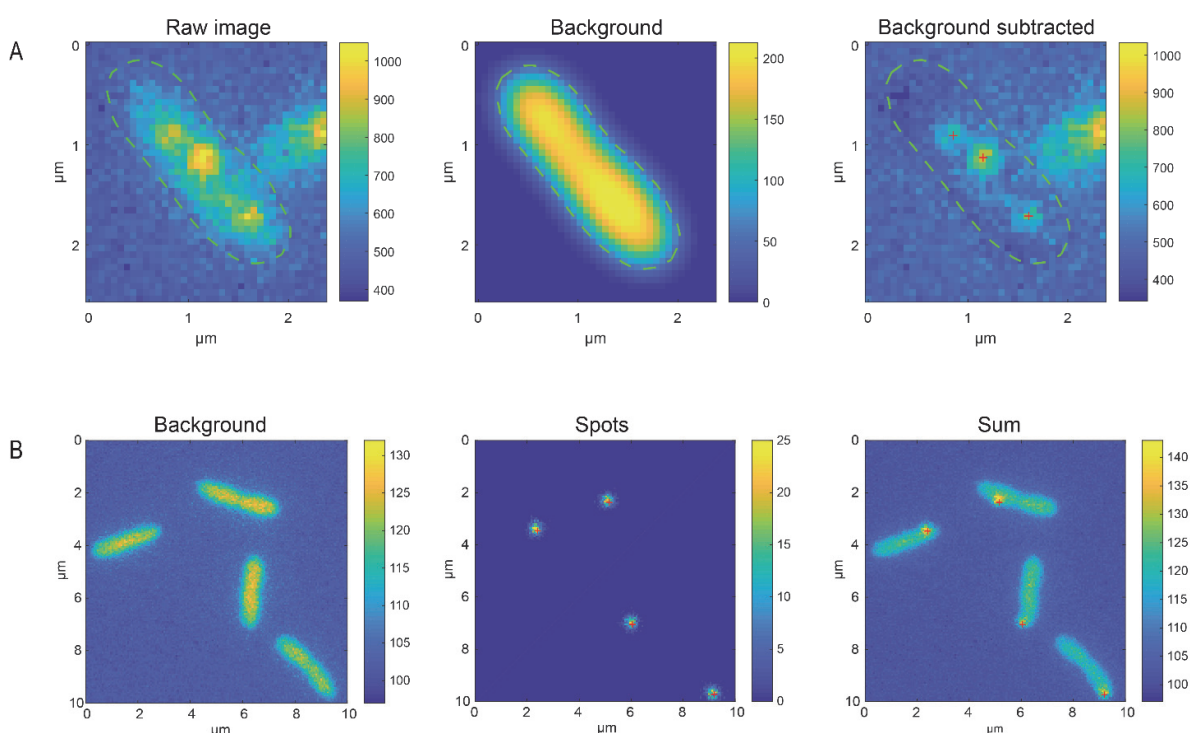


Figure 3-4: Principle and validation of background subtraction method.

A) Principle of background subtraction: The cell contour (green dashed line), measured from the phase contrast image, and the raw fluorescent image (left) are used to create a background image (middle), which is subtracted from the raw image, creating a background subtracted image (right), which is used later for spot detection and fitting (red crosses). **B)** Validation of background subtraction. Images of cells expressing cytosolic YFP are used as background images (left). Images of fluorescent spots with known positions are simulated (middle). The sum of the background and spot images is analyzed (right).

Input data	Background subtraction	RMSE (nm)	True positives	False positives	False negatives	Jaccard index
Background and spots	No	79	140	352	70	25%
Background and spots	Yes	22	191	78	19	66%
Spots only	No	14	176	0	34	84%

Table 3-1: Results of validation of cellular background subtraction.

Root Mean Squared Error (RMSE) is calculated as the root of the mean distance between simulated and measured position. Measured spots are counted as true positives when they are 250 nm to the spot, which is on the order of the spot size. The Jaccard index is the ratio of true positives to the sum of true positives, false positives and false negatives.

3.3.4 Dynamics of Ppk2a foci

We wondered whether dynamics of the Ppk foci could give us a hint about their nature. We performed video-microscopy of them at different timescales (one, five and twenty seconds). For Ppk1 however, the signal was not strong enough and bleached too fast to extract any meaningful data. For Ppk2a, we managed to collect tracks of sufficient length (Figure 3-5 A). As for its localization, we found no difference between the motion of Ppk2a-mNeon foci during exponential phase and after three hours of starvation. We found that Ppk2a-mNeon foci move subdiffusively, with an anomalous exponent around 0.4 (Figure 3-5 B, C). The apparent diffusion coefficient at the 10-second timescale was on the order of $2 \times 10^{-3} \mu\text{m}^2/\text{s}$, but due to experimental imprecision this is only an order of magnitude estimation. This motion is much slower than expected for freely diffusing proteins and protein complexes, which typically have diffusion coefficients on the order of $1 \mu\text{m}^2/\text{s}$ (Philips and Milo 2015). The anomalous diffusion coefficient could indicate that the Ppk2a-mNeon

foci are either part of a big particle that experiences the crowded cytoplasm as a viscoelastic medium or that they are attached to a large polymer, possibly the chromosome or a long polyP molecule (S. C. Weber, Spakowitz, and Theriot 2010).

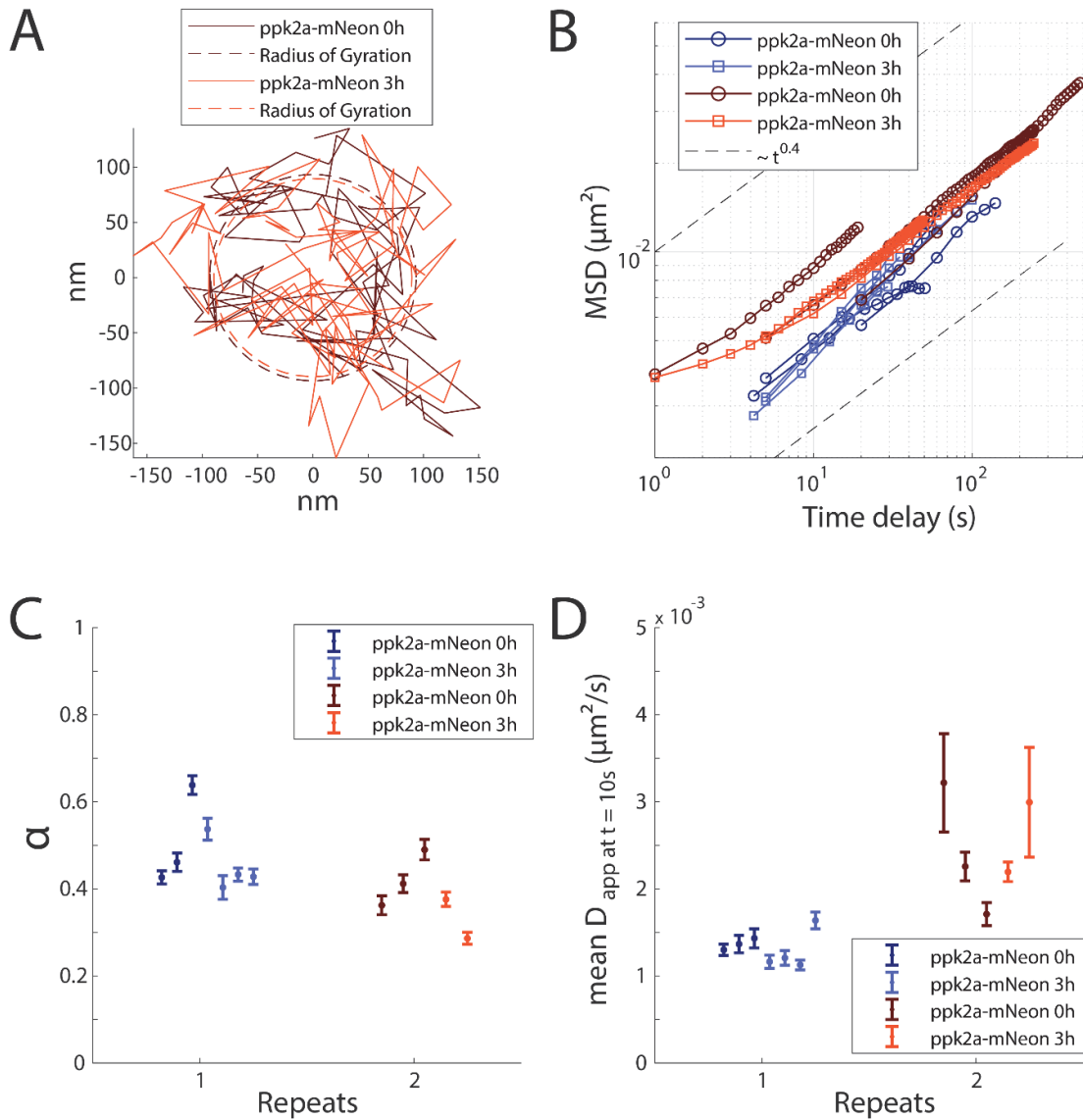


Figure 3-5: Ppk2a-mNeon foci move subdiffusively and their motion is not significantly altered by starvation. **A)** Representative example tracks for Ppk2a-mNeon, from cells in exponential growth (0h) and cells that were starved for three hours (3h). As an indicator of the mobility, the radius of gyration of the track is shown. Both tracks consist of approximately 100 localizations. **B)** MSD plots of Ppk2-mNeon foci from two independent experiments (blue and red). **C)** Average fitted anomalous exponent, α for different experiments. **D)** Average fitted apparent diffusion coefficient at $t = 10\text{s}$ for different experiments. For **C** and **D**, MSD plots of individual tracks were fitted to $\log(\text{MSD}) = \alpha \cdot \log(T) + \log(4D)$, where α and D are free parameters, and T is the time delay. Each plotted point corresponds to the average fit value for one tracking movie, corresponding to between 100 and 1000 tracks. Error bars represent standard error of the mean.

3.4 Discussion

Δ polyP cells fail to exit their cell cycle upon nutrient starvation (Racki et al. 2017), we found that a majority of these cells had DnaX-mApple foci indicative of open replication forks. This observation disproves that the Δ polyP cells are specifically stuck at another stage, such as segregation or septation. Still $\sim 40\%$ of the cells had no visible DnaX-mApple foci. Perhaps the detection efficiency is still too low to detect all open forks. In that case it would be better to use an alternative technique

to probe the fraction of cells with open forks, for example by counting the relative ratio of Origin versus terminus sequences by qPCR or sequencing. Nevertheless, it is possible that the Δ polyP cells are stalled due to a failure to activate downstream effectors of the starvation response and cell cycle exit, and continue their cell cycle until they run out of nitrogen. In this case, the cells would stall at a random point in the cell cycle, and the fraction of cells that is stalled with open forks represents the fraction of the cell cycle that cells spend in DNA replication. For this reason, it would be interesting to measure in the same way the number of cells with open forks during exponential growth in the MOPS medium. In minimal medium with citrate, 80% of *P. aeruginosa* cells have 2 Ori foci and 1 ter focus, indicating they are replicating their DNA (Vallet-Gely and Boccard 2013). Moreover, it would be interesting to see which parts of the starvation response are intact and which ones are not, such as the RpoS sigma factor. This would shed light on what is causing the failure to exit the cell cycle.

Cellular background introduces a bias in spot localization, we developed a background subtraction algorithm to counteract this bias. This tool could prove useful to improve measurements with relatively strong cellular background fluorescence in any rod-like or spherical bacterium. While subtracting the background will reduce all the pixel values to the same average, removing the bias in foci localization, the standard deviation of the pixel values, or noise, will not be changed, and still decrease the localization precision. The quality of the background subtraction heavily depends on how well the model and its assumptions represents the sample. For example, how well the shape of the bacterium is measured.

We found that Ppk1 and Ppk2a form foci before starvation, when there are no polyP granules present that would guide their localization and promote their aggregation. It is possible that low levels of polyP are involved in localizing Ppk's, as was shown to be the case in *C. crescentus* (Henry, Crosson, and Chang 2013) and for aggregation of *P. aeruginosa* Ppk's *in vitro* (Ishige, Zhang, and Kornberg 2002; Parnell et al. 2018). It would be of interest to examine the localization of catalytically inactive Ppk's in the Δ polyP background. It is possible that another cue is required to guide Ppk foci formation in the observed pattern. The chromosome is a structured molecule with lots of specific and unspecific associated proteins and other factors and is therefore a possible candidate to lead Ppk localization. The subdiffusive motion of Ppk2a foci is similar to that of chromosomal loci and is thus consistent with this hypothesis (S. C. Weber, Spakowitz, and Theriot 2010). Further, more in-depth analysis could reveal the physical cause of subdiffusion for the Ppk2a foci, compared to chromosome-associated foci (Meroz and Sokolov 2015). It remains to be tested whether Ppk's interact with DNA, either specifically or unspecifically.

It is not clear whether the Ppk foci are fulfilling a function during exponential growth or whether they are just sequestered awaiting starvation. The growth rate of Δ polyP cells is similar to WT cells, indicating that the Ppk's do not have a critical role during exponential growth, arguing for them rather being on "stand-by". The fact that the Ppk's form foci with a distinct localization pattern suggests that their role is more than just producing or using polyP. Localizing polyP granules in a certain region could be important to position the granules in a way that ensures an even inheritance to the daughter cells. Concentrating polyP production or consumption in a certain region might have the purpose to interact with certain processes at that location. For instance, Ppk1's midcell localization could be related to the midcell localization of the replisome. Perturbing Ppk localization could lead to interesting phenotypes. Although this work only highlighted a few small aspects of the behavior of Ppk's and polyP, it could help to ask more directed questions at how Ppk's fulfill their function and in what processes they are involved during cell cycle exit.

Chapter 4 Conclusion and outlook

4.1 Conclusion

In this thesis, we used microscopy to measure different structures and their dynamics in bacteria. This required both structural and temporal information and thus asked for a methodology to acquire dynamic information with the highest spatial precision, while not perturbing the processes in the cell. Moreover, it had to be compatible with imaging hundreds of cells, to support strong statistical conclusions.

During exponential growth when nutrients are abundant, bacteria have to balance growth with division. While the regulation of cell division was classically associated with controlling constriction onset, the possibility of controlling constriction rate has not been studied previously, in part because resolution seriously limits the extent to which constriction can be measured. The constriction process takes around one hour in slow growing *C. crescentus*, reducing the diameter at midcell from $\sim 0.5 \mu\text{m}$ to zero. Phase contrast microscopy does not have sufficient resolution to measure the constriction diameter beyond halfway constriction (Reshes et al. 2008); SMLM, STED and cryoEM on the other hand offer higher resolution but do not allow to follow the dynamics of a single cell and require population-wide measurements to infer dynamics (Coltharp et al. 2016). SIM doubles the resolution with respect to wide-field microscopy, while still allowing time-lapse imaging of growing cells. This way we could measure constriction kinetics for hundreds of cells down to waist widths of 30%, usually only a few minutes before the end of constriction. Using genetic and pharmacological perturbations, we showed that constriction rate modulation can set cell size. Moreover, we showed that early constriction rate is modulated to compensate for variations in elongation before constriction, leading to a higher fidelity cell size homeostasis. This is the first direct demonstration that constriction rate modulation can be used for cell size regulation in bacteria.

By contrast, when nutrient availability becomes limiting, cells cannot continue exponential growth and need to exit the cell cycle. This process involves the creation of polyP granules. Cells unable to make polyP fail to exit their cell cycle and are severely impaired in responding to stress. PolyP granules are spaced, but it is not clear how this spacing arises and whether it is important for survival. It is unclear what polyP's vital role is during cell cycle exit, and whether they space due to spaced production by the Ppk enzymes or after production due to their properties and interactions. The main Ppk's in our model organism, *Pseudomonas aeruginosa*, Ppk1 and Ppk2a, are low copy number proteins, and for both of them, a significant portion of the population diffuses free throughout the cytoplasm, leading to a weak fluorescent signal in a high cellular background, distorting the apparent position of Ppk1/Ppk2a-foci (Moolman, Kerssemakers, and Dekker 2015). We developed a background subtraction method that improves spot detection efficiency and accuracy and applied this to measure location and diffusion of Ppk foci. We found that both Ppk2a and Ppk1 already form foci prior to starvation and the formation of polyP granules. This is consistent with localized production by Ppk's determining polyP granule location.

4.2 Outlook

4.2.1 Mechanism of constriction rate compensation

In the discussion of the second chapter, we proposed a hypothetical mechanism for constriction rate modulation. A build-up of excess cell wall precursors, proportional to cell volume growth, could lead to faster cell wall remodeling at the division site and hence a faster constriction rate. This build-up of cell wall precursors was predicted previously, based on measurements of surface area to volume ratio (Harris and Theriot 2016). The difference with this work however, is that here we suggest that the precursor level sets constriction rate, rather than trigger onset of constriction rate. It is not known whether cells really allow cell wall metabolites to accumulate. Recent efforts made it possible to measure the levels of metabolites in bacterial populations (Kiefer et al. 2015; Hartl et al. 2017). To look at cell cycle dependence of metabolite concentration, this method was used on a synchronized population of *C. crescentus* cells. Cell wall-related metabolites did accumulate during the first half of the cell cycle, while decreasing again towards the end of the cell cycle (Hartl, personal communication). Whether cell wall precursor levels influence constriction rate could be tested further by providing or depleting cell wall precursors and monitoring the effect on growth and constriction rate. Fosfomycin treatment inhibits cell wall precursor production and indeed slows down constriction rate (Figure 2-2). It would be interesting to provide bacteria with additional cell wall precursors: in the proposed model, constriction rate would increase, while elongation rate would not increase significantly. Moreover, the correlation between elongation before constriction and constriction rate should be weakened. Practically, this could be done by adding GlcNAc and/or MurNAc to the growth medium, many bacteria including *C. crescentus* were shown to be able to take up and use GlcNAc, not only for peptidoglycan synthesis but also as a general carbon source. GlcNAc is a breakdown product of chitin and is one of the main carbon sources in marine environments (Eisenbeis et al. 2008; Riemann and Azam 2002). Another strategy could be overexpressing enzymes of the peptidoglycan metabolism such as MurA. Note that MurA is the target of fosfomycin and its overexpression was shown to confer fosfomycin resistance (Couce et al. 2012). However, the metabolic pathway of peptidoglycan intersects with many others, and unexpected side effects may occur (Jorgenson et al. 2016).

There could be other mechanisms leading to constriction rate compensation, possibly in parallel with cell wall precursor accumulation. DNA replication is thought to play a role in cell size control and homeostasis. In *E. coli*, DNA replication initiates at a constant cell size, and DNA replication and subsequent segregation and division takes the same time on average over a wide variety of conditions (Wallden et al. 2016). If constriction onset is relatively early with respect to DNA replication and segregation, this could be compensated for by factors sensing the state of the chromosome that slow down constriction. If constriction onsets relatively late with respect to DNA replication and segregation, constriction would not be inhibited. It was shown that MatP senses chromosome segregation and regulates constriction rate (Coltharp et al. 2016). It would be informative to monitor chromosome replication and segregation in parallel with constriction kinetics. One can label genetic loci near the terminus of replication to monitor their replication and segregation and see whether constriction rate is correlated to progress in these processes.

4.2.2 Impact of variable constriction rate on pole shape

We noted in chapter 2 that the differences in constriction rate between WT, FtsW^{**1*} and fosfomycin-treated cells lead not only to differences in cell size, but also in pole shape. FtsW^{**1*} cells have blunter/shorter poles; while fosfomycin treated cells have more tapered/longer poles. We wondered if this trend is also true at the single cell level and how well pole shape can be predicted from constriction kinetics. The constriction rate affects pole shape at the single cell level: the overall length of the two new poles is often very close to the elongation during constriction. Since FtsZ localizes most of the cell wall remodeling during constriction within a narrow zone (Coltharp et al.

2016; Holden et al. 2014; Bisson-Filho et al. 2017; Yang et al. 2017), we hypothesized that the shape of the new cell pole can be predicted from the elongation and constriction kinetics. A new cell pole can be drawn by plotting the constriction diameter for each time point as a function of the elongation since constriction onset, divided by two, because there are two new poles. We overlaid the predicted pole with the cell contour of the cell at the time point before division and found that for most cells they overlap quite well (Figure 4-1A). This suggests that most of the cell wall remodeling and its physical deformation, e.g. by turgor pressure, happens in a narrow zone, smaller than the resolution of the SIM microscope and that the new poles do not undergo major shape changes after their synthesis. However, the new poles of some cells showed some asymmetry, e.g. one pole being blunter than the other. A more precise analysis of the evolution of the new pole shape could reveal how new poles are created.

Does the variation in pole shape have any effect on cell biology? The cell poles of many rod-shaped bacteria, such as *E. coli* are approximately hemispherical. The spherical geometry provides a homogeneous distribution of stress (Hearn 1997). *C. crescentus* on the other hand has tapered poles. It is not known whether this pole shape provides a competitive advantage in the lifestyle of *C. crescentus*. One thing that a tapered pole provides is a narrow “tip”, a smaller region with the highest curvature. This might be important for the precise localization of certain structures. Preliminary data indeed shows that while WT cells usually have a stalk at the tip at the end of the pole, the *FtsW^{**I*}* mutants, with their blunter poles, tend to have more variability in the localization of stalks (Figure 4-1B). Other structures at the cell pole of *C. crescentus* include flagella and pili. Therefore, pole shape could possibly affect surface attachment and colonization.

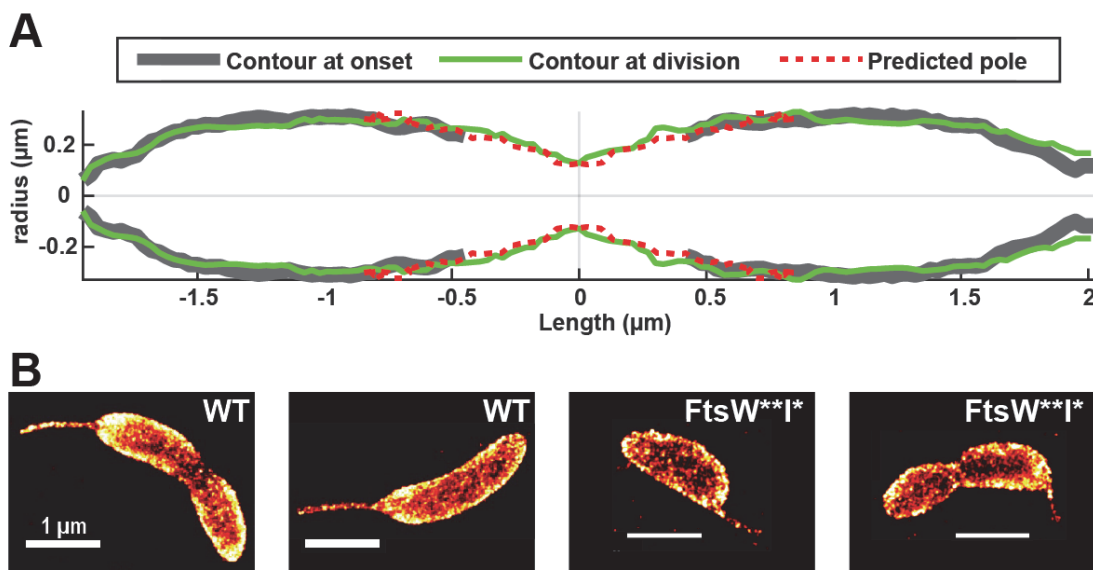


Figure 4-1: Constriction rate, pole shape and impact on the cell.

A) Contour of a cell, from the time-lapse SIM data in chapter 2. The contour at constriction onset (grey) is split at the constriction site and aligned with the cell poles of the contour of the last time point before cell division (green). The predicted pole (red, dashed lines) was created by plotting the minimal width at midcell against the cell length, for each time point, aligned with the center of the contour. **B)** Representative example STORM images of WGA-labelled stalked WT and *FtsW^{**I*}* *C. crescentus* cells. All scale bars are 1 μm .

4.2.3 Location of Ppk foci

Ppk2a and Ppk1 form distinct foci which are significantly less mobile than protein complexes. Specifically, they have diffusion coefficients on the order of $10^{-3} \mu\text{m}^2/\text{s}$, three orders of magnitude smaller than $\sim 1 \mu\text{m}^2/\text{s}$ for large proteins. Ribosomes, being giant RNA-protein complexes of 2 MDa, still have diffusion coefficients of $0.04 \mu\text{m}^2/\text{s}$ (Philips and Milo 2015). Moreover, the Ppk foci seem to move subdiffusively. This could be explained by them being bound to a larger

structure. Ppk2a was shown to form higher order oligomers when bound to polyP (Ishige, Zhang, and Kornberg 2002; Parnell et al. 2018), which could explain their aggregation *in vivo*, especially during starvation, when large polyP granules are formed. Before starvation however, no polyP granules are present, but basal polyP levels could still promote Ppk aggregation. Alternatively or additionally, the Ppk foci could be tethered to a structure such as the nucleoid. This is also consistent with their motion being subdiffusive (S. C. Weber, Spakowitz, and Theriot 2010). If this association is mediated by direct Ppk-DNA interaction, this can be tested with an electrophoretic shift assay.

Ppk location could determine the location of new polyP granules. This could be tested by perturbing Ppk localization, for instance by genetically fusing them to a protein with a specific localization, such as the cell membrane, a specific location on the chromosome, the cell poles, etc. This would presumably relocate the Ppk foci and possibly also the polyP granules. If polyP localization can be perturbed, one could also study if the localization has effects on cell cycle exit or proper cell cycle re-entry after reintroduction to growth medium and the partitioning of polyP granules among daughter cells.

4.3 Final remarks

Microscopy remains a major tool in bacteriology and biology in general, allowing researchers to see and study organization of and within bacteria. Microscopy techniques and subsequent analyses are being improved continuously and are becoming increasingly quantitative, providing further insights than what can be seen at first glance. Ongoing development will continue to improve spatial resolution, temporal resolution and photo-toxicity, expanding the boundaries of microscopy (Z. Liu, Lavis, and Betzig 2015). Work in many labs is directed at developing better labels (De-decker, De Schryver, and Hofkens 2013; Lavis 2017) or better microscopes, for example improving track lengths by an order of magnitude (Balzarotti et al. 2017). However, as all experimental approaches, microscopy provides a single, indirect perspective. It measures intensities of light (or other waves), which usually yields structural or positional information, which requires interpretation by the researcher to infer functional and mechanistic information; seeing is not always equal to understanding. Microscopy or labeling methods do exist to highlight functional information such as interactions, by Förster Resonance Energy Transfer (FRET), Bimolecular Fluorescence Complementation (BIFC), etc., or enzymatic activity, for instance in microscopy-based DNA sequencing or by using incorporation of fluorescent substrates like Fluorescent D-Amino Acids highlighting cell wall remodeling (Kuru et al. 2012). Often still the need remains for complementary experiments, using genetic, biochemical or other approaches to directly test hypotheses. Nevertheless, microscopy offers one of the most straightforward ways to explore and study biology, and probably the best way to study structure, localization and their dynamics.

Chapter 5 Materials and Methods

5.1 Constriction rate modulation can drive cell size control and homeostasis in *Caulobacter crescentus*

Adapted from (Lambert et al. 2018).

5.1.1 Bacterial strains and growth conditions

5.1.1.1 Strains and plasmids

The strains, plasmids, oligonucleotides, restriction sites and modes of constructions used for this study are summarized in Table 5-1, Table 5-2 and Table 5-3. The WT and mutant strains were electroporated with the Pvan mCherry-MTS2 plasmid to yield the Pvan mCherry-MTS2 strain. These strains were then electroporated with the P_{xyl} FtsZ-GFP, P_{xyl} FtsW-GFP or P_{xyl} FtsW^{**}-GFP plasmid to yield the respective dual color strains.

Organisms/strains	Source	Identifier
NA1000, synchronizable derivative of wild-type CB15	(Evinger and Agabian 1977)	CB15N
CB15N <i>ftsW</i> (F145L,A246T); <i>ftsI</i> (I45V)	(Modell et al. 2014)	ML2159
CB15N P _{xyl} :: <i>ftsZ</i> -GFP Pvan:: <i>MTS2</i> -mCherry (GmR/KmR)	This study	CB15NVL1
ML2159 P _{xyl} :: <i>ftsZ</i> -GFP Pvan:: <i>MTS2</i> -mCherry (GmR/KmR)	This study	CB15NVL2
CB15N P _{xyl} :: <i>ftsW</i> -GFP Pvan:: <i>MTS2</i> -mCherry (GmR/KmR)	This study	CB15NVL3
ML2159 P _{xyl} :: <i>ftsW</i> ^{**} -GFP Pvan:: <i>MTS2</i> -mCherry (GmR/KmR)	This study	CB15NVL4
CB15N <i>MreB</i> (Q26P)	(Aaron et al., 2007)	CJW1715
CJW1715 P _{xyl} :: <i>ftsZ</i> -GFP Pvan:: <i>MTS2</i> -mCherry (GmR/KmR)	This study	CB15NVL5
K-12 MG1655 P _{lac} :: <i>ftsZ</i> -GFP P _{BAD} :: <i>MTS2</i> -mCherry (ApR/CmR)	This study	MG1655VL1

Table 5-1: Experimental Models: Organisms and strains

Plasmids	Source	Identifier
P _{xyl} :: <i>VENN-2 FtsW</i> (KmR)	(Goley et al. 2011)	pEG105
P _{xyl} :: <i>VENN-2 FtsW</i> ^{**} (KmR)	This study	pEG1224
P _{xyl} :: <i>GFPN-2</i> (KmR)	(Thanbichler, Iniesta, and Shapiro 2007)	pXGFPN-2
P _{xyl} :: <i>GFPC-2</i> (KmR)	(Thanbichler, Iniesta, and Shapiro 2007)	pXGFPC-2
P _{xyl} :: <i>VENN-2</i> (KmR)	(Thanbichler, Iniesta, and Shapiro 2007)	PXVENN-2
<i>E. coli</i> MTS2 fused to GFP pBAD33 derived plasmid <i>Para-GFP::EcMTS::EcMTS</i> (CmR)	(Szeto et al. 2003)	pSLR92
Pvan:: (KmR)	(Thanbichler, Iniesta, and Shapiro 2007)	pVCHYC-4
P _{xyl} :: <i>ftsZ-dendra2</i> (KmR) used to create pVL1	(Holden et al. 2014)	pX-Ftsz-Dendra2
P _{xyl} :: <i>ftsZ</i> -GFP (KmR)	This study	pVL1
Pvan:: <i>MTS2</i> -mCherry(GmR)	This study	pVL2
P _{xyl} :: <i>GFPN-2 FtsW</i> ^{**} (KmR)	This study	pEG1308
P _{xyl} :: <i>VENN-2 FtsW</i> (KmR)	(Goley et al. 2011)	pEG105
P _{xyl} :: <i>VENN-2 FtsW</i> ^{**} (KmR)	This study	pEG1224
Used to create pEG1305, pEG1308 (KmR)	This study	pXGFPN-2

Table 5-2: Plasmids

Oligonucleotide sequences	source	identifier
5'-AACTTGGTACCTCTAGAGGAAGATCTTTCATCGAGGAG-3'	This study	MTS2_KpnI-F
5'-AACTTGAATTC AAGCTTCTAGGATCCACCGCCG-3'	This study	MTS2_EcoRI-R
5'-CTCGAGCTCCGATGGCCTCCAACGCG-3'	This study	oEG035
5'-GTTCGAATTCTCTCAGGCGTCCGCGCGACC-3'	This study	oEG036
5'-AACTTGGTACCTCTAGAGGAAGATCTTTCATCGAGGAG-3'	This study	MTS2_KpnI-F

Table 5-3: Oligonucleotides

5.1.1.2 Growth conditions

Liquid *C. crescentus* cultures were grown overnight at 28°C with 15 mL of M2G minimal media under mechanical agitation (180 rpm). Each specific inducer for every different condition is described below. Fosfomycin perturbation was achieved with a subminimal inhibitory concentration of 12.5 µg/ml added one hour prior to synchronization. To induce the expression of mCherry-MTS2 from the Pvan promoter, 0.5 mM of vanillate was added to the culture before overnight growth. For the expression of FtsW-eGFP, xylose was added to reach a final concentration of 0.3 % (mass per volume) 2 hours before synchrony as optimized previously (Goley et al. 2011). Pxyl FtsZ-eGFP was induced overnight at 0.003 % xylose in M2G as optimized in a previous study (Holden et al. 2014).

Liquid *E. coli* cultures were grown overnight at 37°C in M9 medium under mechanical agitation (180rpm). mCherry-MTS2 was induced from the PBAD promoter by adding 0.01% (m/V) arabinose during overnight growth. FtsZ-GFP was induced from the Plac promoter using 20 µM Isopropyl β-D-1-thiogalactopyranoside (IPTG) for 2 h prior to the experiment.

5.1.2 Sample preparation

C. crescentus cells were synchronized at 4°C by Percoll density gradient (Schrader and Shapiro 2015) when they reached mid-exponential phase ($OD_{660} = 0.3-0.5$). *E. coli* cells were not synchronized before the experiment, instead cell birth was identified from the time-lapse images. A silicone gasket (Grace Biolabs, 103280) was placed on a rectangular cover slide, and filled with 1% M2G agarose (Ultra Pure™ Agarose, Sigma) containing fosfomycin, xylose and vanillate at the appropriate concentrations when needed. Vanillate was present at 0.5 mM in all experiments with *C. crescentus*, xylose was present at 0.003% for induction of FtsZ-eGFP, but absent for the FtsW-eGFP experiments. Fosfomycin was added to a final concentration of 10 µg/ml for drug perturbation experiments. For the *E. coli* experiments, 0.01% Arabinose was present in the M9-agarose pad. A cover slide was placed on top of the silicone gasket before solidification of the agarose to achieve a flat agarose pad. After 5 min, the top cover slide was removed, and a 1 µL drop of a synchronized cells suspension was placed on the pad. A small piece of agarose (~1 mm) was cut out on two opposing sides to ensure aerobic conditions during imaging. After absorption of the droplet, the pad was sealed with a plasma-cleaned #1.5 round coverslip with a diameter of 25 mm.

5.1.3 Image acquisition

5.1.3.1 Microscope set up

SIM microscopy was performed on the 3D NSIM Nikon microscope, with a CFI Apochromat TIRF objective (100 x, NA 1.49, Nikon). The microscope was equipped with 400 mW, 561 nm and 480mW, 488 nm lasers (Coherent Sapphire) and a back-illuminated EMCCD camera (iXon 3, Andor Technology) with a 512x512 pixel CCD sensor.

5.1.3.2 Acquisition settings

Dual color imaging of the cells was performed at 28°C using the 488 nm and 561 nm lasers for the divisome protein-eGFP channel and the mCherry-MTS2 channel respectively. The camera was operated with a readout speed of 1 MHz and a dynamic range of 16 bit to have the maximum pixel readout speed at the highest dynamic range. The preamplifier gain and the electron multiplication gain were set

to 1 and 200 respectively to maximize the signal to noise at the chosen dynamic range. All raw SIM images were acquired with a camera acquisition time of 200 ms and 100 ms (5 fps and 10 fps) for the 561 and 488 channels. The laser power for both channels was 4 W/cm². These settings yielded a good balance between image quality and photo-bleaching.

All the raw images were acquired in 3D SIM image mode to ensure the highest signal to noise ratio and lateral resolution. Fifteen images were captured of each 30.7×30.7 μm field of view, five phase-shifted images per angle at each of three interference pattern angles. A full raw dual color image stack was acquired in 17 s.

Live-cell fluorescence microscopy over the cell cycle was achieved by performing time-lapse imaging. 3D SIM snapshots were captured at 5 min or 10 min (for fosfomycin-treated cells) time intervals to follow dynamics while minimizing photo-bleaching of the sample during the image acquisition. Multiple fields of view were imaged sequentially at each time point, allowing following up to 200 cells per experiment. Super-resolved SIM images were reconstructed by the Nikon NIS-Elements software.

5.1.4 Bleach correction

For visualization in Figure 2-1A and Figure A-1C, the images were bleach corrected based on the whole field of view, using the Bleach Correction function in ImageJ, using the “Simple Ratio” algorithm, for which the approximate background value was determined manually. Bleach correction was not performed for the analysis.

5.1.5 Quantification and statistical analysis

5.1.5.1 Analysis of cell shape dynamics

The super-resolved SIM images were processed via a custom-made software package called sDADA (Shape Dynamics Automated Data Analysis). sDADA generates scatter plots, histograms and violin plots in order to study key parameters controlling the cell size and homeostasis, such as: elongation rate, constriction duration, length at birth, onset, onset time. sDADA extracts these parameters from the analysis of the cell shape dynamics thanks to semi-interactive modules for image segmentation, edge detection, cell filtering, cell tracking and statistical analysis (See Detailed image analysis workflow). The MATLAB-based software package is available together with its documentation upon request. For the *E. coli* data, the septum is much more vertical than in *C. crescentus*, therefore it is no longer possible to robustly measure the early and late constriction rates with sDaDa, moreover, these cell could not be synchronized. For these data (Figure A-3F), we manually identified cell birth, division onset and division times and lengths.

5.1.5.2 Parameter definition

We assumed as time zero (T_0) the time at which the suspension of synchronized bacteria is added to the agarose pad. This occurred approximately 20-40 minutes before starting time-lapse SIM acquisition. For *E. coli* data, T_0 was the time of first frame after the mother cell divided. T_c , T_z , and T_w refer to the constriction onset time measured with different approaches. T_z is the time of the FtsZ assembly, which we assumed to occur when the fluorescence intensity of FtsZ-eGFP at mid-cell was three times higher than elsewhere. T_w is the FtsW arrival time measured as the moment at which the FtsW signal appeared stable at midcell (Figure A-1C).

T_c is defined as the time at which the constriction invagination depth is equal to a predetermined normalized waist width threshold. To find the optimal threshold, we tested different thresholds in the reasonable range from 80% up to 99% of the maximum diameter, with step sizes of 1 %. Since FtsW arrival time is an alternative readout of the constriction start the T_c values computed from the waist diameter versus time should strongly and robustly correlate with the T_w values. For each threshold, we computed the Pearson's correlation coefficient for the scatter plot of the T_c values versus the T_w values of all the

cells. We found that a threshold of 92% had the best correlation coefficient and minimal least square error for Tc versus Tw.

Generation time (TG) and final length (LG) are the time and the length at which the cell divide. Constriction duration τ is the difference between TG and TC, or when specified, TW. The length at birth, LB and the elongation rate k are extracted from the exponential fitting of the elongation: $L(t) = L_B \cdot e^{kt}$. The length at the constriction onset, LC, LZ or LW, were measured as the lengths at TC, TZ and TW respectively. The total elongation is the difference between LG and LB. Elongation before constriction and during constriction are defined respectively as the difference between LG and LC, and between LC and LB. When specified, LW can be used instead of LC.

5.1.5.3 Statistical tests

For each parameter defined in the section above, the statistical significance of observed differences between strains or conditions was tested. We compared the means of the repeats using Mood's median test. The correlation between variables was analyzed using Pearson's correlation coefficient in the presence of a linear trend or the Spearman's correlation coefficient for non-linear relationship. The experiments were performed in two independent replicates per condition with a minimum of 100 cells analyzed per replicate, and minimum 200 per condition.

5.1.6 Detailed image analysis workflow

5.1.6.1 Cell shape dynamics and fluorescence measurement

A robust semi-automated pipeline was developed to identify, track and measure shape parameters (length, width, waist width) of hundreds of cells imaged in time lapse movies over the all cell cycle. Also distributions of the variables and correlations between variables were analyzed using this pipeline.

5.1.6.2 Drift correction

To simplify the tracking of cells over time, the time-lapse videos were drift-corrected using the Fiji plugin "Descriptor based registration (2d/3d + t)" (Preibisch et al. 2010). The dual-color experiment, registration of both channels was performed based on the drift observed in the red-channel (561nm).

5.1.6.3 sDaDa: a software package for supervised segmentation and measurement of bacterial images

The quantitative image analysis of the cell shape dynamics and of their fluorescent signals was performed with our custom-made software package called sDaDa (Shape Dynamics Automated Data Analysis). sDaDa is an open source MATLAB-based program for time-lapse dual color images of bacteria (FtsZ-GFP, FtsW-GFP (green channel) and mCherry-MTS2 (Szeto et al. 2003) (red channel)).

The program takes as input the time-lapse images stack (each superresolved image with a size of 1024 pixel x 1024 pixel; 30 nm /pixel), the camera parameter (i.e. pixel size) and a set of experimental parameters (i.e. starting time, time interval between two consecutive frames, the field of view (FOV)). The program outputs a data structure containing all the measurements of each cell at each frame and a set of figures with the results of the measurements.

The description of the main features of the sDaDa program and of the general steps in a typical pipeline (Figure A-1) are presented below.

The main pipeline stages of the software are (1) image segmentation and first edge detection guess, (2) cell tracking, (3) edge detection refinement and shape parameters measurement, (4) divisome ring identification (5) shape parameters correlation analysis and outputs display.

More specifically, the segmentation step (1) is based on two processes: the first is based on the Otsu's thresholding method (Otsu, 1979) to distinguish background pixels from foreground one; the second group together a set of pixels by seeing which pixels are connected to each other. The Otsu's method

sets a proper threshold via maximizing the inter-class variance of the bi-modal histogram of the pixel intensities (foreground pixels and background pixels). Connected pixels that have a signal value higher than the threshold are tagged with the same number and identify as part of a cell only if they form an area bigger than $0.5 \mu\text{m}^2$. We used two built-in MATLAB functions (`graythreshold()` and `bwlabel()`) for Otsu's image thresholding and to identify each individual cell.

A `microbeTracker` function named `model2mesh.m` defines the first cell contour guess starting from the edge detection performed with built-in MATLAB functions `bwperim()` and `bwtraceboundary()`. The `model2mesh` function returns two semi-contours, corresponding to the 'left' and 'right' sides of the cell. From the two semi-contours, the bacteria poles (the two farthest apart points on the contour) and the centerline (the average of the two half contour parts) can be easily identified.

Within the segmentation stage, the cell shape search, control and refinement is done thanks to an interactive tool. The user has several tools inspired by the `MicrobeTracker` (Sliusarenko et al. 2011) approach to manipulate the region, such as removing parts, joining two regions, smoothing, expanding. The user can also choose to delete the current time point of the cell or to mark the cell as divided, after which it will no longer be followed.

In order to track the same bacteria in successive frames (step (2)), the program performs a search based on a spatial analysis. The area and the barycenter position belonging to a cell in one frame is compared with the spatial distribution of pixels belonging to the possible corresponding cell in the following frame. The two regions correspond to the same cell if the difference between these two spatial distributions is lower than a user-defined tolerance parameter. The tracking search stops when the cell divides or when one region does not pass the search criteria.

The `FtsZ` and `FtsW` divisome assembly time (T_W and T_Z) is determined by monitoring the intensity profile along the centerline length over the cell cycle (step (4)). T_W and T_Z are the moments at which `FtsZ` and `FtsW` fluorescence signals reach their maximum intensity at the midcell.

The segmented regions, containing a well-identified cell, can therefore enter the second stage (3) where the program extracts and accurately measures the shape parameters described below. The diameter is measured by taking perpendicular slices of the bacteria image along its centerline length. Using the intensity profile along each slice, a histogram with two maxima corresponding to the cell edge will define the diameter. The intersection of the histogram with a line parallel to the abscise axis at half maximum high, identify up to four abscises (two for each maximum). The diameter is the difference between the two furthest apart abscises. Repeating this procedure for each slice of the bacteria, the diameter profile as a function of the length could be achieved (Figure A-2). The minimum between two maxima of the diameter as a function of the length will then define the measure and the position of the constriction site. As a consequence, the waist width will be easily defined: the ratio of the width of the constriction site and the maximum diameter along the cell. Lastly, the length is measured by calculating the arc length of the centerline.

The program examines the temporal evolution of the length and the waist width for all single cells detected in a time-lapse experiment. From these curves, it extracts the elongation rate, the length at birth (L_B) and the division time (T_G). The onset time T_C and the duration of the constriction are measured as explained in the Methods "Parameter definition" section.

The volume and the surface area of a cell are estimated based on the measured widths along the length of the bacterium. The width versus the length profile is first smoothed using a spline function, to filter out the noise that would inflate the surface area estimation. The bacterium is assumed symmetric along its central axis. Therefore, assuming cross-sections perpendicular to the axis are circular, the volume and surface area can be computed by treating the measured 'segments' of the bacterium as a series of conical frusta.

The last stage (5) provides a set of statistical tools to study the correlations between the parameters extracted and to measure their average and variance. The user can generate a scatter plot for each possible couple of parameters combination (e.g. the scatter plots in Figure 2-3). Moreover, the user can generate a violin plot for each parameter to inspect its statistical distribution over the entire population (e.g. the violin plots in Figure 2-2). To conclude the program computes the correlation coefficient of each couple of parameters.

5.1.7 Pole shape analysis

Analysis of cell poles was performed using the Celltool software package ((Pincus and Theriot 2007); <http://zplab.wustl.edu/celltool/>). Image-derived cell shapes were converted into parametric spline curves (Pincus and Theriot 2007), and centerlines were fit to each cell shape (as described in (Sycuro et al. 2010)), again using Celltool. Cell poles were defined as the position on the cell outline closest to the ends of the centerline. The curvature at that position was calculated from the first and second derivatives of the parametric spline $x(t)$, $y(t)$. Curvature = $(x'y'' - y'x'')/(x'^2 + y'^2)^{3/2}$, where prime and double-prime represent the first and second derivatives, respectively. The “pole regions” used for PCA shape analysis were defined as all points within distance d from each endpoint, where d was set to 5% of the total cell perimeter (so 20% of the cell boundary was counted as one pole or the other). Principle modes of pole-shape variation were computed with Celltool, as previously described (Pincus and Theriot 2007).

5.1.8 Estimation of excess peptidoglycan precursor.

The assumptions and derivation are based on the work of Harris and Theriot (Harris and Theriot 2016).

Assumption 1: Peptidoglycan precursor (P) production is proportional to the cell volume (V).

$$\frac{dP}{dt} = \gamma V \quad (1)$$

With γ being the rate constant of P production per unit of V, we assume γ is constant over the cell cycle (it changes over larger timescales than the generation time). $[\gamma] = \frac{\text{mol}}{\mu\text{m}^3}$

Assumption 2: PG precursor consumption is proportional to the increase in cell surface area (A):

$$\frac{dP}{dt} = -\lambda \frac{dA}{dt} \quad (2)$$

With λ being the rate constant of P consumption per unit of A, we assume λ is constant over the cell cycle (it changes over larger timescales than the generation time). $[\lambda] = \frac{\text{mol}}{\mu\text{m}^2}$. The total rate of change in precursor is then:

$$\frac{dP}{dt} = \gamma V - \lambda \frac{dA}{dt} \quad (3)$$

The amount of PG precursors produced between cell birth and an arbitrary time in the cell cycle, t_x , is calculated as follows, using exponential Volume growth:

$$\Delta P = [P]_{t_0}^{t_x} = \int_0^{t_x} \gamma V_0 e^{\alpha t} dt - \lambda(A_c - A_0) = \frac{\gamma}{\alpha} V_0 (e^{\alpha t_x} - 1) - \lambda \Delta A = \frac{\gamma}{\alpha} \Delta V - \lambda \Delta A$$

$$\Delta P = \frac{\gamma}{\alpha} \Delta V - \lambda \Delta A \quad (4)$$

Alternatively:

$$\frac{\Delta P}{\lambda} = \frac{\gamma}{\alpha \lambda} \Delta V - \Delta A \quad (5)$$

With ΔP , ΔV and ΔA being the increase in P, V and A respectively. $\frac{\Delta P}{\lambda}$ is the excess precursor expressed as the surface area that could be built with it. $\frac{\gamma}{\alpha\lambda}$ Expresses how volume growth results in production capacity of surface area. To find its value, we can use a **third assumption**: over a cell cycle, between birth and division of a cell, the amount of precursor that is produced equals the amount that is used, or the net production of precursor is zero:

$$0 = \frac{\Delta P}{\lambda} = \frac{\gamma}{\alpha\lambda} \Delta V - \Delta A$$

$$\frac{\gamma}{\alpha\lambda} = \left\langle \frac{\Delta A}{\Delta V} \right\rangle_{cell\ cycle} \quad (6)$$

If we apply (6) to (5), we get:

$$A_{excess} = \frac{\Delta P}{\lambda} = \left\langle \frac{\Delta A}{\Delta V} \right\rangle_{cell\ cycle} \Delta V - \Delta A \quad (7)$$

At the onset of constriction, when $t = T_C$, this can be written as:

$$A_{excess}(T_C) = \left\langle \frac{\Delta A}{\Delta V} \right\rangle_{cell\ cycle} \Delta V(T_C) - \Delta A(T_C) \quad (8)$$

Note that $\frac{\Delta P}{\lambda} = A_{excess}$ describes the excess precursor as the amount of surface area that could be built with it.

5.1.9 Empirical constriction model.

5.1.9.1 Early and late constriction rate determination

Early constriction rate is defined in nm/min as the difference of diameter over the duration of constriction, during early stage of constriction from a normalized waist width of 90% to 60%):

$$\text{Early constriction rate (nm/min)} = (D_{(w=0,9)} - D_{(w=0,6)}) / (t_{(w=0,6)} - t_{(w=0,9)})$$

Late constriction rate is defined in nm/min as the difference of diameter over the duration of constriction, during late stage of constriction from a normalized waist width of 60% to 30%):

$$\text{Late constriction rate (nm/min)} = (D_{(w=0,6)} - D_{(w=0,3)}) / (t_{(w=0,3)} - t_{(w=0,6)})$$

Diameter and time coordinates at waist 0.9, 0.6, 0.3 were determined using linear interpolation.

5.1.9.2 Instantaneous constriction rate determination

To access instantaneous constriction rate (Figure A-4G, H), we used a previously defined empirical model (Coltharp et al. 2016):

$$W(t) = \frac{D(t)}{D_0} = \sqrt[\alpha]{1 - \left(\frac{t - T_C}{T_G - T_C} \right)^\alpha}$$

Where $D(t)$ is the diameter of the constriction site in function of time, t , while D_0 is the diameter at constriction onset, $W(t)$ is the normalized waist width. T_C is the time at constriction onset, while T_G is the time when constriction and the cell cycle finishes. $T_G - T_C$ is the duration of constriction. α is a variable reflecting the change in constriction rate. For constant constriction rate α equals 1, $W(t) = 1 - \left(\frac{t - T_C}{T_G - T_C} \right)$, while for a constant buildup of the area of hemispherical poles, α equals 2: $\left(\frac{D(t)}{D_0} \right)^2 = 1 - \left(\frac{t - T_C}{T_G - T_C} \right)^2$, or $\left(\frac{t - T_C}{T_G - T_C} \right) = D_0 \sqrt{D_0^2 - D(t)^2}$, which is proportional to the surface area. Average values for α were 1.4 for the WT and 1.5 FtsW**1, suggesting cell wall remodeling rate slows down in both strains.

5.1.10 Data and software availability

All data used and software developed to support the results of this thesis are available: Original data is available on Zenodo, DOI: 10.5281/zenodo.1248441 and 10.5281/zenodo.1241005. Software is available on Zenodo, DOI: 10.5281/zenodo.1173751 and on GitHub: <https://github.com/LEB-EPFL/sDaDa>

Software package	Source	Identifier/website
sDaDa	This study	See Transparent methods and 10.5281/zenodo.1173751
Celltool	(Pincus and Theriot 2007)	http://zplab.wustl.edu/celltool/
ImageJ	(Schneider, Rasband, and Eliceiri 2012)	https://imagej.nih.gov/ij/
MicrobeTracker	(Sliusarenko et al. 2011)	http://microbetracker.org/
MATLAB	The MathWorks, Natick, MA	https://ch.mathworks.com/products/matlab.html
Original data	This study	10.5281/zenodo.1248441 and 10.5281/zenodo.1241005

Table 5-4: Software packages

5.2 The role of polyphosphate in the starvation response of *Pseudomonas aeruginosa*

5.2.1 Bacterial strains and growth conditions

The strains used in chapter 3 are listed in Table 5-5. The growth conditions were the same as in (Racki et al. 2017). For all experiments, cells were first grown overnight at 37°C in MOPS minimal medium. MOPS minimal medium contains: 40 mM sodium succinate, 22 mM NH₄Cl, 43 mM NaCl, 2.2 mM KCl, 1.25 mM NaH₂P₀₄, 1 mM MgSO₄, 0.1 mM CaCl₂, 7.5 μM FeCl₂·4H₂O, 0.8 μM CoCl₂·6H₂O, 0.5 μM MnCl₂·4H₂O, 0.5 μM ZnCl₂, 0.2 μM Na₂MoO₄·2H₂O, 0.1 μM NiCl₂·6H₂O, 0.1 μM H₃BO₃, and 0.01 μM CuCl₂·2H₂O, 50 mM MOPS, pH 7.2. For nitrogen starvation, we used a variant of the MOPS minimal medium with 1 mM instead of 22 mM NH₄Cl, referred to as N-limited MOPS medium.

For the first experiment, with DnaX-mApple, for Figure 3-1, the cells were transferred to N-limited MOPS medium at 37°C and shaking for 24h. Then they were transferred to agarose pads (1% agarose in MOPS minimal medium) on microscope slides for imaging. For the experiments for Ppk localization and mobility (Figure 3-2, Figure 3-3, Figure 3-5), cells from overnight cultures at OD₅₀₀ = 0.4 to 0.6 were split in two populations. The first one was transferred to agarose pads (1% agarose in MOPS minimal medium) on microscope slides for imaging in the case of the non-starved condition (0h). The second population was incubated in N-limited MOPS medium for three hours at 37°C with shaking, and afterwards transferred to agarose pads (1% agarose in N-limited MOPS medium) on microscope slides for imaging in the case of the starved condition (3h).

Identifier	Source	Genotype
LR382	This work	<i>P. aeruginosa</i> UCBPP-PA14 attTn7::mini-Tn7T-Gm ^R ParS ^{pMT1} P _{dnaX} ::(DnaX-mApple2sf, GFP-ParB ^{pMT1})
LR383	This work	<i>P. aeruginosa</i> UCBPP-PA14 Δppk1 Δppk2A Δppk2B Δppk2C attTn7::mini-Tn7T-Gm ^R ParS ^{pMT1} P _{dnaX} ::(DnaX-mApple2sf, GFP-ParB ^{pMT1})
LR183	This work	<i>P. aeruginosa</i> UCBPP-PA14 Ppk1::Ppk1-GFP
LR328	This work	<i>P. aeruginosa</i> UCBPP-PA14 Ppk2A::Ppk2A-mNeonGreen attTn7::mini-Tn7T-Gm ^R ParS ^{pMT1} P _{ssb} ::mApple2sf-ParB ^{pMT1}

Table 5-5: Strains used in Chapter 3

5.2.2 Image acquisition

Image acquisition for Figure 3-2 was done on a Zeiss AxioObserver.A1 using a 100× oil immersion objective (Apo 1.4 PH3). For Figure 3-1 and Figure 3-3 through 5, images were acquired on a Nikon Eclipse Ti-E microscope equipped with an Andor Zyla 5.5 camera. For the second dataset on Figure 3-5, images were acquired on a Zeiss Axio Observer 7 with a Plan-APOCHROMAT 100x/1.4 Oil Ph3 objective, equipped with a Photometrics Prime 95B back-illuminated CMOS camera.

5.2.3 Image segmentation and creation of cell contours

Since the bacteria do not grow or move on the timescale of the tracking experiment, a single phase contrast image was segmented per position. Segmentation was done with SuperSegger, resulting in an image mask, a matrix of ones and zeros where continuous regions of ones correspond to single cells.

For background subtraction and tracking, subpixel meshes were required. The phase contrast image and the image mask with the cell regions were used by Oufiti to create subpixel cell contours, subdivided into “meshes”, dividing the cell into segments along its long axis. Demographs for Figure 3-1, Figure 3-2 and Figure 3-3 were created with Oufiti’s demograph function.

5.2.4 Alignment

To translate the cell meshes from the phase contrast image to the fluorescence image, they have to be corrected for misalignment between these channels as well as for drift over the course of the experiment in the case of the tracking experiments. This displacement is estimated using the cross-correlation method (Guizar-Sicairos, Thurman, and Fienup 2008). Misalignment is measured between the first fluorescence frame and the first phase contrast frame, which is inverted such that the cells appear bright on a darker background. Drift is measured for each phase contrast frame with respect to the first phase contrast frame. For datasets with short lags, too short to allow for the acquisition of a phase image at each frame, the drift in between frames was estimated by interpolating the average drift over the whole acquisition, as determined by the drift between phase images taken before and after the acquisition of the fluorescence images.

5.2.5 Background subtraction and spot finding.

Cellular fluorescent background is removed to prevent its bias on spot position and intensity. The fluorescence image is analyzed on a per-cell basis; a small region around the cell is cropped out of the image. An a-trous wavelet filter identifies pixels with fluorescent foci. Then, the fluorescence background intensity is measured for each segment in the cell mesh, excluding segments with fluorescent foci. Each segment of the cell is approximated by a conical frustum emitting fluorescence homogeneously over its volume. The measured fluorescence per segment is divided by the segments volume. The median of these values is used to generate a background image, where the fluorescence is projected onto a pixelated image. This image is convolved with a 2D Gaussian with the appropriate width to emulate diffraction. The resulting background image is subtracted from the raw image (see Figure 3-4A).

The same a-trous wavelet filter is used again to identify pixels with fluorescent foci. The identified regions are each fitted with a high density Gauss fit, fitting up to four 2D-Gaussians. Fits of insufficient quality or abnormally low or high widths are discarded. Finally, the data is saved as well as exported to the TrackMate format.

Parameter	Value
Wavelet scale	2
Low pass	3
Spot radius	3
Int. threshold	0.5
Min region size	0

Fit radius 2.45

Table 5-6: Spot detection parameters.

5.2.6 Tracking analysis

Spots were tracked using TrackMate, an ImageJ plugin (Tinevez et al. 2017). This allows visual inspection of the localizations as well as the tracking later on. Tracking is done using the “simple tracker” algorithm, based on the linear assignment problem framework (Jaqaman et al. 2008). Gap distances were adjusted to particle motion and density, to maximize linking of particles while keeping false negative connections between nearby foci to a minimum. Typical values were 250 nm link and gap distance, and 10 frame gaps.

Mean square displacement analysis of the tracks was done in MATLAB using MSD analyzer (Tarantino et al. 2014). Drift correction was done based on mean displacement of tracks (the ‘*velocities*’ option).

5.2.7 Software availability

The software described in the previous sections will be made publicly available as a git repository on GitHub, at <https://github.com/AsterVanhecke/tracking-with-BGsub>.

5.3 Outlook: Impact of variable constriction rate on pole shape

5.3.1 Figure 4-1A: prediction of pole contour

Figure 4-1A shows WT data from chapter 3, acquired and analyzed as described in section 5.1. The radius profile was calculated by dividing the diameter profile by two. To create the “final contour”, the profile of the cell in the last frame before the end of constriction was taken. The constriction site on the profile was aligned with length zero. The profile from the frame at constriction onset was split at the constriction site, and halves of the cell were plotted at opposite sides of length zero, at a distance from zero equal to the measured elongation during constriction, representing what these parts of the cell would look like if growth only happened at the constriction site. Finally, the predicted pole was created by plotting the radius at the constriction site versus the length of the cell minus the length of the cell in the frame before constriction, divided by two since two poles are being created. This way the last radius measurement was placed at length zero, and the poles join up with the contour of the cell at constriction onset. The predicted pole is mirrored horizontally. All curves are mirrored vertically.

5.3.2 Figure 4-1B: Impact of pole shape on stalk position

Images were produced as described previously (Douglass et al. 2016). The relevant sections are reproduced here, with slight adaptations.

5.3.2.1 Growth and staining of cells

WT and FtsW^{**I} *C. crescentus* were grown in liquid M2G medium in a mid-exponential phase for 12–16 h. Bacteria were fixed with 2.5% PFA in a PBS solution for 10 min then immediately resuspended in a permeabilization buffer (0.1% Triton X-100 in PBS) for 10 min. The bacteria were then resuspended in 100 µg/ml wheat germ agglutinin (AlexaFluor 647-conjugate, W32466, Life Technologies) solution for 5 h at room temperature, then washed 3 times in PBS solution and post-fixed for 10 min in PBS with 2.5% PFA.

5.3.2.2 Image acquisition and reconstruction

A laser with a wavelength of 642 nm (2RU-VFL-P-2000-642-B1R, MPB Communications) was used to switch off fluorophores on the sample, while a 405 nm laser (OBIS, Coherent) controlled the return rate of the fluorophores to the fluorescence-emitting state. The laser beams were expanded, combined using a dichroic mirror (T425lpxr, Chroma) and then injected into the telescope (f₁ = 100 mm, f_c = 50 mm). The rotating diffuser (2.5° ± 0.25° FWHM at 650 nm, 24-00066, Süss MicroOptics SA) sat

at an adjustable offset of -5 mm from the shared focal planes of the telescope lenses. A series of mirrors was then used to align the beam to both the MLAs (500 μm pitch, 10 mm \times 10 mm, $f = 13.7$ mm, square lenses, 18-00201, Süss MicroOptics SA) and the objective lens (CFI60 PlanApo Lambda $\times 60/\text{NA } 1.4$, Nikon). A custom dichroic (ZT405/561/642/750/850rpc, Chroma) reflected the laser light and transmitted fluorescence emission. Emitted light from the sample was collected by the same objective, passed through the dichroic and was imaged by a tube lens ($f_{\text{TL}} = 200$ mm, MXA20696, Nikon) onto the sCMOS camera (Zyla 4.2, Andor). The width of a square camera pixel corresponds to 106 ± 2 nm on the sample. The emission filter (ET700/75M, Chroma) was combined with a short-pass filter (FF01-842/SP, Semrock) and inserted into the emission path between the tube lens and camera. A separate, 850 nm laser (0.9 mW continuous wave (c.w.) circular beam, 85–238, Thorlabs) passed through a clean-up filter (LL01-852, Semrock) and was reflected from the coverslip by total internal reflection. The reflected beam was directed through an 850 nm band-pass filter (86–090, Edmund Optics) and onto a linear light sensor (TSL1401CL, AMS-TAOS USA, Inc.); changes in the beam position were read using the pgFocus open hardware autofocus module (<http://big.umassmed.edu/wiki/index.php/PgFocus>). This information was used to send a feedback signal to the piezo z stage and lock the objective–coverslip distance to within a standard deviation of 10 nm. Microscope control was orchestrated with Micro-Manager (Version 1.4.22, nightly build 2015-07-27) (Edelstein et al. 2014). The single-molecule localization analysis was performed using a sCMOS-specific maximum likelihood algorithm following a previously described calibration routine (Huang et al. 2013).

The MLAs and rotating diffuser were chosen on the basis of the design specifications from the simulation package and the need to minimize losses in the transmitted laser power. Square lenses provide a complete fill factor and minimize scattering at the lenslet interfaces, while also projecting a square illumination pattern onto the sample. A diffuser with a small divergence angle specification helps to maintain a minimally divergent laser beam profile through the system.

Imaging was performed using an optimized buffer as described previously (Olivier et al. 2013). The bacteria were imaged by acquiring 20,000 frames at 10 ms continuous exposure and 1,400 mW of 642 nm laser light in the objective BFP. Image reconstruction was done using ThunderSTORM (Ovesný et al. 2014), using the parameters in Table 5-7 and Table 5-8.

Parameter	Value
Pixel size [nm]	108
Photoelectrons per A/D count	0.49
Base level [A/D] counts	90
EM Gain	Unchecked

Table 5-7: Camera setup parameters.

Parameter	Value
Filter	Wavelet filter (B-Spline)
B-Spline order	3
B-Spline scale	2
Approx. loc. of molecules: Method	Local maximum
Peak intensity threshold	$2 * \text{std}(\text{Wave.F1})$
Connectivity	8-neighborhood
Sub-pixel loc. of molecules: Method	PSF: Gaussian
Fitting radius [px]	3
Fitting method	Weighted Least Squares
Initial sigma [px]	1.5
Multi-emitter analysis	Not enabled

Table 5-8: Localization analysis parameters.

Appendix A Supplemental information to chapter 2.

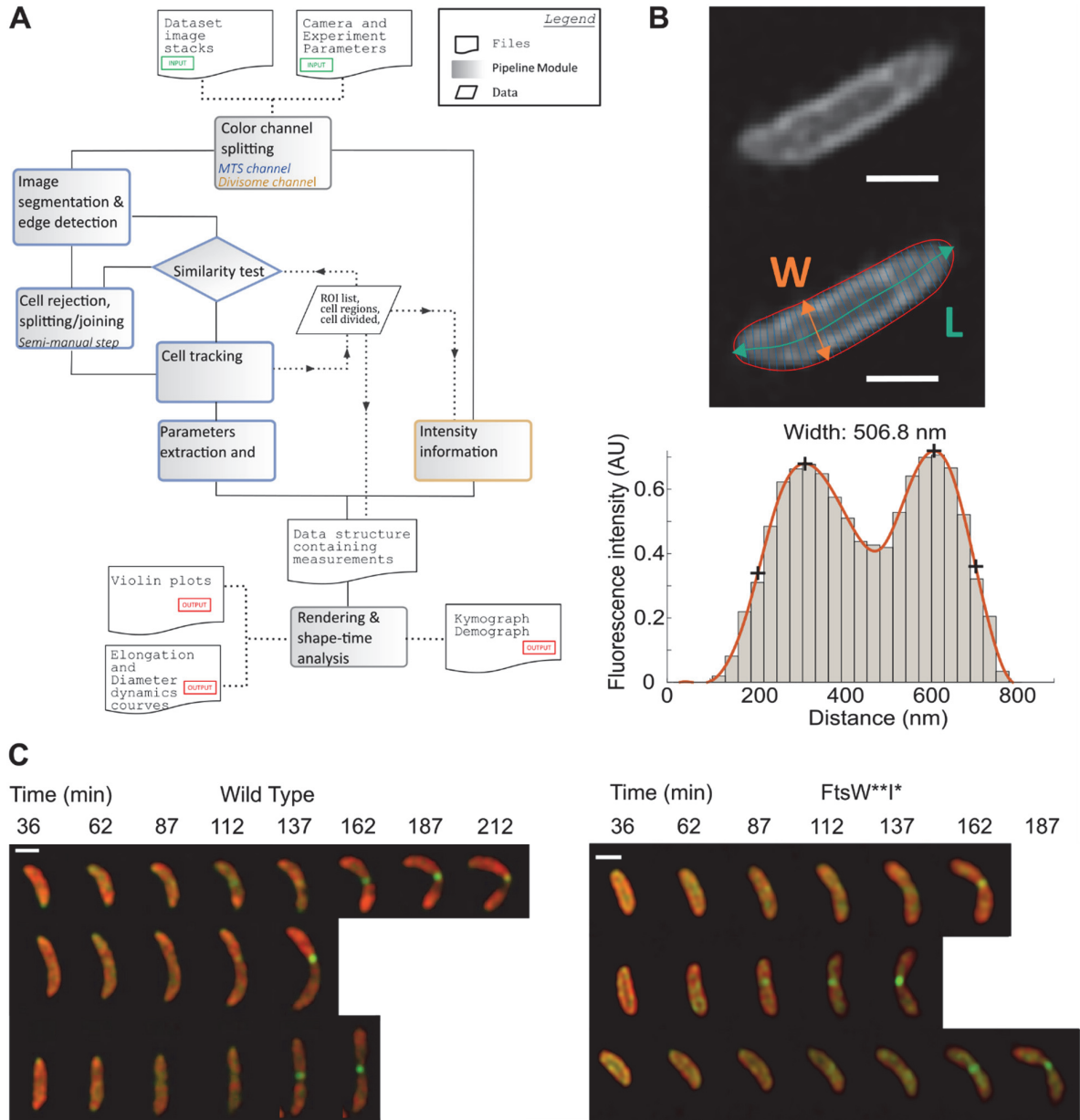


Figure A-1: Image analysis pipeline.

A) Analysis software flowchart. **B)** Analysis of SIM images inner membrane label: from the raw data, the centerline is calculated. At equally spaced points along the centerline, the width is measured by extracting the intensity profile along a line (thin cyan colored line) perpendicular to the centerline (thick cyan colored line) at that point (top panel red line represent the contour). Lower panel: The extracted intensity profile (grey bars) is smoothed by fitting a spline (orange line lower panel). The maxima are calculated (top plus signs on orange line), and the outer position with the half-maximum value is found (lower plus sign on orange line). The distance between these two positions is defined as the width. Scale bar: 700 nm. **C)** SIM images of FtsW onset. Red inner membrane MTS₂-mCherry labeled, FtsW-GFP label Every one in five frames is shown for three representative cells for Wild Type and FtsW**1*. Images were bleach corrected for visualization, see Transparent Methods. Scale bar: 1 μ m.

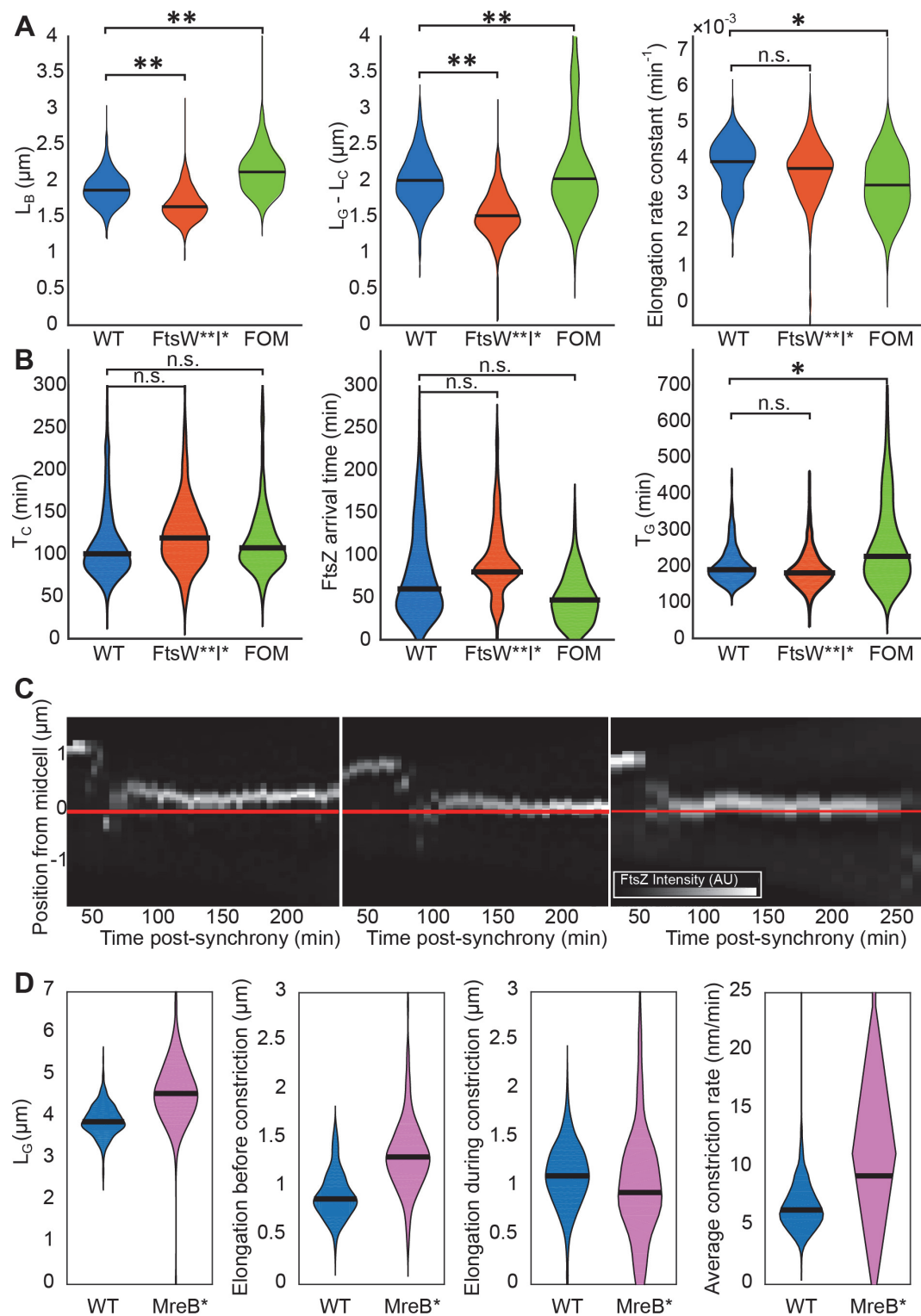


Figure A-2: Differences in size and elongation rate between populations.

A) From left to right: Violin plots distributions of length at birth, violin plots distributions of total elongation, violin plots distributions of elongation rate constant. **B**) From left to right: Violin plots distributions of onset of constriction, violin plots distributions of FtsZ arrival time and violin plots distributions of generation time for the WT, FtsW**I* and fosfomycin treated WT populations. Black horizontal bars represent the median. N: for **(A-B)**: WT: 406, FtsW**I*: 357, FOM: 203, for Significance: **: p < 0.005, *: p < 0.05, n.s.: not significant. **C**) Kymographs of representative cells: FtsZ-GFP intensity distribution along the cell's length (vertical axis), versus cell cycle time (horizontal axis). **D**) From left to right: Violin plots comparison of WT versus MreB* mutant comparison of Length at division, elongation before constriction, elongation during constriction, average constriction rate, N WT: 406, MreB*: 176

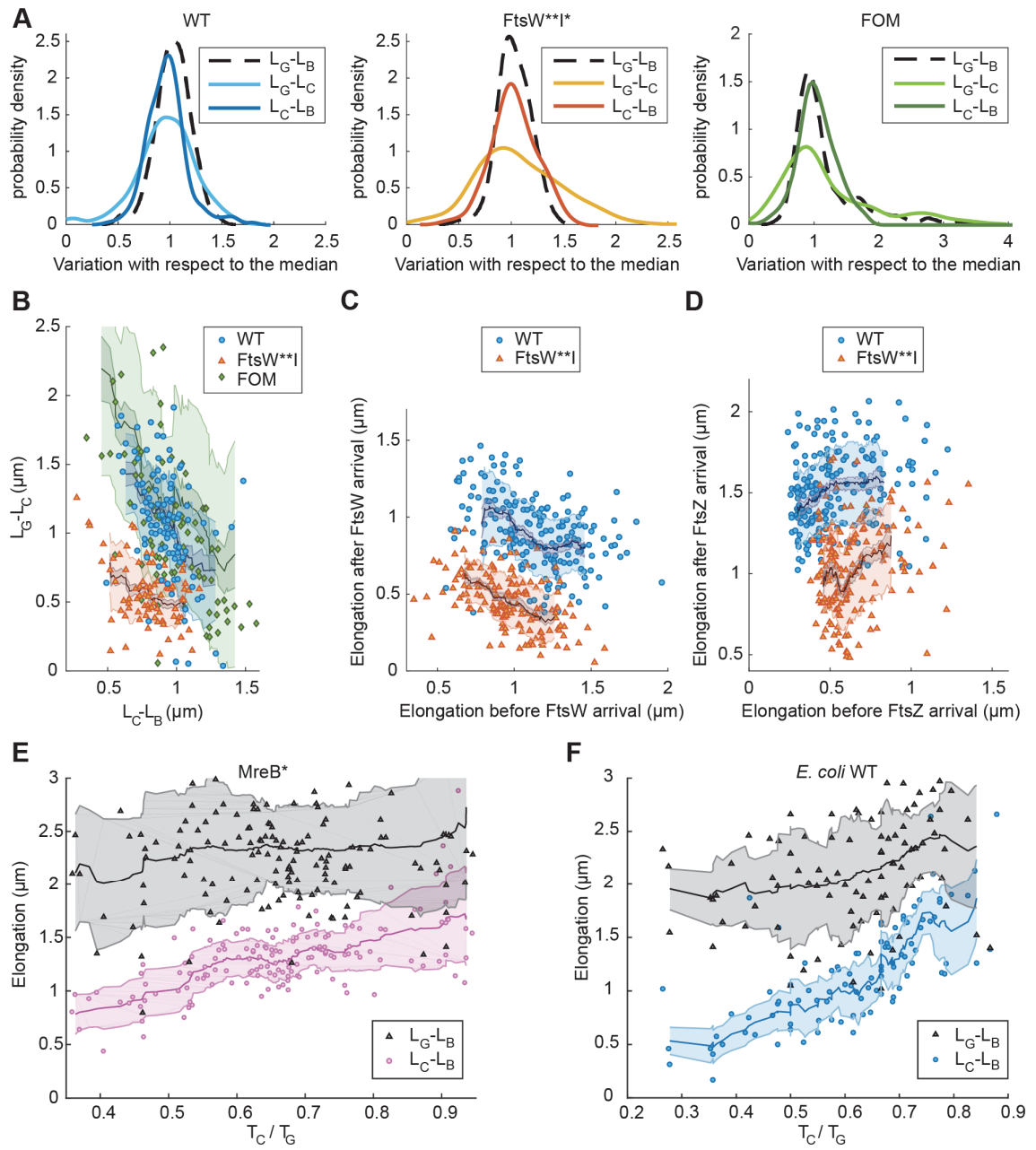


Figure A-3: Constriction rate drives compensation between LG-LC and LC-LB.

A) Variance in total elongation is smaller than the sum of the variance in elongation before and during constriction. Distribution of the measured elongation divided by median elongation. Onset defined by FtsW arrival. The variance of the sum of independent normal random variable a and b is equal to the sum of the variance: $\sigma_{a+b}^2 = \sigma_a^2 + \sigma_b^2$ where a and b are the elongation before and during constriction respectively. $\sigma_a^2 + \sigma_b^2$ is $0.144 \mu\text{m}^2$ for the WT, $0.080 \mu\text{m}^2$ for FtsW**I* and $1.26 \mu\text{m}^2$ for FOM, which is significantly higher than σ_{a+b}^2 measured from the final total elongation distribution, which is $0.101 \mu\text{m}^2$ for WT, $0.045 \mu\text{m}^2$ for FtsW**I* and $1.04 \mu\text{m}^2$ for FOM. **B)** Scatterplot showing the elongation during constriction versus the elongation before constriction. Spearman correlation coefficients are: WT: $r = -0.44$, FtsW**I*: $r = -0.32$, FOM: $r = -0.52$. **C)** Scatterplot of elongation during constriction versus before constriction onset. Spearman correlation: WT: $r = -0.44$, p-value < 0.005, FtsW**I*: $r = -0.49$, p-value < 0.005. **D)** Scatterplot of elongation after versus before FtsZ arrival. Spearman correlation: WT: $\text{Rho} = 0.20$, p < 0.005, Mut: $r = 0.26$, p-value < 0.005. **E)** Total elongation (gray) and elongation before constriction (color) for individual *MreB** mutant cells, as a function of normalized onset time (T_C/T_G). **F)** Total elongation (gray) and elongation before constriction (color) for individual *E. coli* cells, as a function of normalized onset time (T_C/T_G). Dark lines in **(B-F)** represent the 20 cells moving average; the shaded zones represent the moving standard deviation. Extreme outliers, deviating by more than two standard deviations have been omitted for the calculation of the moving average.

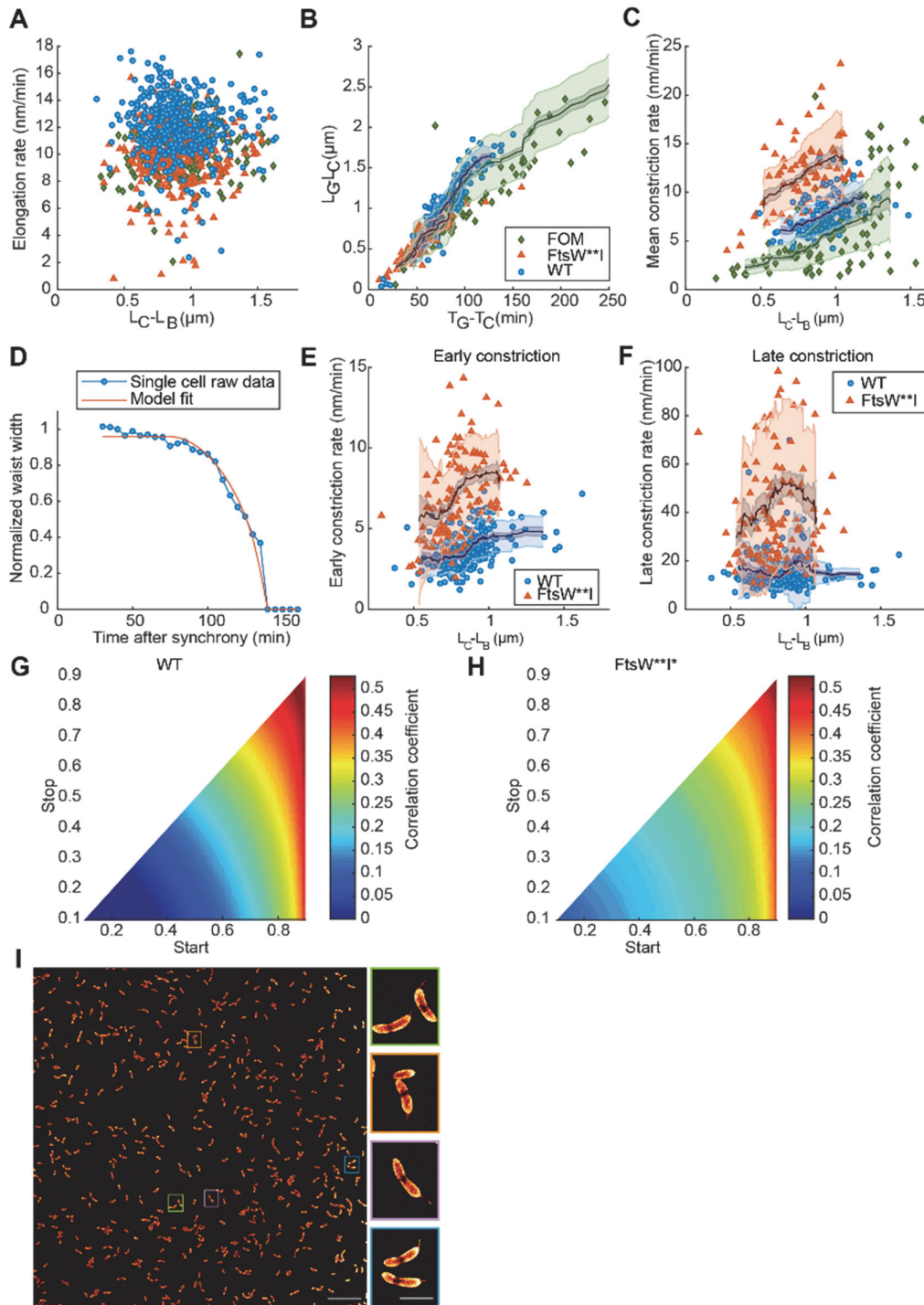


Figure A-4: Constriction rate shows influence of elongation before constriction decreases throughout constriction.

A) Elongation rate during constriction is not responsible for compensation: Overall elongation rate during constriction versus elongation rate before constriction. Constriction onset is defined by visible constriction. N and Spearman's correlation coefficient: WT: N = 408, $r = -0.11$, p-value = 0.026, FtsW**I*: N = 358, $r = -0.023$, p-value = 0.67, FOM: N = 215, $r = 0.30$, p-value = 7×10^{-6} . **B)** Elongation during constriction versus the duration of constriction. Spearman correlation coefficients: WT: $r = 0.90$, FtsW**I*: $r = 0.85$, FOM: $r = 0.94$. N: WT: 96, FtsW**I*: 80, FOM: 102. **C)** Mean constriction rate versus elongation before constriction. Spearman Correlation coefficients: WT: $r = 0.49$ p-value < 0.005, FtsW**I*: $r = 0.46$, p-value < 0.005. N: WT: 96, FtsW**I*: 80, FOM: 102. **D)** Example of a single cell normalized waist width versus time, fit with

the empirical constriction model. **E**) Early constriction rate, (supplemental note 2), in function of elongation before constriction. Early constriction rate is defined as the having a normalized waist width between 0.9 and 0.6. **F**) Late constriction rate as a function of elongation before constriction. Late constriction rate is defined as the difference of diameter over the duration of the constriction, during late stage constriction from a normalized waist width of 60% to 30%. **F**) WT: $r = 0.11$, $p\text{-value} = 0.13$, FtsW**I*: $r = 0.20$, $p\text{-value} = 0.03$. **G**) Heatmap of correlation coefficient between elongation before constriction and constriction rate, as a function of over which portion of constriction the constriction rate is calculated. As in **(E)** and **(F)**, the correlation between elongation before constriction and constriction rate was calculated. This was repeated for the constriction rate during various sub-periods of the constriction process, defined by the normalized waist width at the "start" and "stop" of the sub-period. See also Transparent Methods, Empirical constriction model. **H**) Same as **(G)**, but for FtsW**I*. Dark lines in **(B, C, E and F)** represent the 20 cells moving average; the shaded zones represent the moving standard deviation. Extreme outliers, deviating by more than two standard deviations have been omitted for the calculation of the moving average. **I**) STORM image of fixed *C. crescentus* cells stained with fluorescent wheat germ agglutinin, Right panels: Magnified views of the bacteria colors correspond to the area selected on the left panel. We used WGA-Alexa647 conjugated dye to stain *C. crescentus* cell wall. Scale bars 10 μm (Left panel), and 1 μm (Right panels).

References

- Aaron, Michelle, Godefroid Charbon, Hubert Lam, Heinz Schwarz, Waldemar Vollmer, and Christine Jacobs-Wagner. 2007. "The Tubulin Homologue FtsZ Contributes to Cell Elongation by Guiding Cell Wall Precursor Synthesis in *Caulobacter Crescentus*." *Molecular Microbiology* 64 (4): 938–52. <https://doi.org/10.1111/j.1365-2958.2007.05720.x>.
- Aarsman, Mirjam E. G., André Piette, Claudine Fraipont, Thessa M. F. Vinkenvleugel, Martine Nguyen-Distèche, and Tanneke den Blaauwen. 2005. "Maturation of the *Escherichia Coli* Divisome Occurs in Two Steps." *Molecular Microbiology* 55 (6): 1631–45. <https://doi.org/10.1111/j.1365-2958.2005.04502.x>.
- Adam, M., C. Fraipont, N. Rhazi, M. Nguyen-Distèche, B. Lakaye, J. M. Frère, B. Devreese, et al. 1997. "The Bimodular G57-V577 Polypeptide Chain of the Class B Penicillin-Binding Protein 3 of *Escherichia Coli* Catalyzes Peptide Bond Formation from Thioesters and Does Not Catalyze Glycan Chain Polymerization from the Lipid II Intermediate." *Journal of Bacteriology* 179 (19): 6005–9. <https://doi.org/10.1128/jb.179.19.6005-6009.1997>.
- Adams, David William, Ling Juan Wu, and Jeff Errington. 2014. "Cell Cycle Regulation by the Bacterial Nucleoid." *Current Opinion in Microbiology, Growth and development: eukaryotes/prokaryotes*, 22 (December): 94–101. <https://doi.org/10.1016/j.mib.2014.09.020>.
- Agirrezabala, Xabier, Israel S. Fernández, Ann C. Kelley, David Gil Cartón, Venki Ramakrishnan, and Mikel Valle. 2013. "The Ribosome Triggers the Stringent Response by RelA via a Highly Distorted TRNA." *EMBO Reports* 14 (9): 811–16. <https://doi.org/10.1038/embor.2013.106>.
- Ahn, K., and A. Kornberg. 1990. "Polyphosphate Kinase from *Escherichia Coli*. Purification and Demonstration of a Phosphoenzyme Intermediate." *Journal of Biological Chemistry* 265 (20): 11734–39.
- Amado, Luciana, and Andrei Kuzminov. 2009. "Polyphosphate Accumulation in *Escherichia Coli* in Response to Defects in DNA Metabolism." *Journal of Bacteriology* 191 (24): 7410–16. <https://doi.org/10.1128/JB.01138-09>.
- Amir, Ariel. 2014. "Cell Size Regulation in Bacteria." *Physical Review Letters* 112 (20): 208102. <https://doi.org/10.1103/PhysRevLett.112.208102>.
- . 2017. "Point of View: Is Cell Size a Spandrel?" *ELife*. January 19, 2017. <https://doi.org/10.7554/eLife.22186>.
- Anderson, A. J., and E. A. Dawes. 1990. "Occurrence, Metabolism, Metabolic Role, and Industrial Uses of Bacterial Polyhydroxyalkanoates." *Microbiology and Molecular Biology Reviews* 54 (4): 450–72.
- Annibale, Paolo, Stefano Vanni, Marco Scarselli, Ursula Rothlisberger, and Aleksandra Radenovic. 2011. "Quantitative Photo Activated Localization Microscopy: Unraveling the Effects of Photoblinking." *PLOS ONE* 6 (7): e22678. <https://doi.org/10.1371/journal.pone.0022678>.
- Asakura, Sho, and Fumio Oosawa. 1958. "Interaction between Particles Suspended in Solutions of Macromolecules." *Journal of Polymer Science* 33 (126): 183–92. <https://doi.org/10.1002/pol.1958.1203312618>.
- Ault-Riché, Dana, Cresson D. Fraley, Chi-Meng Tzeng, and Arthur Kornberg. 1998. "Novel Assay Reveals Multiple Pathways Regulating Stress-Induced Accumulations of Inorganic Polyphosphate in *Escherichia Coli*." *Journal of Bacteriology* 180 (7): 1841–47.

References

- Badrinarayanan, Anjana, Tung B.K. Le, and Michael T. Laub. 2015. "Bacterial Chromosome Organization and Segregation." *Annual Review of Cell and Developmental Biology* 31 (1): 171–99. <https://doi.org/10.1146/annurev-cellbio-100814-125211>.
- Bailey, Matthew W., Paola Bisicchia, Boyd T. Warren, David J. Sherratt, and Jaan Männik. 2014. "Evidence for Divisome Localization Mechanisms Independent of the Min System and SlmA in Escherichia Coli." *PLoS Genet* 10 (8): e1004504. <https://doi.org/10.1371/journal.pgen.1004504>.
- Baker, Richard F., and Daniel C. Pease. 1949. "Sectioning of the Bacterial Cell for the Electron Microscope." *Nature* 163 (4138): 282. <https://doi.org/10.1038/163282a0>.
- Balzarotti, Francisco, Yvan Eilers, Klaus C. Gwosch, Arvid H. Gynnå, Volker Westphal, Fernando D. Stefani, Johan Elf, and Stefan W. Hell. 2017. "Nanometer Resolution Imaging and Tracking of Fluorescent Molecules with Minimal Photon Fluxes." *Science* 355 (6325): 606–12. <https://doi.org/10.1126/science.aak9913>.
- Banerjee, Shiladitya, Klevin Lo, Matthew K. Daddysman, Alan Selewa, Thomas Kuntz, Aaron R. Dinner, and Norbert F. Scherer. 2017. "Biphasic Growth Dynamics Control Cell Division in Caulobacter Crescentus." *Nature Microbiology* 2 (July): 17116. <https://doi.org/10.1038/nmicrobiol.2017.116>.
- Barker, Melanie M, Tamas Gaal, and Richard L Gourse. 2001. "Mechanism of Regulation of Transcription Initiation by PpGpp. II. Models for Positive Control Based on Properties of RNAP Mutants and Competition for RNAP." *Journal of Molecular Biology* 305 (4): 689–702. <https://doi.org/10.1006/jmbi.2000.4328>.
- Barker, Melanie M., Tamas Gaal, Cathleen A. Josaitis, and Richard L. Gourse. 2001. "Mechanism of Regulation of Transcription Initiation by PpGpp. I. Effects of PpGpp on Transcription Initiation in Vivo and in Vitro." *Journal of Molecular Biology* 305 (4): 673–88. <https://doi.org/10.1006/jmbi.2000.4327>.
- Barreteau, H el ene, Andreja Kova c, Audrey Boniface, Matej Sova, Stanislav Gobec, and Didier Blanot. 2008. "Cytoplasmic Steps of Peptidoglycan Biosynthesis." *FEMS Microbiology Reviews* 32 (2): 168–207. <https://doi.org/10.1111/j.1574-6976.2008.00104.x>.
- Bates, David, and Nancy Kleckner. 2005. "Chromosome and Replisome Dynamics in E. Coli: Loss of Sister Cohesion Triggers Global Chromosome Movement and Mediates Chromosome Segregation." *Cell* 121 (6): 899–911. <https://doi.org/10.1016/j.cell.2005.04.013>.
- Battesti, Aurelia, Nadim Majdalani, and Susan Gottesman. 2011. "The RpoS-Mediated General Stress Response in Escherichia Coli." *Annual Review of Microbiology* 65 (1): 189–213. <https://doi.org/10.1146/annurev-micro-090110-102946>.
- Beaufay, Fran ois, J er me Coppine, Aur elie Mayard, G eraldine Laloux, Xavier De Bolle, and R egis Hallez. 2015. "A NAD-dependent Glutamate Dehydrogenase Coordinates Metabolism with Cell Division in Caulobacter Crescentus." *The EMBO Journal* 34 (13): 1786–1800. <https://doi.org/10.15252/emboj.201490730>.
- Bergkessel, Megan, David W. Basta, and Dianne K. Newman. 2016. "The Physiology of Growth Arrest: Uniting Molecular and Environmental Microbiology." *Nature Reviews Microbiology* 14 (9): 549–62. <https://doi.org/10.1038/nrmicro.2016.107>.
- Bernhardt, Thomas G., and Piet A. J. de Boer. 2005. "SlmA, a Nucleoid-Associated, FtsZ Binding Protein Required for Blocking Septal Ring Assembly over Chromosomes in E. Coli." *Molecular Cell* 18 (5): 555–64. <https://doi.org/10.1016/j.molcel.2005.04.012>.
- Betzig, Eric, George H. Patterson, Rachid Sougrat, O. Wolf Lindwasser, Scott Olenych, Juan S. Bonifacino, Michael W. Davidson, Jennifer Lippincott-Schwartz, and Harald F. Hess. 2006. "Imaging Intracellular Fluorescent Proteins at Nanometer Resolution." *Science* 313 (5793): 1642–45. <https://doi.org/10.1126/science.1127344>.

References

- Beveridge, T.J. 1988. "The Bacterial Surface: General Considerations towards Design and Function." *Canadian Journal of Microbiology* 34 (4): 363–72.
- Bi, Erfei, and Joe Lutkenhaus. 1991. "FtsZ Ring Structure Associated with Division in *Escherichia Coli*." *Nature* 354 (6349): 161–64. <https://doi.org/10.1038/354161a0>.
- . 1993. "Cell Division Inhibitors SulA and MinCD Prevent Formation of the FtsZ Ring." *Journal of Bacteriology* 175 (4): 1118–25. <https://doi.org/10.1128/jb.175.4.1118-1125.1993>.
- Billings, Gabriel, Nikolay Ouzounov, Tristan Ursell, Samantha M. Desmarais, Joshua Shaevitz, Zemer Gitai, and Kerwyn Casey Huang. 2014. "De Novo Morphogenesis in L-Forms via Geometric Control of Cell Growth." *Molecular Microbiology* 93 (5): 883–96. <https://doi.org/10.1111/mmi.12703>.
- Bisson-Filho, Alexandre W., Yen-Pang Hsu, Georgia R. Squyres, Erkin Kuru, Fabai Wu, Calum Jukes, Yingjie Sun, et al. 2017. "Treadmilling by FtsZ Filaments Drives Peptidoglycan Synthesis and Bacterial Cell Division." *Science* 355 (6326): 739–43. <https://doi.org/10.1126/science.aak9973>.
- Blaauwen, Tanneke den, Leendert W Hamoen, and Petra Anne Levin. 2017. "The Divisome at 25: The Road Ahead." *Current Opinion in Microbiology*, Cell regulation, 36 (April): 85–94. <https://doi.org/10.1016/j.mib.2017.01.007>.
- Boutte, Cara C., Jonathan T. Henry, and Sean Crosson. 2012. "PpGpp and Polyphosphate Modulate Cell Cycle Progression in *Caulobacter Crescentus*." *Journal of Bacteriology* 194 (1): 28–35. <https://doi.org/10.1128/JB.05932-11>.
- Bresan, Stephanie, Anna Sznajder, Waldemar Hauf, Karl Forchhammer, Daniel Pfeiffer, and Dieter Jendrossek. 2016. "Polyhydroxyalkanoate (PHA) Granules Have No Phospholipids." *Scientific Reports* 6 (May): 26612. <https://doi.org/10.1038/srep26612>.
- Buss, Jackson, Carla Coltharp, Gleb Shtengel, Xinxing Yang, Harald Hess, and Jie Xiao. 2015. "A Multi-Layered Protein Network Stabilizes the *Escherichia Coli* FtsZ-Ring and Modulates Constriction Dynamics." *PLoS Genet* 11 (4): e1005128. <https://doi.org/10.1371/journal.pgen.1005128>.
- Campos, Manuel, Ivan V. Surovtsev, Setsu Kato, Ahmad Paintdakhi, Bruno Beltran, Sarah E. Ebmeier, and Christine Jacobs-Wagner. 2014. "A Constant Size Extension Drives Bacterial Cell Size Homeostasis." *Cell* 159 (6): 1433–46. <https://doi.org/10.1016/j.cell.2014.11.022>.
- Chatterji, Dipankar, and Anil Kumar Ojha. 2001. "Revisiting the Stringent Response, PpGpp and Starvation Signaling." *Current Opinion in Microbiology* 4 (2): 160–65. [https://doi.org/10.1016/S1369-5274\(00\)00182-X](https://doi.org/10.1016/S1369-5274(00)00182-X).
- Chiancone, Emilia, and Pierpaolo Ceci. 2010. "The Multifaceted Capacity of Dps Proteins to Combat Bacterial Stress Conditions: Detoxification of Iron and Hydrogen Peroxide and DNA Binding." *Biochimica et Biophysica Acta (BBA) - General Subjects*, Ferritin: Structures, Properties and Applications, 1800 (8): 798–805. <https://doi.org/10.1016/j.bbagen.2010.01.013>.
- Chowdhury, Chiranjit, Sharmistha Sinha, Sunny Chun, Todd O. Yeates, and Thomas A. Bobik. 2014. "Diverse Bacterial Microcompartment Organelles." *Microbiol. Mol. Biol. Rev.* 78 (3): 438–68. <https://doi.org/10.1128/MMBR.00009-14>.
- Colavin, Alexandre, Handuo Shi, and Kerwyn Casey Huang. 2018. "RodZ Modulates Geometric Localization of the Bacterial Actin MreB to Regulate Cell Shape." *Nature Communications* 9 (1): 1280. <https://doi.org/10.1038/s41467-018-03633-x>.
- Coltharp, Carla, Jackson Buss, Trevor M. Plumer, and Jie Xiao. 2016. "Defining the Rate-Limiting Processes of Bacterial Cytokinesis." *Proceedings of the National Academy of Sciences*, February, 201514296. <https://doi.org/10.1073/pnas.1514296113>.

References

- Cooper, Stephen, and Charles E. Helmstetter. 1968. "Chromosome Replication and the Division Cycle of *Escherichia Coli* Br." *Journal of Molecular Biology* 31 (3): 519–40. [https://doi.org/10.1016/0022-2836\(68\)90425-7](https://doi.org/10.1016/0022-2836(68)90425-7).
- Couce, Alejandro, Alejandra Briales, Alexandro Rodríguez-Rojas, Coloma Costas, Álvaro Pascual, and Jesús Blázquez. 2012. "Genome-Wide Overexpression Screen for Fosfomycin Resistance in *Escherichia Coli*: MurA Confers Clinical Resistance at Low Fitness Cost." *Antimicrobial Agents and Chemotherapy*, February, AAC.06122-11. <https://doi.org/10.1128/AAC.06122-11>.
- Crooke, E., M. Akiyama, Narayana N. Rao, and Arthur Kornberg. 1994. "Genetically Altered Levels of Inorganic Polyphosphate in *Escherichia Coli*." *Journal of Biological Chemistry* 269 (9): 6290–95.
- De Nobili, M, M Contin, C Mondini, and P. C Brookes. 2001. "Soil Microbial Biomass Is Triggered into Activity by Trace Amounts of Substrate." *Soil Biology and Biochemistry* 33 (9): 1163–70. [https://doi.org/10.1016/S0038-0717\(01\)00020-7](https://doi.org/10.1016/S0038-0717(01)00020-7).
- Dedecker, Peter, Frans C. De Schryver, and Johan Hofkens. 2013. "Fluorescent Proteins: Shine on, You Crazy Diamond." *Journal of the American Chemical Society* 135 (7): 2387–2402. <https://doi.org/10.1021/ja309768d>.
- den Blaauwen, T., L.W. Hamoen, and P.A. Levin. 2017. "The Divisome at 25: The Road Ahead." *Current Opinion in Microbiology* 36: 85–94. <https://doi.org/10.1016/j.mib.2017.01.007>.
- Dillon, Shane C., and Charles J. Dorman. 2010. "Bacterial Nucleoid-Associated Proteins, Nucleoid Structure and Gene Expression." *Nature Reviews Microbiology* 8 (3): 185–95. <https://doi.org/10.1038/nrmicro2261>.
- Dion, Michael, Mrinal Kapoor, Yingjie Sun, Sean Wilson, Joel Ryan, Antoine Vigouroux, Sven van Teeffelen, Rudolf Oldenbourg, and Ethan C. Garner. 2018. "Cell Diameter in *Bacillus Subtilis* Is Determined by the Opposing Actions of Two Distinct Cell Wall Synthetic Systems." *BioRxiv*, August, 392837. <https://doi.org/10.1101/392837>.
- Domínguez-Escobar, Julia, Arnaud Chastanet, Alvaro H. Crevenna, Vincent Fromion, Roland Wedlich-Söldner, and Rut Carballido-López. 2011. "Processive Movement of MreB-Associated Cell Wall Biosynthetic Complexes in Bacteria." *Science* 333 (6039): 225–28. <https://doi.org/10.1126/science.1203466>.
- Donachie, W. D. 1968. "Relationship between Cell Size and Time of Initiation of DNA Replication." *Nature* 219 (5158): 1077–79. <https://doi.org/10.1038/2191077a0>.
- Donachie, W.D., and K.J. Begg. 1989. "Cell Length, Nucleoid Separation, and Cell Division of Rod-Shaped and Spherical Cells of *Escherichia Coli*." *Journal of Bacteriology* 171 (9): 4633–39.
- Douglass, K.M., C. Sieben, A. Archetti, A. Lambert, and S. Manley. 2016. "Super-Resolution Imaging of Multiple Cells by Optimized Flat-Field Epi-Illumination." *Nature Photonics* 10 (11): 705–8. <https://doi.org/10.1038/nphoton.2016.200>.
- Dubochet, J., A. W. McDowell, B. Menge, E. N. Schmid, and K. G. Lickfeld. 1983. "Electron Microscopy of Frozen-Hydrated Bacteria." *Journal of Bacteriology* 155 (1): 381–90.
- Durfee, Tim, Anne-Marie Hansen, Huijun Zhi, Frederick R. Blattner, and Ding Jun Jin. 2008. "Transcription Profiling of the Stringent Response in *Escherichia Coli*." *Journal of Bacteriology* 190 (3): 1084–96. <https://doi.org/10.1128/JB.01092-07>.
- Edelstein, Arthur D., Mark A. Tsuchida, Nenad Amodaj, Henry Pinkard, Ronald D. Vale, and Nico Stuurman. 2014. "Advanced Methods of Microscope Control Using MManager Software." *Journal of Biological Methods* 1 (2): e10. <https://doi.org/10.14440/jbm.2014.36>.

References

- Eisenbeis, Simone, Stefanie Lohmiller, Marianne Valdebenito, Stefan Leicht, and Volkmar Braun. 2008. "NagA-Dependent Uptake of N-Acetyl-Glucosamine and N-Acetyl-Chitin Oligosaccharides across the Outer Membrane of *Caulobacter Crescentus*." *Journal of Bacteriology* 190 (15): 5230–38. <https://doi.org/10.1128/JB.00194-08>.
- English, Brian P., Vasili Haurlyliuk, Arash Sanamrad, Stoyan Tankov, Nynke H. Dekker, and Johan Elf. 2011. "Single-Molecule Investigations of the Stringent Response Machinery in Living Bacterial Cells." *Proceedings of the National Academy of Sciences* 108 (31): E365–73. <https://doi.org/10.1073/pnas.1102255108>.
- Erickson, Harold P. 1995. "FtsZ, a Prokaryotic Homolog of Tubulin?" *Cell* 80 (3): 367–70.
- . 1997. "FtsZ, a Tubulin Homologue in Prokaryote Cell Division." *Trends in Cell Biology* 7 (9): 362–67. [https://doi.org/10.1016/S0962-8924\(97\)01108-2](https://doi.org/10.1016/S0962-8924(97)01108-2).
- Erickson, Harold P., David E. Anderson, and Masaki Osawa. 2010. "FtsZ in Bacterial Cytokinesis: Cytoskeleton and Force Generator All in One." *Microbiology and Molecular Biology Reviews* 74 (4): 504–28. <https://doi.org/10.1128/MMBR.00021-10>.
- Espéli, Olivier, Romain Borne, Pauline Dupaigne, Axel Thiel, Emmanuelle Gigant, Romain Mercier, and Frédéric Boccard. 2012. "A MatP-Divisome Interaction Coordinates Chromosome Segregation with Cell Division in *E. Coli*." *The EMBO Journal* 31 (14): 3198–3211. <https://doi.org/10.1038/emboj.2012.128>.
- Evinger, M., and N. Agabian. 1977. "Envelope-Associated Nucleoid from *Caulobacter Crescentus* Stalked and Swarmer Cells." *Journal of Bacteriology* 132 (1): 294–301.
- Fu, Guo, Tao Huang, Jackson Buss, Carla Coltharp, Zach Hensel, and Jie Xiao. 2010. "In Vivo Structure of the *E. Coli* FtsZ-Ring Revealed by Photoactivated Localization Microscopy (PALM)." *PLoS ONE* 5 (9): e12680. <https://doi.org/10.1371/journal.pone.0012680>.
- Gahlmann, Andreas, and W. E. Moerner. 2014. "Exploring Bacterial Cell Biology with Single-Molecule Tracking and Super-Resolution Imaging." *Nature Reviews Microbiology* 12 (1): 9–22. <https://doi.org/10.1038/nrmicro3154>.
- Gamba, Pamela, Jan-Willem Veening, Nigel J. Saunders, Leendert W. Hamoen, and Richard A. Daniel. 2009. "Two-Step Assembly Dynamics of the *Bacillus Subtilis* Divisome." *Journal of Bacteriology* 191 (13): 4186–94. <https://doi.org/10.1128/JB.01758-08>.
- Garcia, Hernan E., Ricardo. A. Locarnini, Timothy P. Boyer, John I. Antonov, Olga K. Baranova, Melissa M. Zweng, James R. Reagan, and Daphne R. Johnson. 2013. "World Ocean Atlas 2013. Vol. 4: Dissolved Inorganic Nutrients (Phosphate, Nitrate, Silicate)." Technical Ed. NOAA Atlas NESDIS. https://data.nodc.noaa.gov/woa/WOA13/DOC/woa13_vol4.pdf.
- Garner, Ethan C., Remi Bernard, Wenqin Wang, Xiaowei Zhuang, David Z. Rudner, and Tim Mitchison. 2011. "Coupled, Circumferential Motions of the Cell Wall Synthesis Machinery and MreB Filaments in *B. Subtilis*." *Science* 333 (6039): 222–25. <https://doi.org/10.1126/science.1203285>.
- Godin, Michel, Francisco Feijó Delgado, Sungmin Son, William H. Grover, Andrea K. Bryan, Amit Tzur, Paul Jorgensen, et al. 2010. "Using Buoyant Mass to Measure the Growth of Single Cells." *Nature Methods* 7 (5): 387–90. <https://doi.org/10.1038/nmeth.1452>.
- Goley, Erin D., Luis R. Comolli, Katherine E. Fero, Kenneth H. Downing, and Lucy Shapiro. 2010. "DipM Links Peptidoglycan Remodeling to Outer Membrane Organization in *Caulobacter*." *Molecular Microbiology* 77 (1): 56–73. <https://doi.org/10.1111/j.1365-2958.2010.07222.x>.
- Goley, Erin D., Yi-Chun Yeh, Sun-Hae Hong, Michael J. Fero, Eduardo Abeliuk, Harley H. McAdams, and Lucy Shapiro. 2011. "Assembly of the *Caulobacter* Cell Division Machine." *Molecular Microbiology* 80 (6): 1680–98. <https://doi.org/10.1111/j.1365-2958.2011.07677.x>.

References

- Gray, Michael J, and Ursula Jakob. 2015. "Oxidative Stress Protection by Polyphosphate—New Roles for an Old Player." *Current Opinion in Microbiology*, Cell regulation, 24 (April): 1–6. <https://doi.org/10.1016/j.mib.2014.12.004>.
- Guizar-Sicairos, Manuel, Samuel T. Thurman, and James R. Fienup. 2008. "Efficient Subpixel Image Registration Algorithms." *Optics Letters* 33 (2): 156–58. <https://doi.org/10.1364/OL.33.000156>.
- Gustafsson, M. G. L. 2000. "Surpassing the Lateral Resolution Limit by a Factor of Two Using Structured Illumination Microscopy." *Journal of Microscopy* 198 (2): 82–87. <https://doi.org/10.1046/j.1365-2818.2000.00710.x>.
- Gustafsson, Mats G. L., Lin Shao, Peter M. Carlton, C. J. Rachel Wang, Inna N. Golubovskaya, W. Zacheus Cande, David A. Agard, and John W. Sedat. 2008. "Three-Dimensional Resolution Doubling in Wide-Field Fluorescence Microscopy by Structured Illumination." *Biophysical Journal* 94 (12): 4957–70. <https://doi.org/10.1529/biophysj.107.120345>.
- Hacker, William C., Shuxiang Li, and Adrian H. Elcock. 2017. "Features of Genomic Organization in a Nucleotide-Resolution Molecular Model of the Escherichia Coli Chromosome." *Nucleic Acids Research* 45 (13): 7541–54. <https://doi.org/10.1093/nar/gkx541>.
- Harris, Leigh K., and Julie A. Theriot. 2016. "Relative Rates of Surface and Volume Synthesis Set Bacterial Cell Size." *Cell* 165 (6): 1479–92. <https://doi.org/10.1016/j.cell.2016.05.045>.
- Harry, E. J., J. Rodwell, and R. G. Wake. 1999. "Co-Ordinating DNA Replication with Cell Division in Bacteria: A Link between the Early Stages of a Round of Replication and Mid-Cell Z Ring Assembly." *Molecular Microbiology* 33 (1): 33–40. <https://doi.org/10.1046/j.1365-2958.1999.01439.x>.
- Hartl, Johannes, Patrick Kiefer, Fabian Meyer, and Julia A. Vorholt. 2017. "Longevity of Major Coenzymes Allows Minimal de Novo Synthesis in Microorganisms." *Nature Microbiology* 2 (7): 17073. <https://doi.org/10.1038/nmicrobiol.2017.73>.
- Hearn, E. J. 1997. *Mechanics of Materials Volume 1: An Introduction to the Mechanics of Elastic and Plastic Deformation of Solids and Structural Materials*. Elsevier.
- Heilemann, Mike, Sebastian van de Linde, Mark Schüttelpelz, Robert Kasper, Britta Seefeldt, Anindita Mukherjee, Philip Tinnefeld, and Markus Sauer. 2008. "Subdiffraction-Resolution Fluorescence Imaging with Conventional Fluorescent Probes." *Angewandte Chemie International Edition* 47 (33): 6172–76. <https://doi.org/10.1002/anie.200802376>.
- Hell, Stefan W., and Jan Wichmann. 1994. "Breaking the Diffraction Resolution Limit by Stimulated Emission: Stimulated-Emission-Depletion Fluorescence Microscopy." *Optics Letters* 19 (11): 780–82. <https://doi.org/10.1364/OL.19.000780>.
- Henry, Jonathan T., Sean Crosson, and Fred Chang. 2013. "Chromosome Replication and Segregation Govern the Biogenesis and Inheritance of Inorganic Polyphosphate Granules." *Molecular Biology of the Cell* 24 (20): 3177–86. <https://doi.org/10.1091/mbc.e13-04-0182>.
- Hess, Samuel T., Thanu P. K. Girirajan, and Michael D. Mason. 2006. "Ultra-High Resolution Imaging by Fluorescence Photoactivation Localization Microscopy." *Biophysical Journal* 91 (11): 4258–72. <https://doi.org/10.1529/biophysj.106.091116>.
- Hill, Norbert S., Paul J. Buske, Yue Shi, and Petra Anne Levin. 2013. "A Moonlighting Enzyme Links Escherichia Coli Cell Size with Central Metabolism." *PLoS Genet* 9 (7): e1003663. <https://doi.org/10.1371/journal.pgen.1003663>.
- Ho, Po-Yi, and Ariel Amir. 2015. "Simultaneous Regulation of Cell Size and Chromosome Replication in Bacteria." *Frontiers in Microbiology* 6. <https://doi.org/10.3389/fmicb.2015.00662>.

References

- Holden, Seamus J., Thomas Pengo, Karin L. Meibom, Carmen Fernandez Fernandez, Justine Collier, and Suliana Manley. 2014. “High Throughput 3D Super-Resolution Microscopy Reveals *Caulobacter Crescentus* in Vivo Z-Ring Organization.” *Proceedings of the National Academy of Sciences* 111 (12): 4566–71. <https://doi.org/10.1073/pnas.1313368111>.
- Hu, Zonglin, and Joe Lutkenhaus. 1999. “Topological Regulation of Cell Division in *Escherichia Coli* Involves Rapid Pole to Pole Oscillation of the Division Inhibitor MinC under the Control of MinD and MinE.” *Molecular Microbiology* 34 (1): 82–90. <https://doi.org/10.1046/j.1365-2958.1999.01575.x>.
- Huang, Fang, Tobias M. P. Hartwich, Felix E. Rivera-Molina, Yu Lin, Whitney C. Duim, Jane J. Long, Pradeep D. Uchil, et al. 2013. “Video-Rate Nanoscopy Using SCMOS Camera-Specific Single-Molecule Localization Algorithms.” *Nature Methods* 10 (7): 653–58. <https://doi.org/10.1038/nmeth.2488>.
- Hussain, Saman, Carl N. Wivagg, Piotr Szwedziak, Felix Wong, Kaitlin Schaefer, Thierry Izoré, Lars D. Renner, et al. 2018. “MreB Filaments Align along Greatest Principal Membrane Curvature to Orient Cell Wall Synthesis.” *ELife*. February 22, 2018. <https://doi.org/10.7554/eLife.32471>.
- Ishige, Kazuya, Haiyu Zhang, and Arthur Kornberg. 2002. “Polyphosphate Kinase (PPK2), a Potent, Polyphosphate-Driven Generator of GTP.” *Proceedings of the National Academy of Sciences* 99 (26): 16684–88. <https://doi.org/10.1073/pnas.262655299>.
- Jaqaman, Khuloud, Dinah Loerke, Marcel Mettlen, Hirotaka Kuwata, Sergio Grinstein, Sandra L. Schmid, and Gaudenz Danuser. 2008. “Robust Single-Particle Tracking in Live-Cell Time-Lapse Sequences.” *Nature Methods* 5 (8): 695–702. <https://doi.org/10.1038/nmeth.1237>.
- Jones, Laura J. F., Rut Carballido-López, and Jeffery Errington. 2001. “Control of Cell Shape in Bacteria: Helical, Actin-like Filaments in *Bacillus Subtilis*.” *Cell* 104 (6): 913–22. [https://doi.org/10.1016/S0092-8674\(01\)00287-2](https://doi.org/10.1016/S0092-8674(01)00287-2).
- Jorgenson, Matthew A., Suresh Kannan, Mary E. Laubacher, and Kevin D. Young. 2016. “Dead-End Intermediates in the Enterobacterial Common Antigen Pathway Induce Morphological Defects in *Escherichia Coli* by Competing for Undecaprenyl Phosphate.” *Molecular Microbiology* 100 (1): 1–14. <https://doi.org/10.1111/mmi.13284>.
- Jun, Suckjoon, and Sattar Taheri-Araghi. 2015. “Cell-Size Maintenance: Universal Strategy Revealed.” *Trends in Microbiology* 23 (1): 4–6. <https://doi.org/10.1016/j.tim.2014.12.001>.
- Kahan, F.M., J.S. Kahan, P.J. Cassidy, and H. Kropp. 1974. “The Mechanism of Action of Fosfomycin (Phosphonomycin).” *Annals of the New York Academy of Sciences* 235 (1): 364–86. <https://doi.org/10.1111/j.1749-6632.1974.tb43277.x>.
- Katzmann, Emanuel, Frank D. Müller, Claus Lang, Maxim Messerer, Michael Winklhofer, Jürgen M. Plitzko, and Dirk Schüler. 2011. “Magnetosome Chains Are Recruited to Cellular Division Sites and Split by Asymmetric Septation.” *Molecular Microbiology* 82 (6): 1316–29. <https://doi.org/10.1111/j.1365-2958.2011.07874.x>.
- Kerfeld, Cheryl A., Sabine Heinhorst, and Gordon C. Cannon. 2010. “Bacterial Microcompartments.” *Annual Review of Microbiology* 64 (1): 391–408. <https://doi.org/10.1146/annurev.micro.112408.134211>.
- Khakimova, Malika, Heather G. Ahlgren, Joe J. Harrison, Ann M. English, and Dao Nguyen. 2013. “The Stringent Response Controls Catalases in *Pseudomonas Aeruginosa* and Is Required for Hydrogen Peroxide and Antibiotic Tolerance.” *Journal of Bacteriology* 195 (9): 2011–20. <https://doi.org/10.1128/JB.02061-12>.
- Kiefer, Patrick, Uwe Schmitt, Jonas E. N. Müller, Johannes Hartl, Fabian Meyer, Florian Ryffel, and Julia A. Vorholt. 2015. “DynaMet: A Fully Automated Pipeline for Dynamic

References

- LC-MS Data.” *Analytical Chemistry* 87 (19): 9679–86. <https://doi.org/10.1021/acs.analchem.5b01660>.
- Kiekebusch, Daniela, Katharine A. Michie, Lars-Oliver Essen, Jan Löwe, and Martin Thanbichler. 2012. “Localized Dimerization and Nucleoid Binding Drive Gradient Formation by the Bacterial Cell Division Inhibitor MipZ.” *Molecular Cell* 46 (3): 245–59. <https://doi.org/10.1016/j.molcel.2012.03.004>.
- Klar, Thomas A., Stefan Jakobs, Marcus Dyba, Alexander Egner, and Stefan W. Hell. 2000. “Fluorescence Microscopy with Diffraction Resolution Barrier Broken by Stimulated Emission.” *Proceedings of the National Academy of Sciences* 97 (15): 8206–10. <https://doi.org/10.1073/pnas.97.15.8206>.
- Koch, A. L. 1996. “What Size Should a Bacterium Be? A Question of Scale.” *Annual Review of Microbiology* 50: 317–48. <https://doi.org/10.1146/annurev.micro.50.1.317>.
- Koch, A. L., and M. Schaechter. 1962. “A Model for Statistics of the Cell Division Process.” *Microbiology* 29 (3): 435–54. <https://doi.org/10.1099/00221287-29-3-435>.
- Komeili, Arash, Zhuo Li, Dianne K. Newman, and Grant J. Jensen. 2006. “Magnetosomes Are Cell Membrane Invaginations Organized by the Actin-Like Protein MamK.” *Science* 311 (5758): 242–45. <https://doi.org/10.1126/science.1123231>.
- Kornberg, Arthur, S. R. Kornberg, and Ernest S. Simms. 1956. “Metaphosphate Synthesis by an Enzyme from Escherichia Coli.” *Biochimica et Biophysica Acta* 20 (January): 215–27. [https://doi.org/10.1016/0006-3002\(56\)90280-3](https://doi.org/10.1016/0006-3002(56)90280-3).
- Kornberg, S. R. 1957. “Adenosine Triphosphate Synthesis from Polyphosphate by an Enzyme from Escherichia Coli.” *Biochimica et Biophysica Acta* 26 (2): 294–300. [https://doi.org/10.1016/0006-3002\(57\)90008-2](https://doi.org/10.1016/0006-3002(57)90008-2).
- Kuroda, Akio, Helen Murphy, Michael Cashel, and Arthur Kornberg. 1997. “Guanosine Tetra- and Pentaphosphate Promote Accumulation of Inorganic Polyphosphate in Escherichia Coli.” *Journal of Biological Chemistry* 272 (34): 21240–43. <https://doi.org/10.1074/jbc.272.34.21240>.
- Kuroda, Akio, Kazutaka Nomura, Ryo Ohtomo, Junichi Kato, Tsukasa Ikeda, Noboru Takiguchi, Hisao Ohtake, and Arthur Kornberg. 2001. “Role of Inorganic Polyphosphate in Promoting Ribosomal Protein Degradation by the Lon Protease in E. Coli.” *Science* 293 (5530): 705–8. <https://doi.org/10.1126/science.1061315>.
- Kuroda, Akio, Shoutaro Tanaka, Tsukasa Ikeda, Junichi Kato, Noboru Takiguchi, and Hisao Ohtake. 1999. “Inorganic Polyphosphate Kinase Is Required to Stimulate Protein Degradation and for Adaptation to Amino Acid Starvation in Escherichia Coli.” *Proceedings of the National Academy of Sciences* 96 (25): 14264–69. <https://doi.org/10.1073/pnas.96.25.14264>.
- Kuru, Erkin, H. Velocity Hughes, Pamela J. Brown, Edward Hall, Srinivas Tekkam, Felipe Cava, Miguel A. de Pedro, Yves V. Brun, and Michael S. VanNieuwenhze. 2012. “In Situ Probing of Newly Synthesized Peptidoglycan in Live Bacteria with Fluorescent D-Amino Acids.” *Angewandte Chemie International Edition* 51 (50): 12519–23. <https://doi.org/10.1002/anie.201206749>.
- Lambert, Ambroise, Aster Vanhecke, Anna Archetti, Seamus Holden, Felix Schaber, Zachary Pincus, Michael T. Laub, Erin Goley, and Suliana Manley. 2018. “Constriction Rate Modulation Can Drive Cell Size Control and Homeostasis in C. Crescentus.” *iScience* 4 (June): 180–89. <https://doi.org/10.1016/j.isci.2018.05.020>.
- Lange, R., D. Fischer, and R. Hengge-Aronis. 1995. “Identification of Transcriptional Start Sites and the Role of PpGpp in the Expression of RpoS, the Structural Gene for the Sigma S Subunit of RNA Polymerase in Escherichia Coli.” *Journal of Bacteriology* 177 (16): 4676–80. <https://doi.org/10.1128/jb.177.16.4676-4680.1995>.

References

- Lariviere, Patrick J., Piotr Szwedziak, Christopher R. Mahone, Jan Löwe, and Erin D. Goley. 2018. "FzIA, an Essential Regulator of FtsZ Filament Curvature, Controls Constriction Rate during Caulobacter Division." *Molecular Microbiology* 107 (2): 180–97. <https://doi.org/10.1111/mmi.13876>.
- Laub, M. T., H. H. McAdams, T. Feldblyum, C. M. Fraser, and L. Shapiro. 2000. "Global Analysis of the Genetic Network Controlling a Bacterial Cell Cycle." *Science (New York, N.Y.)* 290 (5499): 2144–48.
- Lavis, Luke D. 2017. "Chemistry Is Dead. Long Live Chemistry!" *Biochemistry* 56 (39): 5165–70. <https://doi.org/10.1021/acs.biochem.7b00529>.
- Le, Tung B. K., Maxim V. Imakaev, Leonid A. Mirny, and Michael T. Laub. 2013. "High-Resolution Mapping of the Spatial Organization of a Bacterial Chromosome." *Science* 342 (6159): 731–34. <https://doi.org/10.1126/science.1242059>.
- Lee, Philina S., and Alan D. Grossman. 2006. "The Chromosome Partitioning Proteins Soj (ParA) and Spo0J (ParB) Contribute to Accurate Chromosome Partitioning, Separation of Replicated Sister Origins, and Regulation of Replication Initiation in *Bacillus Subtilis*." *Molecular Microbiology* 60 (4): 853–69. <https://doi.org/10.1111/j.1365-2958.2006.05140.x>.
- Lee, T. K., C. Tropini, J. Hsin, S. M. Desmarais, T. S. Ursell, E. Gong, Z. Gitai, R. D. Monds, and K. C. Huang. 2014. "A Dynamically Assembled Cell Wall Synthesis Machinery Buffers Cell Growth." *Proceedings of the National Academy of Sciences* 111 (12): 4554–59. <https://doi.org/10.1073/pnas.1313826111>.
- Leitao, Ricardo M., and Douglas R. Kellogg. 2017. "The Duration of Mitosis and Daughter Cell Size Are Modulated by Nutrients in Budding Yeast." *J Cell Biol*, September, jcb.201609114. <https://doi.org/10.1083/jcb.201609114>.
- Li, Zhuo, Michael J Trimble, Yves V Brun, and Grant J Jensen. 2007. "The Structure of FtsZ Filaments in Vivo Suggests a Force-Generating Role in Cell Division." *The EMBO Journal* 26 (22): 4694–4708. <https://doi.org/10.1038/sj.emboj.7601895>.
- Liu, Kuanqing, Alycia N Bittner, and Jue D Wang. 2015. "Diversity in (p)PpGpp Metabolism and Effectors." *Current Opinion in Microbiology*, Cell regulation, 24 (April): 72–79. <https://doi.org/10.1016/j.mib.2015.01.012>.
- Liu, Zhe, Luke D. Lavis, and Eric Betzig. 2015. "Imaging Live-Cell Dynamics and Structure at the Single-Molecule Level." *Molecular Cell* 58 (4): 644–59. <https://doi.org/10.1016/j.molcel.2015.02.033>.
- Løbner-Olesen, Anders, Kirsten Skarstad, Flemming G. Hansen, Kaspar von Meyenburg, and Erik Boye. 1989. "The DnaA Protein Determines the Initiation Mass of *Escherichia Coli* K-12." *Cell* 57 (5): 881–89. [https://doi.org/10.1016/0092-8674\(89\)90802-7](https://doi.org/10.1016/0092-8674(89)90802-7).
- Logsdon, Michelle M., Po-Yi Ho, Kadamba Papavinasasundaram, Kirill Richardson, Murat Cokol, Christopher M. Sasseti, Ariel Amir, and Bree B. Aldridge. 2017. "A Parallel Adder Coordinates Mycobacterial Cell-Cycle Progression and Cell-Size Homeostasis in the Context of Asymmetric Growth and Organization." *Current Biology* 27 (21): 3367–3374.e7. <https://doi.org/10.1016/j.cub.2017.09.046>.
- Löwe, Jan, and Linda A. Amos. 1998. "Crystal Structure of the Bacterial Cell-Division Protein FtsZ." *Nature* 391 (6663): 203–6. <https://doi.org/10.1038/34472>.
- Ma, Xiaolan, David W. Ehrhardt, and William Margolin. 1996. "Colocalization of Cell Division Proteins FtsZ and FtsA to Cytoskeletal Structures in Living *Escherichia Coli* Cells by Using Green Fluorescent Protein." *Proceedings of the National Academy of Sciences* 93 (23): 12998–3. <https://doi.org/10.1073/pnas.93.23.12998>.

References

- MacCready, Joshua S., Pusparanee Hakim, Eric J. Young, Longhua Hu, Jian Liu, Katherine W. Osteryoung, Anthony G. Vecchiarelli, and Daniel C. Ducat. 2018. "Protein Gradients on the Nucleoid Position the Carbon-Fixing Organelles of Cyanobacteria." *BioRxiv*, May, 334813. <https://doi.org/10.1101/334813>.
- Manley, Suliana, Jennifer M. Gillette, George H. Patterson, Hari Shroff, Harald F. Hess, Eric Betzig, and Jennifer Lippincott-Schwartz. 2008. "High-Density Mapping of Single-Molecule Trajectories with Photoactivated Localization Microscopy." *Nature Methods* 5 (2): 155–57. <https://doi.org/10.1038/nmeth.1176>.
- Marczynski, Gregory T. 1999. "Chromosome Methylation and Measurement of Faithful, Once and Only Once per Cell Cycle Chromosome Replication In *Caulobacter Crescentus*." *Journal of Bacteriology* 181 (7): 1984–93.
- Marenduzzo, Davide, Cristian Micheletti, and Peter R. Cook. 2006. "Entropy-Driven Genome Organization." *Biophysical Journal* 90 (10): 3712–21. <https://doi.org/10.1529/biophysj.105.077685>.
- Marsh, R. C., and A. Worcel. 1977. "A DNA Fragment Containing the Origin of Replication of the *Escherichia Coli* Chromosome." *Proceedings of the National Academy of Sciences* 74 (7): 2720–24. <https://doi.org/10.1073/pnas.74.7.2720>.
- Martinez, A., and R. Kolter. 1997. "Protection of DNA during Oxidative Stress by the Non-specific DNA-Binding Protein Dps." *Journal of Bacteriology* 179 (16): 5188–94. <https://doi.org/10.1128/jb.179.16.5188-5194.1997>.
- Mathews, C K. 1993. "The Cell-Bag of Enzymes or Network of Channels?" *Journal of Bacteriology* 175 (20): 6377–81.
- Meer, Gerrit van, Dennis R. Voelker, and Gerald W. Feigenson. 2008. "Membrane Lipids: Where They Are and How They Behave." *Nature Reviews Molecular Cell Biology* 9 (2): 112–24. <https://doi.org/10.1038/nrm2330>.
- Meeske, Alexander J., Eammon P. Riley, William P. Robins, Tsuyoshi Uehara, John J. Mekalanos, Daniel Kahne, Suzanne Walker, Andrew C. Kruse, Thomas G. Bernhardt, and David Z. Rudner. 2016. "SEDS Proteins Are a Widespread Family of Bacterial Cell Wall Polymerases." *Nature* advance online publication (August). <https://doi.org/10.1038/nature19331>.
- Meroz, Yasmine, and Igor M. Sokolov. 2015. "A Toolbox for Determining Subdiffusive Mechanisms." *Physics Reports*, A toolbox for determining subdiffusive mechanisms, 573 (April): 1–29. <https://doi.org/10.1016/j.physrep.2015.01.002>.
- Meyenburg, K. von, F. G. Hansen, E. Riise, H. E. N. Bergmans, M. Meijer, and W. Messer. 1979. "Origin of Replication, OriC, of the *Escherichia Coli* K12 Chromosome: Genetic Mapping and Minichromosome Replication." *Cold Spring Harbor Symposia on Quantitative Biology* 43 (January): 121–28. <https://doi.org/10.1101/SQB.1979.043.01.018>.
- Miller, J. J. 1984. "In Vitro Experiments Concerning the State of Polyphosphate in the Yeast Vacuole." *Canadian Journal of Microbiology* 30 (2): 236–46. <https://doi.org/10.1139/m84-035>.
- Modell, J.W., T.K. Kambara, B.S. Perchuk, and M.T. Laub. 2014. "A DNA Damage-Induced, SOS-Independent Checkpoint Regulates Cell Division in *Caulobacter Crescentus*." *PLoS Biology* 12 (10). <https://doi.org/10.1371/journal.pbio.1001977>.
- Mohl, Dane A., Jesse Easter, and James W. Gober. 2001. "The Chromosome Partitioning Protein, ParB, Is Required for Cytokinesis in *Caulobacter Crescentus*." *Molecular Microbiology* 42 (3): 741–55. <https://doi.org/10.1046/j.1365-2958.2001.02643.x>.
- Möll, Andrea, Susan Schlimpert, Ariane Briegel, Grant J. Jensen, and Martin Thanbichler. 2010. "DipM, a New Factor Required for Peptidoglycan Remodelling during Cell Division in *Caulobacter Crescentus*." *Molecular Microbiology* 77 (1): 90–107. <https://doi.org/10.1111/j.1365-2958.2010.07224.x>.

References

- Moolman, M. Charl, Jacob W. J. Kerssemakers, and Nynke H. Dekker. 2015. “Quantitative Analysis of Intracellular Fluorescent Foci in Live Bacteria.” *Biophysical Journal* 109 (5): 883–91. <https://doi.org/10.1016/j.bpj.2015.07.013>.
- Morales Angeles, Danae, Yun Liu, Alwin M. Hartman, Marina Borisova, Anabela de Sousa Borges, Niels de Kok, Katrin Beilharz, et al. 2017. “Pentapeptide-Rich Peptidoglycan at the Bacillus Subtilis Cell-Division Site.” *Molecular Microbiology* 104 (2): 319–33. <https://doi.org/10.1111/mmi.13629>.
- Morgenstein, Randy M., Benjamin P. Bratton, Jeffrey P. Nguyen, Nikolay Ouzounov, Joshua W. Shaevitz, and Zemer Gitai. 2015. “RodZ Links MreB to Cell Wall Synthesis to Mediate MreB Rotation and Robust Morphogenesis.” *Proceedings of the National Academy of Sciences* 112 (40): 12510–15. <https://doi.org/10.1073/pnas.1509610112>.
- Müller, Axel, Morgan Beeby, Alasdair W. McDowall, Janet Chow, Grant J. Jensen, and William M. Clemons. 2014. “Ultrastructure and Complex Polar Architecture of the Human Pathogen Campylobacter Jejuni.” *MicrobiologyOpen* 3 (5): 702–10. <https://doi.org/10.1002/mbo3.200>.
- National Research Council (US) Steering Group for the Workshop on Size Limits of Very Small Microorganisms. 1999. *Size Limits of Very Small Microorganisms: Proceedings of a Workshop*. Washington (DC): National Academies Press (US). <http://www.ncbi.nlm.nih.gov/books/NBK224756/>.
- Nguyen, Dao, Amruta Joshi-Datar, Francois Lepine, Elizabeth Bauerle, Oyebode Olakanmi, Karlyn Beer, Geoffrey McKay, et al. 2011. “Active Starvation Responses Mediate Antibiotic Tolerance in Biofilms and Nutrient-Limited Bacteria.” *Science* 334 (6058): 982–86. <https://doi.org/10.1126/science.1211037>.
- Nielsen, Henrik J., Jesper R. Ottesen, Brenda Youngren, Stuart J. Austin, and Flemming G. Hansen. 2006. “The Escherichia Coli Chromosome Is Organized with the Left and Right Chromosome Arms in Separate Cell Halves.” *Molecular Microbiology* 62 (2): 331–38. <https://doi.org/10.1111/j.1365-2958.2006.05346.x>.
- NOBUYUKI OTSU. 1979. “A Threshold Selection Method from Gray-Level Histograms.” *IEEE TRANSACTIONS ON SYSTEMS, MAN, AND CYBERNETICS*, SMC-9, (1).
- Nolivos, Sophie, and David Sherratt. 2014. “The Bacterial Chromosome: Architecture and Action of Bacterial SMC and SMC-like Complexes.” *FEMS Microbiology Reviews* 38 (3): 380–92. <https://doi.org/10.1111/1574-6976.12045>.
- Oikonomou, Catherine M., Yi-Wei Chang, and Grant J. Jensen. 2016. “A New View into Prokaryotic Cell Biology from Electron Cryotomography.” *Nature Reviews Microbiology* 14 (4): 205–20. <https://doi.org/10.1038/nrmicro.2016.7>.
- Olivier, Nicolas, Debora Keller, Pierre Gönczy, and Suliana Manley. 2013. “Resolution Doubling in 3D-STORM Imaging through Improved Buffers.” *PLOS ONE* 8 (7): e69004. <https://doi.org/10.1371/journal.pone.0069004>.
- Osawa, Masaki, David E. Anderson, and Harold P. Erickson. 2009. “Curved FtsZ Protofilaments Generate Bending Forces on Liposome Membranes.” *The EMBO Journal* 28 (22): 3476–84. <https://doi.org/10.1038/emboj.2009.277>.
- Osawa, Masaki, and Harold P. Erickson. 2013. “Liposome Division by a Simple Bacterial Division Machinery.” *Proceedings of the National Academy of Sciences* 110 (27): 11000–4. <https://doi.org/10.1073/pnas.1222254110>.
- Osella, Matteo, Eileen Nugent, and Marco Cosentino Lagomarsino. 2014. “Concerted Control of Escherichia Coli Cell Division.” *Proceedings of the National Academy of Sciences of the United States of America* 111 (9): 3431–35. <https://doi.org/10.1073/pnas.1313715111>.
- Ouzounov, Nikolay, Jeffrey P. Nguyen, Benjamin P. Bratton, David Jacobowitz, Zemer Gitai, and Joshua W. Shaevitz. 2016. “MreB Orientation Correlates with Cell Diameter in

References

- Escherichia Coli.” *Biophysical Journal* 111 (5): 1035–43. <https://doi.org/10.1016/j.bpj.2016.07.017>.
- Ovesný, Martin, Pavel Křížek, Josef Borkovec, Zdeněk Svindrych, and Guy M. Hagen. 2014. “ThunderSTORM: A Comprehensive ImageJ Plug-in for PALM and STORM Data Analysis and Super-Resolution Imaging.” *Bioinformatics (Oxford, England)* 30 (16): 2389–90. <https://doi.org/10.1093/bioinformatics/btu202>.
- Parnell, Alice E., Silja Mordhorst, Florian Kemper, Mariacarmela Giurandino, Josh P. Prince, Nikola J. Schwarzer, Alexandre Hofer, et al. 2018. “Substrate Recognition and Mechanism Revealed by Ligand-Bound Polyphosphate Kinase 2 Structures.” *Proceedings of the National Academy of Sciences* 115 (13): 3350–55. <https://doi.org/10.1073/pnas.1710741115>.
- Paul, Brian J., Melanie M. Barker, Wilma Ross, David A. Schneider, Cathy Webb, John W. Foster, and Richard L. Gourse. 2004. “DksA: A Critical Component of the Transcription Initiation Machinery That Potentiates the Regulation of RRNA Promoters by PpGpp and the Initiating NTP.” *Cell* 118 (3): 311–22. <https://doi.org/10.1016/j.cell.2004.07.009>.
- Pedro, Miguel A. de, and Felipe Cava. 2015. “Structural Constraints and Dynamics of Bacterial Cell Wall Architecture.” *Frontiers in Microbiology* 6. <https://doi.org/10.3389/fmicb.2015.00449>.
- Philips, Rob, and Ron Milo. 2015. “What Are the Time Scales for Diffusion in Cells?” In *Cell Biology by the Numbers*. Garland Science. <http://book.bionumbers.org/what-are-the-time-scales-for-diffusion-in-cells/>.
- Pincus, Z., and J. A. Theriot. 2007. “Comparison of Quantitative Methods for Cell-Shape Analysis.” *Journal of Microscopy* 227 (Pt 2): 140–56. <https://doi.org/10.1111/j.1365-2818.2007.01799.x>.
- Poggio, Sebastian, Constantin N. Takacs, Waldemar Vollmer, and Christine Jacobs-Wagner. 2010. “A Protein Critical for Cell Constriction in the Gram-Negative Bacterium *Caulobacter Crescentus* Localizes at the Division Site through Its Peptidoglycan-Binding LysM Domains.” *Molecular Microbiology* 77 (1): 74–89. <https://doi.org/10.1111/j.1365-2958.2010.07223.x>.
- Popp, Felix, Judith P. Armitage, and Dirk Schüler. 2014. “Polarity of Bacterial Magnetotaxis Is Controlled by Aerotaxis through a Common Sensory Pathway.” *Nature Communications* 5 (November): 5398. <https://doi.org/10.1038/ncomms6398>.
- Potrykus, Katarzyna, Helen Murphy, Nadège Philippe, and Michael Cashel. 2011. “PpGpp Is the Major Source of Growth Rate Control in *E. Coli*.” *Environmental Microbiology* 13 (3): 563–75. <https://doi.org/10.1111/j.1462-2920.2010.02357.x>.
- Preibisch, Stephan, Stephan Saalfeld, Johannes Schindelin, and Pavel Tomancak. 2010. “Software for Bead-Based Registration of Selective Plane Illumination Microscopy Data.” *Nature Methods* 7 (6): 418–19. <https://doi.org/10.1038/nmeth0610-418>.
- Racki, Lisa R., Elitza I. Tocheva, Michael G. Dieterle, Meaghan C. Sullivan, Grant J. Jensen, and Dianne K. Newman. 2017. “Polyphosphate Granule Biogenesis Is Temporally and Functionally Tied to Cell Cycle Exit during Starvation in *Pseudomonas Aeruginosa*.” *Proceedings of the National Academy of Sciences* 114 (12): E2440–49. <https://doi.org/10.1073/pnas.1615575114>.
- Raetz, C. R., and W. Dowhan. 1990. “Biosynthesis and Function of Phospholipids in *Escherichia Coli*.” *The Journal of Biological Chemistry* 265 (3): 1235–38.
- Rao, Narayana N., María R. Gómez-García, and Arthur Kornberg. 2009. “Inorganic Polyphosphate: Essential for Growth and Survival.” *Annual Review of Biochemistry* 78 (1): 605–47. <https://doi.org/10.1146/annurev.biochem.77.083007.093039>.

References

- Rao, Narayana N., and Arthur Kornberg. 1996. "Inorganic Polyphosphate Supports Resistance and Survival of Stationary-Phase Escherichia Coli." *Journal of Bacteriology* 178 (5): 1394–1400. <https://doi.org/10.1128/jb.178.5.1394-1400.1996>.
- Rashevsky, N. 1938. "The Relation of Mathematical Biophysics to Experimental Biology." *Acta Biotheoretica* 4 (2): 133–53. <https://doi.org/10.1007/BF01557301>.
- Raskin, David M., and Piet A. J. de Boer. 1999a. "Rapid Pole-to-Pole Oscillation of a Protein Required for Directing Division to the Middle of Escherichia Coli." *Proceedings of the National Academy of Sciences* 96 (9): 4971–76. <https://doi.org/10.1073/pnas.96.9.4971>.
- . 1999b. "MinDE-Dependent Pole-to-Pole Oscillation of Division Inhibitor MinC in Escherichia Coli." *Journal of Bacteriology* 181 (20): 6419–24.
- Reshes, G., S. Vanounou, I. Fishov, and M. Feingold. 2008. "Timing the Start of Division in E. Coli: A Single-Cell Study." *Physical Biology* 5 (4): 046001. <https://doi.org/10.1088/1478-3975/5/4/046001>.
- Riemann, Lasse, and Farooq Azam. 2002. "Widespread N-Acetyl-d-Glucosamine Uptake among Pelagic Marine Bacteria and Its Ecological Implications." *Appl. Environ. Microbiol.* 68 (11): 5554–62. <https://doi.org/10.1128/AEM.68.11.5554-5562.2002>.
- Rojas, Enrique R., Gabriel Billings, Pascal D. Odermatt, George K. Auer, Lillian Zhu, Amanda Miguel, Fred Chang, Douglas B. Weibel, Julie A. Theriot, and Kerwyn Casey Huang. 2018. "The Outer Membrane Is an Essential Load-Bearing Element in Gram-Negative Bacteria." *Nature* 559 (7715): 617–21. <https://doi.org/10.1038/s41586-018-0344-3>.
- Rollins, Geoffrey C., Jae Yen Shin, Carlos Bustamante, and Steve Pressé. 2014. "Stochastic Approach to the Molecular Counting Problem in Superresolution Microscopy." *Proceedings of the National Academy of Sciences*, December, 201408071. <https://doi.org/10.1073/pnas.1408071112>.
- Rust, Michael J., Mark Bates, and Xiaowei Zhuang. 2006. "Sub-Diffraction-Limit Imaging by Stochastic Optical Reconstruction Microscopy (STORM)." *Nature Methods* 3 (10): 793–96. <https://doi.org/10.1038/nmeth929>.
- Saint-Ruf, Claude, Josipa Pesut, Mary Sopta, and Ivan Matic. 2007. "Causes and Consequences of DNA Repair Activity Modulation During Stationary Phase in Escherichia Coli." *Critical Reviews in Biochemistry and Molecular Biology* 42 (4): 259–70. <https://doi.org/10.1080/10409230701495599>.
- Sargent, M G. 1975. "Control of Cell Length in Bacillus Subtilis." *Journal of Bacteriology* 123 (1): 7–19.
- Schaechter, M., O. Maaløe, and N. O. Kjeldgaard. 1958. "Dependency on Medium and Temperature of Cell Size and Chemical Composition during Balanced Growth of Salmonella Typhimurium." *Microbiology* 19 (3): 592–606. <https://doi.org/10.1099/00221287-19-3-592>.
- Schneider, Caroline A., Wayne S. Rasband, and Kevin W. Eliceiri. 2012. "NIH Image to ImageJ: 25 Years of Image Analysis." *Nature Methods* 9 (7): 671–75.
- Schrader, Jared M., and Lucy Shapiro. 2015. "Synchronization of Caulobacter Crescentus for Investigation of the Bacterial Cell Cycle." *JoVE (Journal of Visualized Experiments)*, no. 98 (April): e52633–e52633. <https://doi.org/10.3791/52633>.
- Schulz, H.N., and B.B. Jørgensen. 2001. "Big Bacteria." *Annual Review of Microbiology* 55: 105–37. <https://doi.org/10.1146/annurev.micro.55.1.105>.
- Shaner, Nathan C., Gerard G. Lambert, Andrew Chammas, Yuhui Ni, Paula J. Cranfill, Michelle A. Baird, Brittney R. Sell, et al. 2013. "A Bright Monomeric Green Fluorescent Protein Derived from Branchiostoma Lanceolatum." *Nature Methods* 10 (5): 407–9. <https://doi.org/10.1038/nmeth.2413>.

References

- Shaner, Nathan C., Michael Z. Lin, Michael R. McKeown, Paul A. Steinbach, Kristin L. Hazelwood, Michael W. Davidson, and Roger Y. Tsien. 2008. "Improving the Photostability of Bright Monomeric Orange and Red Fluorescent Proteins." *Nature Methods* 5 (6): 545–51. <https://doi.org/10.1038/nmeth.1209>.
- Shi, Handuo, Benjamin P. Bratton, Zemer Gitai, and Kerwyn Casey Huang. 2018. "How to Build a Bacterial Cell: MreB as the Foreman of E. Coli Construction." *Cell* 172 (6): 1294–1305. <https://doi.org/10.1016/j.cell.2018.02.050>.
- Shi, Handuo, Alexandre Colavin, Marty Bigos, Carolina Tropini, Russell D. Monds, and Kerwyn Casey Huang. 2017. "Deep Phenotypic Mapping of Bacterial Cytoskeletal Mutants Reveals Physiological Robustness to Cell Size." *Current Biology* 27 (22): 3419–3429.e4. <https://doi.org/10.1016/j.cub.2017.09.065>.
- Shim, Sang-Hee, Chenglong Xia, Guisheng Zhong, Hazen P. Babcock, Joshua C. Vaughan, Bo Huang, Xun Wang, Cheng Xu, Guo-Qiang Bi, and Xiaowei Zhuang. 2012. "Super-Resolution Fluorescence Imaging of Organelles in Live Cells with Photoswitchable Membrane Probes." *Proceedings of the National Academy of Sciences* 109 (35): 13978–83. <https://doi.org/10.1073/pnas.1201882109>.
- Si, Fangwei, Dongyang Li, Sarah E. Cox, John T. Sauls, Omid Azizi, Cindy Sou, Amy B. Schwartz, et al. 2017. "Invariance of Initiation Mass and Predictability of Cell Size in Escherichia Coli." *Current Biology* 27 (9): 1278–87. <https://doi.org/10.1016/j.cub.2017.03.022>.
- Sigal, Yaron M., Ruobo Zhou, and Xiaowei Zhuang. 2018. "Visualizing and Discovering Cellular Structures with Super-Resolution Microscopy." *Science* 361 (6405): 880–87. <https://doi.org/10.1126/science.aau1044>.
- Silhavy, Thomas J., Daniel Kahne, and Suzanne Walker. 2010. "The Bacterial Cell Envelope." *Cold Spring Harbor Perspectives in Biology*, April, a000414. <https://doi.org/10.1101/cshperspect.a000414>.
- Skerker, J.M., and M.T. Laub. 2004. "Cell-Cycle Progression and the Generation of Asymmetry in Caulobacter Crescentus." *Nature Reviews Microbiology* 2 (4): 325–37. <https://doi.org/10.1038/nrmicro864>.
- Sliusarenko, Oleksii, Jennifer Heinritz, Thierry Emonet, and Christine Jacobs-Wagner. 2011. "High-Throughput, Subpixel Precision Analysis of Bacterial Morphogenesis and Intracellular Spatio-Temporal Dynamics." *Molecular Microbiology* 80 (3): 612–27. <https://doi.org/10.1111/j.1365-2958.2011.07579.x>.
- Smith, Isabel W., J. F. Wilkinson, and J. P. Duguid. 1954. "VOLUTIN PRODUCTION IN AEROBACTER AEROGENES DUE TO NUTRIENT IMBALANCE." *Journal of Bacteriology* 68 (4): 450–63.
- Sompayrac, L., and O. Maaløe. 1973. "Autorepressor Model for Control of DNA Replication." *Nature New Biology* 241 (109): 133–35. <https://doi.org/10.1038/newbio241133a0>.
- Stirling, J W. 1990. "Immuno- and Affinity Probes for Electron Microscopy: A Review of Labeling and Preparation Techniques." *Journal of Histochemistry & Cytochemistry* 38 (2): 145–57. <https://doi.org/10.1177/38.2.2405054>.
- Strauss, Michael P., Andrew T. F. Liew, Lynne Turnbull, Cynthia B. Whitchurch, Leigh G. Monahan, and Elizabeth J. Harry. 2012. "3D-SIM Super Resolution Microscopy Reveals a Bead-Like Arrangement for FtsZ and the Division Machinery: Implications for Triggering Cytokinesis." *PLoS Biol* 10 (9): e1001389. <https://doi.org/10.1371/journal.pbio.1001389>.
- Surovtsev, Ivan V., and Christine Jacobs-Wagner. 2018. "Subcellular Organization: A Critical Feature of Bacterial Cell Replication." *Cell* 172 (6): 1271–93. <https://doi.org/10.1016/j.cell.2018.01.014>.

References

- Swulius, Matthew T., and Grant J. Jensen. 2012. "The Helical MreB Cytoskeleton in *Escherichia Coli* MC1000/PLE7 Is an Artifact of the N-Terminal Yellow Fluorescent Protein Tag." *Journal of Bacteriology* 194 (23): 6382–86. <https://doi.org/10.1128/JB.00505-12>.
- Sycuro, Laura K., Zachary Pincus, Kimberley D. Gutierrez, Jacob Biboy, Chelsea A. Stern, Waldemar Vollmer, and Nina R. Salama. 2010. "Peptidoglycan Crosslinking Relaxation Promotes *Helicobacter Pylori*'s Helical Shape and Stomach Colonization." *Cell* 141 (5): 822–33. <https://doi.org/10.1016/j.cell.2010.03.046>.
- Szeto, Tim H., Susan L. Rowland, Cheryl L. Habrukowich, and Glenn F. King. 2003. "The MinD Membrane Targeting Sequence Is a Transplantable Lipid-Binding Helix." *Journal of Biological Chemistry* 278 (41): 40050–56. <https://doi.org/10.1074/jbc.M306876200>.
- Szwedziak, Piotr, Qing Wang, Tanmay A M Bharat, Matthew Tsim, and Jan Löwe. 2014. "Architecture of the Ring Formed by the Tubulin Homologue FtsZ in Bacterial Cell Division." *eLife* 3 (December). <https://doi.org/10.7554/eLife.04601>.
- Taheri-Araghi, Sattar, Serena Bradde, John T. Sauls, Norbert S. Hill, Petra Anne Levin, Johan Paulsson, Massimo Vergassola, and Suckjoon Jun. 2015. "Cell-Size Control and Homeostasis in Bacteria." *Current Biology* 25 (3): 385–91. <https://doi.org/10.1016/j.cub.2014.12.009>.
- Tarantino, Nadine, Jean-Yves Tinevez, Elizabeth Faris Crowell, Bertrand Boisson, Ricardo Henriques, Musa Mhlanga, Fabrice Agou, Alain Israël, and Emmanuel Laplantine. 2014. "TNF and IL-1 Exhibit Distinct Ubiquitin Requirements for Inducing NEMO–IKK Supramolecular Structures." *J Cell Biol* 204 (2): 231–45. <https://doi.org/10.1083/jcb.201307172>.
- Teeffelen, Sven van, Siyuan Wang, Leon Furchtgott, Kerwyn Casey Huang, Ned S. Wingreen, Joshua W. Shaevitz, and Zemer Gitai. 2011. "The Bacterial Actin MreB Rotates, and Rotation Depends on Cell-Wall Assembly." *Proceedings of the National Academy of Sciences* 108 (38): 15822–27. <https://doi.org/10.1073/pnas.1108999108>.
- Thanbichler, Martin, Antonio A. Iniesta, and Lucy Shapiro. 2007. "A Comprehensive Set of Plasmids for Vanillate- and Xylose-Inducible Gene Expression in *Caulobacter Crescentus*." *Nucleic Acids Research* 35 (20): e137. <https://doi.org/10.1093/nar/gkm818>.
- Thanbichler, Martin, and Lucy Shapiro. 2006. "MipZ, a Spatial Regulator Coordinating Chromosome Segregation with Cell Division in *Caulobacter*." *Cell* 126 (1): 147–62. <https://doi.org/10.1016/j.cell.2006.05.038>.
- Tindall, B. J., G. Sutton, and G. M. Garrity. 2017. "Enterobacter Aerogenes Hormaeche and Edwards 1960 (Approved Lists 1980) and *Klebsiella Mobilis* Bascomb et Al. 1971 (Approved Lists 1980) Share the Same Nomenclatural Type (ATCC 13048) on the Approved Lists and Are Homotypic Synonyms, with Consequences for the Name *Klebsiella Mobilis* Bascomb et Al. 1971 (Approved Lists 1980)." *International Journal of Systematic and Evolutionary Microbiology* 67 (2): 502–4. <https://doi.org/10.1099/ijsem.0.001572>.
- Tinevez, Jean-Yves, Nick Perry, Johannes Schindelin, Genevieve M. Hoopes, Gregory D. Reynolds, Emmanuel Laplantine, Sebastian Y. Bednarek, Spencer L. Shorte, and Kevin W. Eliceiri. 2017. "TrackMate: An Open and Extensible Platform for Single-Particle Tracking." *Methods, Image Processing for Biologists*, 115 (February): 80–90. <https://doi.org/10.1016/j.ymeth.2016.09.016>.
- Tocheva, Elitza I., Anne E. Dekas, Shawn E. McGlynn, Dylan Morris, Victoria J. Orphan, and Grant J. Jensen. 2013. "Polyphosphate Storage during Sporulation in the Gram-Negative Bacterium *Acetonebacterium Longum*." *Journal of Bacteriology* 195 (17): 3940–46. <https://doi.org/10.1128/JB.00712-13>.

References

- Traxler, Matthew F., Sean M. Summers, Huyen-Tran Nguyen, Vineetha M. Zacharia, G. Aaron Hightower, Joel T. Smith, and Tyrrell Conway. 2008. "The Global, PpGpp-Mediated Stringent Response to Amino Acid Starvation in Escherichia Coli." *Molecular Microbiology* 68 (5): 1128–48. <https://doi.org/10.1111/j.1365-2958.2008.06229.x>.
- Traxler, Matthew F., Vineetha M. Zacharia, Stafford Marquardt, Sean M. Summers, Huyen-Tran Nguyen, S. Elizabeth Stark, and Tyrrell Conway. 2011. "Discretely Calibrated Regulatory Loops Controlled by PpGpp Partition Gene Induction across the 'Feast to Famine' Gradient in Escherichia Coli." *Molecular Microbiology* 79 (4): 830–45. <https://doi.org/10.1111/j.1365-2958.2010.07498.x>.
- Tropini, Carolina, Timothy K. Lee, Jen Hsin, Samantha M. Desmarais, Tristan Ursell, Russell D. Monds, and Kerwyn Casey Huang. 2014. "Principles of Bacterial Cell-Size Determination Revealed by Cell-Wall Synthesis Perturbations." *Cell Reports* 9 (4): 1520–27. <https://doi.org/10.1016/j.celrep.2014.10.027>.
- Tsien, Roger Y. 1998. "The Green Fluorescent Protein." *Annual Review of Biochemistry* 67 (1): 509–44. <https://doi.org/10.1146/annurev.biochem.67.1.509>.
- Turner, Robert D., Stéphane Mesnage, Jamie K. Hobbs, and Simon J. Foster. 2018. "Molecular Imaging of Glycan Chains Couples Cell-Wall Polysaccharide Architecture to Bacterial Cell Morphology." *Nature Communications* 9 (1): 1263. <https://doi.org/10.1038/s41467-018-03551-y>.
- Typas, Athanasios, Manuel Banzhaf, Carol A. Gross, and Waldemar Vollmer. 2012. "From the Regulation of Peptidoglycan Synthesis to Bacterial Growth and Morphology." *Nature Reviews Microbiology* 10 (2): 123–36. <https://doi.org/10.1038/nrmicro2677>.
- Uebe, René, and Dirk Schüler. 2016. "Magnetosome Biogenesis in Magnetotactic Bacteria." *Nature Reviews Microbiology* 14 (10): 621–37. <https://doi.org/10.1038/nrmicro.2016.99>.
- Ursell, Tristan S., Jeffrey Nguyen, Russell D. Monds, Alexandre Colavin, Gabriel Billings, Nikolay Ouzounov, Zemer Gitai, Joshua W. Shaevitz, and Kerwyn Casey Huang. 2014. "Rod-like Bacterial Shape Is Maintained by Feedback between Cell Curvature and Cytoskeletal Localization." *Proceedings of the National Academy of Sciences* 111 (11): E1025–34. <https://doi.org/10.1073/pnas.1317174111>.
- Vadia, Stephen, Jessica L. Tse, Rafael Lucena, Zhizhou Yang, Douglas R. Kellogg, Jue D. Wang, and Petra Anne Levin. 2017. "Fatty Acid Availability Sets Cell Envelope Capacity and Dictates Microbial Cell Size." *Current Biology* 27 (12): 1757–1767.e5. <https://doi.org/10.1016/j.cub.2017.05.076>.
- Valens, Michèle, Stéphanie Penaud, Michèle Rossignol, François Cornet, and Frédéric Boccard. 2004. "Macrodomain Organization of the Escherichia Coli Chromosome." *The EMBO Journal* 23 (21): 4330–41. <https://doi.org/10.1038/sj.emboj.7600434>.
- Vallet-Gely, Isabelle, and Frédéric Boccard. 2013. "Chromosomal Organization and Segregation in Pseudomonas Aeruginosa." *PLOS Genetics* 9 (5): e1003492. <https://doi.org/10.1371/journal.pgen.1003492>.
- Viollier, Patrick H., Martin Thanbichler, Patrick T. McGrath, Lisandra West, Maliwan Meehan, Harley H. McAdams, and Lucy Shapiro. 2004. "Rapid and Sequential Movement of Individual Chromosomal Loci to Specific Subcellular Locations during Bacterial DNA Replication." *Proceedings of the National Academy of Sciences* 101 (25): 9257–62. <https://doi.org/10.1073/pnas.0402606101>.
- Vollmer, Waldemar, Didier Blanot, and Miguel A. de Pedro. 2008. "Peptidoglycan Structure and Architecture." *FEMS Microbiology Reviews* 32 (2): 149–67. <https://doi.org/10.1111/j.1574-6976.2007.00094.x>.

References

- Wallden, Mats, David Fange, Ebba Gregorsson Lundius, Özden Baltekin, and Johan Elf. 2016. "The Synchronization of Replication and Division Cycles in Individual *E. Coli* Cells." *Cell* 166 (3): 729–39. <https://doi.org/10.1016/j.cell.2016.06.052>.
- Wang, Ping, Lydia Robert, James Pelletier, Wei Lien Dang, Francois Taddei, Andrew Wright, and Suckjoon Jun. 2010. "Robust Growth of *Escherichia Coli*." *Current Biology* 20 (12): 1099–1103. <https://doi.org/10.1016/j.cub.2010.04.045>.
- Wang, Siyuan, and Ned S. Wingreen. 2013. "Cell Shape Can Mediate the Spatial Organization of the Bacterial Cytoskeleton." *Biophysical Journal* 104 (3): 541–52. <https://doi.org/10.1016/j.bpj.2012.12.027>.
- Wang, Xindan, Xun Liu, Christophe Possoz, and David J. Sherratt. 2006. "The Two *Escherichia Coli* Chromosome Arms Locate to Separate Cell Halves." *Genes & Development* 20 (13): 1727–31. <https://doi.org/10.1101/gad.388406>.
- Wang, Xindan, Paula Montero Llopis, and David Z. Rudner. 2013. "Organization and Segregation of Bacterial Chromosomes." *Nature Reviews Genetics* 14 (3): 191–203. <https://doi.org/10.1038/nrg3375>.
- Wang, Xindan, Christophe Possoz, and David J. Sherratt. 2005. "Dancing around the Divisome: Asymmetric Chromosome Segregation in *Escherichia Coli*." *Genes & Development* 19 (19): 2367–77. <https://doi.org/10.1101/gad.345305>.
- Weart, Richard B., Amy H. Lee, An-Chun Chien, Daniel P. Haeusser, Norbert S. Hill, and Petra Anne Levin. 2007. "A Metabolic Sensor Governing Cell Size in Bacteria." *Cell* 130 (2): 335–47. <https://doi.org/10.1016/j.cell.2007.05.043>.
- Weber, Harald, Tino Polen, Johanna Heuveling, Volker F. Wendisch, and Regine Hengge. 2005. "Genome-Wide Analysis of the General Stress Response Network in *Escherichia Coli*: Σ S-Dependent Genes, Promoters, and Sigma Factor Selectivity." *Journal of Bacteriology* 187 (5): 1591–1603. <https://doi.org/10.1128/JB.187.5.1591-1603.2005>.
- Weber, Stephanie C., Andrew J. Spakowitz, and Julie A. Theriot. 2010. "Bacterial Chromosomal Loci Move Subdiffusively through a Viscoelastic Cytoplasm." *Physical Review Letters* 104 (23): 238102. <https://doi.org/10.1103/PhysRevLett.104.238102>.
- Wehrens, Martijn, Dmitry Ershov, Rutger Rozendaal, Noreen Walker, Daniel Schultz, Roy Kishony, Petra Anne Levin, and Sander J. Tans. 2018. "Size Laws and Division Ring Dynamics in Filamentous *Escherichia Coli* Cells." *Current Biology* 28 (6): 972-979.e5. <https://doi.org/10.1016/j.cub.2018.02.006>.
- Weidel, W., and H. Pelzer. 1964. "Bagshaped Macromolecules—A New Outlook on Bacterial Cell Walls." In *Advances in Enzymology and Related Areas of Molecular Biology*, 193–232. Wiley-Blackwell. <https://doi.org/10.1002/9780470122716.ch5>.
- Westfall, Corey S., and Petra Anne Levin. 2017. "Bacterial Cell Size: Multifactorial and Multifaceted." *Annual Review of Microbiology* 71 (1): 499–517. <https://doi.org/10.1146/annurev-micro-090816-093803>.
- Westphal, Volker, Silvio O. Rizzoli, Marcel A. Lauterbach, Dirk Kamin, Reinhard Jahn, and Stefan W. Hell. 2008. "Video-Rate Far-Field Optical Nanoscopy Dissects Synaptic Vesicle Movement." *Science* 320 (5873): 246–49. <https://doi.org/10.1126/science.1154228>.
- Wong, Felix, Lars D. Renner, Gizem Özbaykal, Jayson Paulose, Douglas B. Weibel, Sven van Teeffelen, and Ariel Amir. 2017. "Mechanical Strain Sensing Implicated in Cell Shape Recovery in *Escherichia Coli*." *Nature Microbiology* 2 (9): 17115. <https://doi.org/10.1038/nmicrobiol.2017.115>.
- Wu, Ling Juan, and Jeff Errington. 2004. "Coordination of Cell Division and Chromosome Segregation by a Nucleoid Occlusion Protein in *Bacillus Subtilis*." *Cell* 117 (7): 915–25. <https://doi.org/10.1016/j.cell.2004.06.002>.

References

- Yahashiri, A., M.A. Jorgenson, and D.S. Weiss. 2015. "Bacterial SPOR Domains Are Recruited to Septal Peptidoglycan by Binding to Glycan Strands That Lack Stem Peptides." *Proceedings of the National Academy of Sciences of the United States of America* 112 (36): 11347–52. <https://doi.org/10.1073/pnas.1508536112>.
- Yang, Xinxing, Zhixin Lyu, Amanda Miguel, Ryan McQuillen, Kerwyn Casey Huang, and Jie Xiao. 2017. "GTPase Activity–Coupled Treadmilling of the Bacterial Tubulin FtsZ Organizes Septal Cell Wall Synthesis." *Science* 355 (6326): 744–47. <https://doi.org/10.1126/science.aak9995>.
- Yeates, Todd O., Cheryl A. Kerfeld, Sabine Heinhorst, Gordon C. Cannon, and Jessup M. Shively. 2008. "Protein-Based Organelles in Bacteria: Carboxysomes and Related Microcompartments." *Nature Reviews Microbiology* 6 (9): 681–91. <https://doi.org/10.1038/nrmicro1913>.
- Yildirim, Asli, and Michael Feig. 2018. "High-Resolution 3D Models of Caulobacter Crescentus Chromosome Reveal Genome Structural Variability and Organization." *Nucleic Acids Research* 46 (8): 3937–52. <https://doi.org/10.1093/nar/gky141>.
- York, Andrew G., Panagiotis Chandris, Damian Dalle Nogare, Jeffrey Head, Peter Wawrzusin, Robert S. Fischer, Ajay Chitnis, and Hari Shroff. 2013. "Instant Super-Resolution Imaging in Live Cells and Embryos via Analog Image Processing." *Nature Methods* 10 (11): 1122–26. <https://doi.org/10.1038/nmeth.2687>.
- Young, Kevin D. 2006. "The Selective Value of Bacterial Shape." *Microbiology and Molecular Biology Reviews* 70 (3): 660–703. <https://doi.org/10.1128/MMBR.00001-06>.
- Youngren, Brenda, Henrik Jörk Nielsen, Suckjoon Jun, and Stuart Austin. 2014. "The Multifork Escherichia Coli Chromosome Is a Self-Duplicating and Self-Segregating Thermodynamic Ring Polymer." *Genes & Development* 28 (1): 71–84. <https://doi.org/10.1101/gad.231050.113>.
- Zhang, Haiyu, Kazuya Ishige, and Arthur Kornberg. 2002. "A Polyphosphate Kinase (PPK2) Widely Conserved in Bacteria." *Proceedings of the National Academy of Sciences* 99 (26): 16678–83. <https://doi.org/10.1073/pnas.262655199>.
- Zheng, Hai, Po-Yi Ho, Meiling Jiang, Bin Tang, Weirong Liu, Dengjin Li, Xuefeng Yu, Nancy E. Kleckner, Ariel Amir, and Chenli Liu. 2016. "Interrogating the Escherichia Coli Cell Cycle by Cell Dimension Perturbations." *Proceedings of the National Academy of Sciences* 113 (52): 15000–5. <https://doi.org/10.1073/pnas.1617932114>.

Curriculum Vitae

Aster Vanhecke

place Chauderon 34, 1003 Lausanne, CH - astervanhecke@hotmail.com - +4178/834.26.09

EDUCATION

- 2014 – present: Ecole Polytechnique Fédérale de Lausanne, PhD
 - Project management, experimental design
 - Use, calibration and modification of custom superresolution microscopes
 - Development of an image analysis pipeline in MATLAB, using git(hub) for version control
 - Data visualization and statistical analysis in MATLAB/Jupyter
 - Presenting results, both in written form as in figures (Matlab, adobe illustrator)
 - Orally presenting results at international conferences (posters as well as oral presentations),
- 2014 KULeuven, 2 month student job.
 - Collect and analyze additional data leading to a publication
- 2012-2014 MSc in Biochemistry & Biotechnology (129 ECTS)
 - Graduated with distinction in 2014
 - Master's thesis: '*A study of the SeqA using Photo-Activated Localization Microscopy*':
 - Molecular cloning, Super-resolution microscopy
- 2009-2012 BSc in Biochemistry & Biotechnology (184 ECTS)
 - Graduated with distinction in 2012

PROFESSIONAL QUALIFICATIONS

- Molecular biology, microbiology
- Building optical set-ups
- Computer skills
 - Matlab
 - Jupyter Notebook
 - git, GitHub
 - Microsoft office

AWARDS

- Selected talk and BacNet travel award at Bacnet 2017
- Best poster prize at D.DAY UNIL 2017 by ADAS (Association des Doctorants et Assistants) and SVSN (Société Vaudoise des Sciences Naturelles)

PUBLICATIONS

Constriction rate modulation can drive cell size control and homeostasis in *C. crescentus*. Lambert A.*, Vanhecke A.* et al. 2018, *iScience* 4 (June): 180–89.

A study of SeqA subcellular localization in *Escherichia coli* using photo-activated localization microscopy, JT Mika JT*, Vanhecke A.*, et al. 2015, *Faraday Discuss.*, 184, 425-450

LANGUAGE SKILLS

- Dutch – Native speaker
- English – Professional proficiency
- French – Fluent

INTERESTS

- Reading about nature, science, technology, history, politics, economy, etc.
- Going into nature: Hiking, biking, snowboarding, diving, etc.

